VOLUME 33 NOVEMBER 1955 NUMBER 11

Canadian Journal of Physics

NOTICE TO AUTHORS

Enclosed in this issue is an announcement of a change in the system of citing references in the *Canadian Journal of Physics*. Authors are requested to consult the announcement for details of the new system.

Editor: G. M. VOLKOFF

Associate Editors:

L. G. ELLIOTT, *Atomic Energy of Canada, Ltd., Chalk River*
J. S. FOSTER, *McGill University*
G. HERZBERG, *National Research Council of Canada*
L. LEPRINCE-RINGUET, *Ecole Polytechnique, Paris*
R. W. PRINGLE, *University of Manitoba*
B. W. SARGENT, *Queen's University*
Sir FRANCIS SIMON, *Clarendon Laboratory, University of Oxford*
W. H. WATSON, *University of Toronto*

Published by THE NATIONAL RESEARCH COUNCIL

OTTAWA CANADA

CANADIAN JOURNAL OF PHYSICS

(*Formerly Section A, Canadian Journal of Research*)

Under the authority of the Chairman of the Committee of the Privy Council on Scientific and Industrial Research, the National Research Council issues THE CANADIAN JOURNAL OF PHYSICS and six other journals devoted to the publication, in English or French, of the results of original scientific research. Matters of general policy concerning these journals are the responsibility of a joint Editorial Board consisting of: members representing the National Research Council of Canada; the Editors of the Journals; and members representing the Royal Society of Canada and four other scientific societies.

EDITORIAL BOARD

Representatives of the National Research Council

A. N. Campbell, *University of Manitoba*
G. E. Hall, *University of Western Ontario*
E. G. D. Murray, *McGill University*
D. L. Thomson, *McGill University*
W. H. Watson (Chairman), *University of Toronto*

Editors of the Journals

D. L. Bailey, *University of Toronto*
T. W. M. Cameron, *Macdonald College*
J. B. Collip, *University of Western Ontario*
G. A. Ledingham, *National Research Council*
Léo Marion, *National Research Council*
R. G. E. Murray, *University of Western Ontario*
G. M. Volkoff, *University of British Columbia*

Representatives of Societies

D. L. Bailey, *University of Toronto*
Royal Society of Canada
T. W. M. Cameron, *Macdonald College*
Royal Society of Canada
J. B. Collip, *University of Western Ontario*
Canadian Physiological Society
R. G. E. Murray, *University of Western Ontario*
Canadian Society of Microbiologists
H. G. Thode, *McMaster University*
Chemical Institute of Canada
T. Thorvaldson, *University of Saskatchewan*
Royal Society of Canada
G. M. Volkoff, *University of British Columbia*
Royal Society of Canada; Canadian Association of Physicists

Ex officio

Léo Marion (Editor-in-Chief), *National Research Council*

Manuscripts for publication should be submitted to Dr. Léo Marion, Editor-in-Chief, Canadian Journal of Physics, National Research Council, Ottawa 2, Canada.
(For instructions on preparation of copy, see **Notes to Contributors** (inside back cover).)

Proof, correspondence concerning proof, and orders for reprints should be sent to the Manager, Editorial Office (Research Journals), Division of Administration, National Research Council, Ottawa 2, Canada.

Subscriptions, renewals, requests for single or back numbers, and all remittances should be sent to Division of Administration, National Research Council, Ottawa 2, Canada. Remittances should be made payable to the Receiver General of Canada, credit National Research Council.

The journals published, frequency of publication, and prices are:

Canadian Journal of Biochemistry and Physiology	Bimonthly	$3.00 a year
Canadian Journal of Botany	Bimonthly	$4.00 a year
Canadian Journal of Chemistry	Monthly	$5.00 a year
Canadian Journal of Microbiology*	Bimonthly	$3.00 a year
Canadian Journal of Physics	Monthly	$4.00 a year
Canadian Journal of Technology	Bimonthly	$3.00 a year
Canadian Journal of Zoology	Bimonthly	$3.00 a year

The price of single numbers of all journals is 75 cents.

*Volume 1 will combine three numbers published in 1954 with six published in 1955 and will be available at the regular annual subscription rate of $3.00.

REFERENCES—CANADIAN JOURNAL OF PHYSICS

This is to announce a change from the present system of citing references. Beginning in January 1956, reference citations will be unnumbered and will be referred to in the text by the author and date. Authors are requested to follow the new system in all manuscripts submitted henceforth, noting especially the following details.

In the List of References

1. References should be arranged alphabetically according to the names of the authors of the publications.

2. The year of publication should follow the initials of the last author.

3. Citations of work accepted for publication should include the year and place of publication followed by "In press". References to work that has not been published should be given simply as "Unpublished".

4. If two or more publications are listed for the same author or authors, the name(s) of the author(s) should be replaced by a dash in the second and subsequent citations.

5. Two or more publications listed for the same author or authors in the same year should be differentiated by *a*, *b*, etc., following the year.

6. In citations from periodicals the volume number will be printed in bold-face type and thus in the manuscript the number should be underlined by a wavy line.

EXAMPLES:

Atkins, K. R. 1954. Can. J. Phys. **32**: 347.
Dirac, P. A. M. 1947. The principles of quantum mechanics. 3rd ed. Oxford at the Clarendon Press.
——— 1948*a*. Phil. Mag. **39**: 31.
——— 1948*b*. Phys. Rev. **74**: 817.
——— 1952. Proc. Roy. Soc. (London), A, **212**: 330.
Smith, A. B. Unpublished.
Smith, A. B. and Allen, R. O. 1956. Can. J. Phys. In press.
Sumner, J. B. and Somers, G. F. 1944. Laboratory experiments in biological chemistry. Academic Press, Inc., New York, N.Y.

In the Text

The following examples indicate how to refer in the text to citations given in the reference list: (Atkins 1954), (Dirac 1948*a*, *b*, 1952), (Dirac 1947; Smith and Allen 1956), (Smith unpublished). When the names of authors form part of the text, only the date will appear in parentheses, e.g. "Atkins (1954) found . . ."

Canadian Journal of Physics

Issued by THE NATIONAL RESEARCH COUNCIL OF CANADA

VOLUME 33 NOVEMBER 1955 NUMBER 11

VERTICAL EXTENT OF AURORAL ARCS AND BANDS[1]

BY B. W. CURRIE AND J. T. WEAVER

ABSTRACT

Measurements of the vertical extent of quiet arcs and bands from 181 auroral photographs, taken at Chesterfield (63.3° N., 90.7° W.), Coppermine (67.8° N., 115.2° W.), and Saskatoon (52.1° N., 106.6° W.), indicate that these forms are confined to a narrow layer of the atmosphere immediately above the 100-km. level. The most frequent thickness of this layer is between 20 and 40 km. Values in excess of 50 km. rarely occur. The percentage of auroral time that the luminosity is restricted to this layer is uncertain. The ratio of the number of arcs and bands to the total number of observed forms suggests a value exceeding 50%. When the occurrence of each form is weighted according to the angular field covered by it, a value as high as 60% is indicated.

INTRODUCTION

Little is known about the range of heights within which each type of aurora commonly occurs, and the percentage of auroral time with each type as the dominant form. As a result, it is quite usual to assume vertical extents of several hundreds of kilometers in interpreting spectra, radio reflections, and magnetic and ionospheric disturbances observed during auroral displays. This is because heights for the upper limits of rays, as determined by parallactic methods, often range up to 300 and 400 km. and occasionally to over 1000 km. (5).

A reliable determination of an auroral height from a pair of parallactic photographs depends on (*a*) well-defined edges to the structure and (*b*) an orientation of the edges roughly perpendicular to the direction of the base-line joining the photographic stations. The first condition is usually satisfied by the lower edges of arcs and bands, and the vertical edges of isolated rays. The brightness of arcs and bands rises rapidly to a maximum close to the lower edge and then drops slowly toward their upper edge until they are of the same general brightness as the sky. The brightness of rays is nearly uniform throughout their length. The second condition cannot be met by a single base-line for parallactic photography. Arcs and bands are nearly horizontal; rays are nearly vertical. A compromise is usually made, a direction for the base-line being selected that will give parallactic displacements making acute angles of about 45° with the edges of both types of structures. As a result, a small error in locating the edge of aurora on one photograph relative to that on the other can lead to a large error in the parallactic displacement.

[1]*Manuscript received July 25, 1955.*
Contribution from the Physics Department, University of Saskatchewan, Saskatoon, Saskatchewan.

An example will indicate the possible error in a measured height, due to an error Δp in a parallactic displacement p. For an auroral point 140 km. above the earth's surface, and at an altitude of 20° in the most favorable orientation (the vertical plane through the base-line joining the photographic stations), p is about 1.5° for a base-line of 25 km. The relative error in a measured height is approximately $\Delta p/\sin p$ (see page 83 of Ref. 8). The scale of the projected drawings is usually one degree to a centimeter, so that a total error of as little as 0.5 cm. in locating the contours could result in a height error of roughly 45 km. in this case. For the upper limit of arcs and bands the error in p is sometimes so large that computed heights less than the height for the lower limit of the same form are obtained. For the upper limit of rays the error is due largely to the small parallactic angles.

A better approximation to the height of the upper edge of an arc is obtained by measuring the height of a point on the lower edge and the angular distance between this point and a point on the upper edge in the same azimuthal plane, and then by assuming that the two points are on an arc of a circle with radius equal to the distance to the lower point. If the vertical extent of the aurora of the afore-mentioned example were 40 km., the angular distance between bottom and top would be about 6°; and an error of 1 cm. in locating the upper edge on the projected drawing would result in an error of approximately 7 km. in its measured height.

The assumption that elements of an auroral structure lie along arcs of circles in vertical planes is obviously faulty, and would lead to very large errors in the vertical extent of arcs for directions departing much from normal to them. Auroral rays lie along, or nearly along, the lines of the earth's magnetic field, the exciting particles apparently spiralling down the magnetic lines. Presumably, the same excitation mechanism is applicable to homogeneous arcs and bands—suggesting that the vertical extent of these forms should be found by taking the difference between the upper and lower heights for points on a common line of the magnetic field. The fact that rays occasionally appear in such forms and are orientated in the direction of the magnetic field gives added support for this procedure.

PROCEDURE

Since a large number of photographs were available, both single- and double-station, that had been taken at Chesterfield (63.3° N., 90.7° W.), Coppermine (67.8° N., 115.2° W.), and Saskatoon (52.1° N., 106.6° W.), measurements were limited to quiet arcs and bands that crossed the geomagnetic meridian plane for each place. Evaluations for these cases were comparatively easy to make. They required measurement of the altitudes of the upper and lower auroral points in the plane of the geomagnetic meridian, a knowledge of the height of the lower auroral points, and a suitable chart on which the auroral points could be located and from which the vertical extent could be read. Much the same procedures were followed as for determining heights by double-station photographs (1, 5, 8). Outlines of the upper and lower contours of an arc or band were placed on tracing paper by projecting the photograph. The

tracing was placed on the appropriate "net" for azimuth–altitude measurements, and the altitudes of the upper and lower auroral points for the azimuth of the geomagnetic meridian were read from it. If the photograph was one from a set for parallactic measurements, the height of the lower edge was already known or could be determined; if not, a height of 100 km. was assumed. The reasons for selecting 100 km. for statistical studies are substantial, and have been discussed previously (2, 3). (Errors in the vertical extent due to height differences from the 100 km. value will be considered later.) A set of conveniently-spaced lines, representing the magnetic lines in the geomagnetic meridian plane for the place in question, was drawn on the chart generally used for determining the height and the distance to the horizontal projection of an auroral point (see Fig. 37 of Ref. 5). The magnetic lines were located according to the equation $r/\sin^2 \alpha = \text{constant}$, where r is the distance from the center of a magnetic dipole at the earth's center to a point on the magnetic line and α is the angle between the straight line joining the afore-mentioned points and the axis of the dipole. Errors due to the fact that the field cannot be represented exactly by a dipole located at the center of the earth are small in comparison with errors from other sources. The magnetic line on which the structure was located could then be found from the height and the altitude of the lower auroral point. The height of the upper auroral point was found by following this line to the point with the altitude of the upper auroral point. The difference between the two heights gave the vertical extent.

The percentage of auroral time that the luminosity is likely to be restricted to the range of heights given by the vertical extent for arcs and bands was found by counting the number of each form (arc, band, ray, drapery, etc.) as reported for Chesterfield during the Second International Polar-Year, 1932–33, and computing the percentage ratio of arcs and bands to the total number of forms. A similar count and computation was made for the 1932–33 Coppermine data, although these were in less suitable form. Auroral glows were excluded, since they are of low intensity, and little is known about their heights.

A more useful quantity is one indicating a combination of time and angular field covered by particular forms. The 1932–33 Chesterfield records were particularly suitable for estimating this quantity. Each observation included a sketch of the aurora on a zenithal-equidistant projection. A lucite disk of the same size as the projection was divided rather arbitrarily into 21 parts so that each part covered approximately the same angular field. The zenithal one was circular; the others were bounded by arcs of circles and radial lines. The disk was placed on each sketch, and a count made of the number of parts crossed or occupied by each form. This number was used to weight the occurrence. The percentage ratio of the weighted total of arcs and bands to the weighted total of all forms was then computed—again omitting auroral glows.

RESULTS

Figure 1 shows the statistical distribution of vertical extent for 144 quiet arcs and bands (52 Chesterfield, 33 Coppermine, and 59 Saskatoon) assuming a lower height of 100 km. Each point on the graph shows the number of occur-

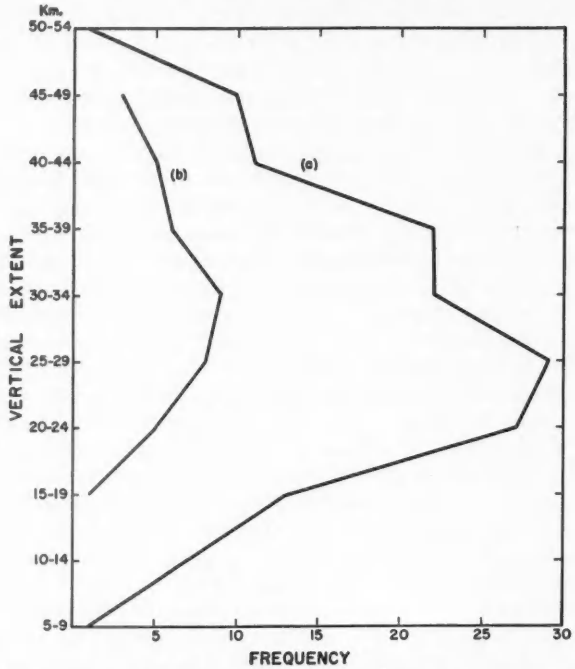

FIG. 1. The frequency distribution of vertical extents of quiet auroral arcs and bands. Curve (*a*) is from 144 single-station photographs assuming a lower height of 100 km.; curve (*b*) is from 37 sets of parallactic photographs with known lower heights.

rences within the indicated range. On the same figure is shown the corresponding distribution for 37 arcs and bands at Chesterfield for which the lower heights had been measured by parallactic methods.

While the number of these is small, the distribution is essentially the same as for the ones with the assumed height of 100 km. The lower heights for these ranged from 82 to 117 km., and the average value was about 102 km. The additional 2 km. in the average height explains in part the larger vertical extent for the maximum of this distribution.

The percentage time ratio of arcs and bands to the total number of forms was 54% at Coppermine, and 76% at Chesterfield. The percentage time ratio of arcs and bands to the total number of forms after weighting according to the angular field covered by each group was 67% at Chesterfield.

DISCUSSION

Several sources of error enter into the major distribution of Fig. 1, none of which are likely to alter the conclusion that the auroral luminosity for quiet forms is confined largely to a 50-km. layer of the atmosphere located mostly above the 100-km. level. These are (*a*) the difficulty in locating the upper edge

of the arcs and bands, (*b*) the possibility that the elements of an arc or band are not directed along the magnetic lines, (*c*) the assumption that the lower height was 100 km., and (*d*) the variation in density of the photographs.

Numerous trials on different photographs indicate that error (*a*) seldom results in a departure of more than one degree in altitude from the average altitude for 10 trials on each photograph. Since altitudes both larger and smaller than the true altitudes are equally probable, all this error could do is to flatten out the distribution—leaving the maximum in the same place.

The horizontal direction of arcs and quiet bands is nearly normal to the geomagnetic meridians (2, 3). Hence, measurements in the geomagnetic meridian plane would not have been altered appreciably by assuming other orientations for the elements, for example, along arcs of circles or vertically above the earth, as long as the angular altitude of the aurora was not large. For this reason, measurements were made mostly on arcs and bands within the altitude range from 15 to 25 degrees.

While the effect of error (*c*) can be evaluated for particular cases, the total effect on the distribution of vertical extents is complex and can only be estimated qualitatively. Assuming that there is no error in the observed altitude of the lower edge, a difference between the true height and the assumed height of 100 km. affects primarily the distance to the selected point on the aurora. The difference between the true distance and the computed distance depends on the altitude of the aurora. The relative error in the distance, $\Delta r/r$, due to a departure ΔH km. from the assumed height of 100 km. is given by

$$\frac{\Delta r}{r} = \frac{\Delta H}{x(x-y)}$$

where

$$x = (6272 \sin^2\theta + 198.5)^{\frac{1}{2}},$$

$$y = 79.20 \sin\theta.$$

θ is the angular altitude of the auroral point. The derivation of the above relationship is lengthy but not difficult. A constant radius of 6371 km. is assumed for the earth. Figure 2 shows the variation in the percentage error in r for altitudes up to 30° corresponding to $\Delta H = 5$, 10, 15, and 20 km. For altitudes greater than 30°, the percentage error in r is practically the same as the percentage error in H. As the altitude decreases the percentage error in r decreases relative to that for H. A diagram showing several vertical extents for different values of r will show readily that the percentage error in the vertical extent is the same as the percentage error in r as long as the altitudes of the auroral points are the same.

About one-third of many thousands of parallactic measurements on all types of aurora by Stormer (6) gave heights between 90 and 120 km. About two-thirds of the parallactic measurements at Chesterfield (1) gave heights between 90 and 130 km. for quiet arcs and bands. All measurements have shown a marked maximum of heights at about 105 km., and relatively few heights below 100 km. It is reasonable to assume that the true heights of the arcs and bands used in this investigation should have a similar distribution;

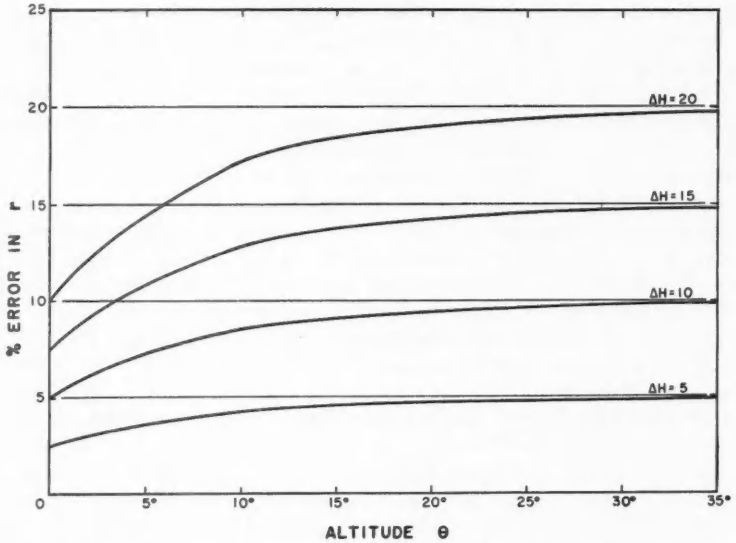

FIG. 2. Plots of the percentage error in the distance to an auroral point against its altitude for departures of 5, 10, 15, and 20 km. from an assumed height of 100 km.

and that the most frequent vertical extent shown by Fig. 1 is not in error by more than 10%. It is likely that larger vertical extents than shown by Fig. 1 occasionally occur, the assumed value of 100 km. biasing the distribution toward lower values.

Since the auroral luminosity at the tops of arcs and most bands gradually merges into the general brightness of the sky, the density of the photographic image may affect the vertical extent, the denser photographs giving greater vertical extents. To test this point, the difference in density between the blackest part of each form and the general fog was measured for each photograph of the Saskatoon group. This was a homogeneous group with respect to photographic emulsion and developer. They were subdivided into four groups according to density and vertical extent, densities below the average for all forms and vertical extents below the maximum in their distribution curve being considered small. The number with small density and small vertical extent was 20; large density and small vertical extent, 9; small density and large vertical extent, 13; and large density and large vertical extent, 17. A chi-squared test of these values gives a probability slightly less than 0.05, suggesting that the larger vertical extents are associated with the denser photographs. An alternative hypothesis that the larger vertical extent occurs with the brighter aurora could not be checked. Neither exposure times nor visual estimates of the brightness of the aurora had been recorded in many cases.

Because of association of the errors (*a*), (*b*), and (*c*) with altitude of the aurora some significant variation of the vertical extent with altitude might be expected. A scatter diagram of vertical extent against altitude failed to show this. Chi-squared tests for various ranges of altitudes were also unsuccessful. Similar tests were made for variations of vertical extent with time of night, season, and latitude. All showed random variations relative to these variables, although a significant variation relative to the last was suggested by an average vertical extent of 27.9 km. for the Chesterfield and Coppermine photographs, and 31.0 km. for the Saskatoon photographs.

Values greater than 50% for the percentage time ratio of arcs and bands to the total number of all forms are supported by similar estimates from data for other places. Fuller (4) in reports on auroral observations for the years 1931–34 at College, Alaska, gives curves showing daily variations in the number of aurorae of each type seen at each half-hour. An average value of about 69% is obtained by measuring the areas below the curves for each type with a planimeter (glows excluded). Values given by Sverdrup (7) for the years 1922–25 for the Arctic Ocean to the north of Siberia vary from 36 to 67% (glows again excluded). Conceivably, values of this quantity may vary according to the phase of sunspot cycle, and to the location relative to the zone of maximum auroral occurrence. While the idea of a percentage time ratio weighted according to the angular field covered by each form is not new, values for it do not appear in auroral literature. This may be due to insufficient observational data for most places.

ACKNOWLEDGMENTS

This investigation was made possible through financial assistance provided by the Radio Physics Laboratory, Defence Research Board of Canada. It also depended on the availability of auroral photographs taken at the Canadian geophysical stations during the Second International Polar-Year, 1932–33, and held in trust by the Physics Department, University of Saskatchewan.

REFERENCES

1. Currie, B. W. Terrestrial Magnetism and Atm. Elec. 39: 293. 1934.
2. Currie, B. W. and Jensen, R. E. J. Geophys. Research, 58: 201. 1953.
3. Currie, B. W. and Jones, C. K. Terrestrial Magnetism and Atm. Elec. 46: 269. 1941.
4. Fuller, V. R. Terrestrial Magnetism and Atm. Elec. 38: 207. 1933; 40: 269. 1935.
5. Harang, L. The aurorae. Chapman & Hall, Ltd., London. 1951.
6. Stormer, C. Terrestrial Magnetism and Atm. Elec. 51: 501. 1946.
7. Sverdrup, H. U. Carnegie Inst. Wash. Publ. No. 175, Vol. VI. 1927.
8. Vegard, L. and Krogness, O. Geofys. Publikasjoner, Vol. 1, No. 1. 1919.

ON THE EFFICIENCY OF AN ACOUSTIC LINE SOURCE WITH PROGRESSIVE PHASE SHIFT[1]

By G. J. Thiessen

ABSTRACT

The introduction of a small continuous phase shift along the length of a finite line source does not result in a decrease of energy radiated but simply causes the directionality pattern to change. When the phase shift is such that it corresponds to the phase shift with distance in a sound wave, then the directionality pattern has changed through 90° and the energy radiated begins to drop rapidly. At this point the slope of the energy vs. phase shift parameter curve increases with increasing frequency.

I. INTRODUCTION

Various special problems involving line sources have been discussed previously in the literature. Olson (4) has considered directional characteristics of line microphones with a time delay introduced between adjacent lines and shows the effect on the directionality pattern. Others have considered the effect of a grounded slab (5) and a conducting half plane (6) on the radiation of a line source. Junger (2) has calculated the impedance ratio for various modes from an infinite cylindrical source in which the dynamic configuration of the cylindrical radiator is periodic in ϕ and z where z is measured along the axis. The subject of this discussion is the effect of a progressive phase shift along an acoustic line radiator of finite length on the directionality pattern and the efficiency. The term efficiency as used here is not the absolute efficiency but that relative to a line source which is in phase throughout its length.

II. DIRECTIONALITY PATTERN

Consider a line source of length l lying on the x-axis with the center at the origin as shown in Fig. 1. Let the source be such that the volume of fluid flow for unit length is given by

$$Q(t) = Q_0 e^{i\omega t}.$$

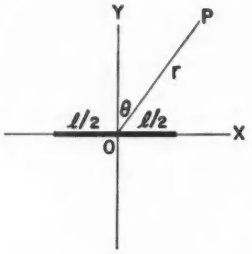

Fig. 1.

[1]*Manuscript received July 21, 1955.*
Contribution from the Division of Applied Physics, National Research Council, Ottawa, Canada. Issued as N.R.C. No. 3752.

Then at large distances r at the point P the pressure due to an element dx of the source located at the origin will be given by (Ref. 3)

$$dp = i\frac{k\rho c}{4\pi r} Q_0 e^{ik(ct-r)} dx$$

where $k = \omega/c = 2\pi/\lambda$, ω is the angular frequency, λ is the wavelength, ρ is the density of the medium, c is the velocity of sound in the medium, and t is the time. If the element is at x, then the path to P is effectively reduced to $r - x\sin\theta$. If in addition there is a phase shift along the source which varies with x so that the equivalent increase in path length is αx, then the pressure at P for an element at x will be

$$dp = i\frac{k\rho c}{4\pi r} Q_0 e^{ik(ct-r+x\sin\theta-\alpha x)} dx.$$

The total pressure p due to the whole line is obtained by a simple integration giving, after dropping the phase factor $\sin k(ct-r)$,

[1] $$p_{\max} = -\frac{\rho c Q_0}{2\pi r}\frac{\sin[kl/2(\sin\theta-\alpha)]}{\sin\theta-\alpha}.$$

The form of this expression is, of course, well known in optics and occurs as the directionality pattern of a long slit. The phase shift term α is less well

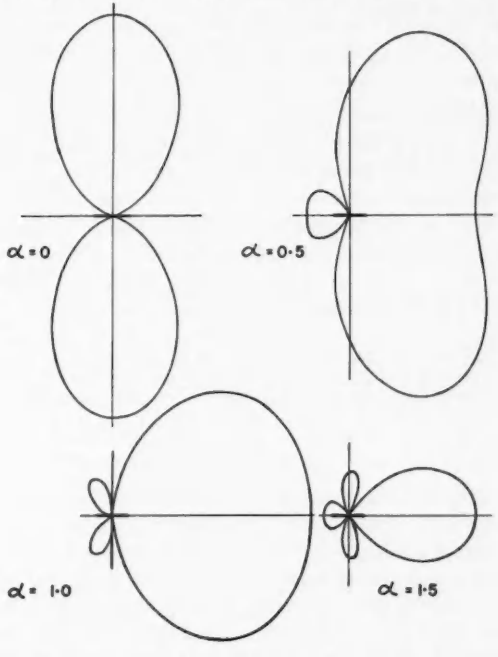

FIG. 2. Directionality pattern for the sound pressure due to a line source as shown with a length $l = \lambda$ and with a progressive phase retardation toward the right which is measured by the parameter α.

known and would occur if the slit were illuminated at an angle and even then the value of α would be limited. It is of interest to see the effect of varying α on the directionality pattern. In Fig. 2 are plotted such patterns for values of α indicated on each curve for the case where $l/\lambda = 1.0$. Although it is the pressure that is plotted here, it is obvious that the power radiated is not decreasing very rapidly until $\alpha = 1$.

III. TOTAL ENERGY RADIATED

For the total energy E radiated we must integrate over all angles the expression

$$p_{\max}^2/2\rho c,$$

which gives

$$E = \frac{\rho c Q_0^2}{4\pi} \int_{-\pi/2}^{+\pi/2} \frac{\sin^2[kl/2(\sin\theta-\alpha)]}{(\sin\theta-\alpha)^2} \cos\theta \, d\theta$$

$$= \frac{kl\rho c Q_0^2}{8\pi} \int_{-\pi R(1+\alpha)}^{\pi R(1-\alpha)} \frac{\sin^2 x}{x^2} \, dx, \tag{2}$$

where $x = kl/2(\sin\theta-\alpha)$ and $R = l/\lambda$. Equation [2] can be changed into (see Reference 1, page 316ff.)

$$E = \frac{kl\rho c Q_0^2}{8} \int_{-\pi R(1+\alpha)}^{\pi R(1-\alpha)} \frac{J_{\frac{1}{2}}^2}{x} \, dx, \tag{3}$$

where it is understood that $J_{\frac{1}{2}}$ is $J_{\frac{1}{2}}(x)$. For limits of zero and infinity this integral has a very simple form (7). However, the indefinite integral is somewhat more complex. The general expression for integrals of this kind (1) contains an indeterminate term for this particular case, but can be evaluated from the derivative of the numerator and denominator leading to the final result

$$E = -\frac{kl\rho c Q_0^2}{16}\left[\frac{8x}{3} J_{\frac{1}{2}} J_{-\frac{1}{2}} + J_{\frac{1}{2}}^2\right]_{-\pi R(1+\alpha)}^{\pi R(1-\alpha)} + \frac{kl\rho c Q_0^2}{16}\left[\frac{4x}{3}\left(J_{-\frac{1}{2}} \sum_{n=1}^{\infty} (-1)^{n+1} \frac{4n+1}{3n} J_{2n+\frac{1}{2}} - J_{\frac{1}{2}} \sum_{n=1}^{\infty} (-1)^{n+1} \frac{4n-1}{n} J_{2n-\frac{1}{2}}\right)\right]_{-\pi R(1+\alpha)}^{\pi R(1-\alpha)}. \tag{4}$$

Although equation [4] is a complete analytical expression for the total power radiated it is not an attractive one to use. However, its behavior as a function of α for the particular cases of $l/\lambda = 5$, 10, and 20 is shown in Fig. 3 where the energy radiated is compared with that for $\alpha = 0$ and is plotted on the ordinate in decibels. The qualitative observation made previously that an appreciable decrease in energy radiated occurs only when α is near unity or greater is now more obvious. Furthermore, the slope of the curve at the point $\alpha = 1$ increases with increasing values of l/λ.

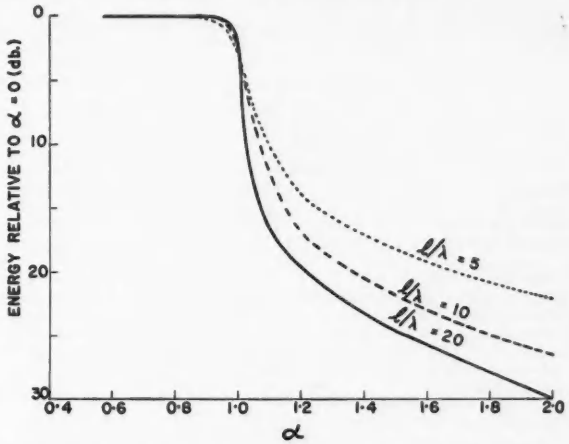

FIG. 3. The variation of the total energy output with α for $l/\lambda = 5$, 10, and 20.

IV. CONCLUSIONS

A continuous phase variation along the length of a line source affects mainly the directionality. Only when the rate of phase variation is comparable to, or greater than, that occurring along the sound wave (i.e. a phase variation of 2π for a distance of λ along the line) will the energy radiated be appreciably decreased. Although the calculations were performed for an acoustical line source, very similar results apply to an electromagnetic radiator such as an antenna.

REFERENCES

1. JAHNKE, E. and EMDE, F. Tables of functions. 4th ed. Dover Publications, New York. 1943. pp. 130, 146.
2. JUNGER, M. C. J. Acoust. Soc. Amer. 25: 40. 1953.
3. MORSE, P. M. Vibration and sound. 2nd ed. McGraw-Hill Book Company, Inc., New York. 1948. p. 313.
4. OLSON, H. F. Proc. Inst. Radio Engrs. 27: 438. 1939.
5. TAI, C. T. J. Appl. Phys. 22: 405. 1951.
6. WAIT, J. R. J. Appl. Phys. 24: 1928. 1953.
7. WATSON, G. N. Theory of Bessel functions. 2nd ed. Cambridge: At the University Press. 1948. p. 396.

LOW ENERGY NEUTRON CROSS SECTION OF MANGANESE[1]

By R. Krotkov[2]

ABSTRACT

The total neutron cross section of Mn^{55} has three (predominantly scattering) resonances in the energy range 300–2500 ev. In the present paper these resonances are examined in detail from the point of view of the R matrix formalism. It is found that quite good (but not perfect) agreement with the experimental cross section curve is obtained by assigning (in order of increasing resonance energy) spins (2, 3, 3) and neutron widths (23, 11, 395 ev.) to the resonances. The addition of a constant increment $\Delta R_{11} = 0.16 \times 10^{-12}$ cm. representing the contribution of distant, positive energy, $J = 3$ resonances to the R matrix element for s-neutron scattering improves agreement with experiment on the high energy side of the highest energy resonance. The (n, γ) cross section at 0.025 ev. is fitted well by a constant radiation width of 0.5 ev. However, with no set of parameters was it possible to fit both the experimental total cross section curve, and the observed coherent scattering cross section at 0 ev., although the sign of the latter was accounted for correctly. The discrepancy is 2.0 barns (calculated) compared to 1.7 barns (observed).

INTRODUCTION

From the point of view of neutron resonance reactions, manganese is a well-known and relatively simple nucleus. There is only one naturally occurring isotope, Mn^{55} (with 25 protons, 30 neutrons), with spin 5/2, and with a total neutron cross section (4, 19, 20, 14) as shown in the experimental curve of any of the figures.[3] The three peaks are at 337, 1080, and 2360 ev.; they are essentially scattering resonances (9, 1, 12), the only other process of importance being the (n, γ) reaction, (as is usual at these energies). Even this reaction is unlikely compared to elastic S wave scattering. The 337 ev. peak has been known for a long time (in 1947 Barbre and Goldhaber (1) estimated its width to be about 10 ev.), while the 1080 peak was found fairly recently (20, 4). The coherent and absorption cross sections at thermal energies are also known.

In 1950, Harris, Hibdon, and Muehlhause (11) examined the then known experimental data to see if they could be fitted by a two-level Breit–Wigner formula (the 1080 ev. level was as yet undiscovered). They were able to obtain good agreement at several points, though they did not try to fit the curve in detail. They concluded that the 337 ev. peak had a neutron width of 21.6 ev., a radiation width of $\backsim$0.6 ev., and a spin $J = 3$, while the corresponding values for the 2360 ev. peak were 304 ev., $\backsim$0 ev., $J = 2$.

A more detailed attempt to fit the experimental curve was carried out by Bollinger, Palmer, and Dahlberg (5), who took all three levels into account and found that best fit was obtained for a spin assignment $J = 2, 3, 3$, neutron widths $\Gamma_n = 22, 14, 336$ ev., and a constant radiation width of about 0.6 ev. However, no choice of level widths was able to give complete quantitative agreement.

The fast choppers at Brookhaven (20) and Argonne (4), together with work at Columbia (19) and Knolls (8), have recently given detailed data on the

[1]*Manuscript received May 31, 1955.*
Contribution from the Palmer Physical Laboratory, Princeton, New Jersey, U.S.A.
[2]*Present address: Palmer Physical Laboratory, Princeton, New Jersey, U.S.A.*
[3]*This curve is taken from the compilation of Reference (17).*

Mn^{55} total cross section; the coherent and incoherent scattering cross sections at thermal energies are known from the early work of Fermi and Marshall (7), Bendt and Ruderman (2), and from the later work of Shull and Wollan (21). The activation cross section at 2200 meters/second has been measured by Pomerance *et al.* (15, 18), Colmer and Littler (6), Grimeland *et al.* (10), and Harris *et al.* (13). In the present paper an effort will be made to fit the experimental data from thermal energy to 4 kev. by the R matrix theory; the work of Harris *et al.* (11) and Bollinger *et al.* (5) has certainly shown that this theory can fit the curve in its essentials. It would be encouraging to verify that the full R matrix formalism can really "explain" the experimental data in detail. The next section will set up the equations to be used in numerical computations.

MATHEMATICAL PRELIMINARIES

As is well known, R matrix calculations apply to two-particle reactions and are carried out as follows (22). The total cross section is essentially specified by resonance energies E_λ and reduced widths $\gamma_{\lambda s}$ (the subscript s labels the channels, i.e. the possible two-particle states). These parameters determine the real, symmetric R matrix (with dimension equal to the number of channels) through the formula

[1] $$R_{st} = \sum_\lambda \frac{\gamma_{\lambda s}\gamma_{\lambda t}}{E_\lambda - E},$$

where E is the energy of the incident neutron (in the center of mass system) and R_{st} is the st matrix element of R.

The next step is to find the scattering matrix U, which is given by

[2] $$U = \omega \frac{1+iBRB-iC}{1-iBRB+iC}\omega$$

in terms of R and the diagonal matrices ω, B, C. The latter are defined in terms of incoming waves I_s in the various channels, all evaluated at the nuclear radius a_s:

[3] $$\omega_s = i\, I_s'/|I_s'|,$$
$$b_s = [\mathrm{Im}(I_s/I_s')]^{-\frac{1}{2}},$$
$$c_s = \frac{\mathrm{Re}(I_s/I_s')}{\mathrm{Im}(I_s/I_s')}.$$

I_s' is the derivative of I_s with respect to the channel radius r_s. ω, B, and C also give the partial widths $\Gamma_{\lambda s}$ in terms of the reduced widths $\gamma_{\lambda s}$:

[4] $$\Gamma_{\lambda s} = \frac{2b_s^2}{1+c_s^2}\gamma_{\lambda s}^2.$$

If R has more than two or three dimensions, U is difficult to calculate because it is hard to find the inverse of $1-iBRB+iC$. However, once U is known, its elements give the experimentally measured cross sections directly:

[5] $$\sigma_{st} = \frac{\pi}{k_s^2}|U_{st}|^2 \quad (s \neq t, \text{ i.e. a true reaction}),$$
$$\sigma_{ss} = \frac{\pi}{k_s^2}|1-U_{ss}|^2 \quad (\text{elastic scattering in channel } s).$$

In [5], k_s is the wave number of the incident neutron.

For us, there will be a channel for elastic neutron scattering (with $l = 0$), and a channel for each mode of γ-decay (i.e. for each excited state of the residual nucleus), but these latter channels will be "weak" (matrix elements of R between these channels are small compared to the diagonal matrix element for the elastic scattering channel). Some modification of the standard scheme is required here, because, strictly speaking, the pair γ-ray plus residual nucleus is not a two-particle system: it is not clear what should be used for the I and I' (or B and C) corresponding to this channel. However, this difficulty can be avoided, and at the same time the inverse of the matrix $1-iBRB+iC$ calculated, by proceeding as follows:

The radiation reduced widths $\gamma_{\lambda s}$ (s now refers to a γ-ray channel) are small compared to the neutron reduced widths $\gamma_{\lambda 1}$, which suggests that we break R up into two parts:

$$R = R_0+\epsilon;$$

[6]
$$R_0 = \left[\begin{array}{c|c} R_{11} & 0 \\ \hline 0 & 0 \end{array}\right], \quad \epsilon = \left[\begin{array}{c|ccc} 0 & R_{12} & R_{13} & \cdots \\ \hline R_{21} & R_{22} & R_{23} & \cdots \\ R_{31} & R_{32} & R_{33} & \cdots \\ \vdots & \vdots & \vdots & \\ \vdots & \vdots & \vdots & \end{array}\right]$$

with ϵ small compared to R_0. We put $s = 1$ for the neutron channel. The matrices ω, B, and C appearing in the expression [2] for U are unknown, except for the elements referring to channel 1. These elements are:

[7]
$$\omega = e^{-ika},$$
$$B = k^{\frac{1}{2}},$$
$$C = 0$$

(a being the radius of the Mn^{56} compound nucleus). The elements b_s, c_s referring to the γ-ray channels we will have to determine somehow later; for the present we write:

[8]
$$B = \begin{bmatrix} k^{\frac{1}{2}} & & & \\ & b_2 & 0 & \\ & & & \\ 0 & & b_3 & \\ & & & \ddots \end{bmatrix}, \quad C = \begin{bmatrix} 0 & & & \\ & c_2 & 0 & \\ & & & \\ 0 & & c_3 & \\ & & & \ddots \end{bmatrix}.$$

U can then be calculated by using a power series expansion for the matrix

$$(1-iBR_0B+iC-iB\epsilon B)^{-1}$$

and keeping only the first order terms (in ϵ).

This expansion is (for two possibly non-commuting matrices A and $i\eta$, η being small compared to A)

$$(A-i\eta)^{-1} = A^{-1}(1+i\eta A^{-1}+i\eta A^{-1}i\eta A^{-1}+i\eta A^{-1}i\eta A^{-1}i\eta A^{-1}+\ldots).$$

In our case we put

$$A = 1-iBR_0B+iC$$

and

$$\eta = B\epsilon B.$$

For this A, $A+\bar{A} = 2$ ($\bar{A}$ = complex conjugate of A), and the matrix of interest, $\omega^{-1}U\omega^{-1}$, becomes

[9] $$\omega^{-1}U\omega^{-1} = \frac{\bar{A}+i\eta}{A-i\eta} = \frac{\bar{A}}{A}+2iA^{-1}\eta A^{-1}+\ldots.$$

A straightforward calculation then gives the following expressions for the elastic scattering and (n, γ) cross section, σ_{sc} and $\sigma_{n\gamma}$ respectively:

[10a] $$\sigma_{sc} = \frac{\pi}{k^2}\left|1-e^{-2ika}\frac{1+ikR_{11}}{1-ikR_{11}}\right|^2,$$

[10b] $$\sigma_{n\gamma} = \sum_s \sigma_{1s} = \frac{4\pi}{k}\frac{1}{1+k^2R_{11}{}^2}\sum_s \frac{b_s{}^2}{1+c_s{}^2}R_{1s}{}^2.$$

s now refers to the γ-ray channels only; the ω_s for the γ-ray channels do not enter into [10] because they are of absolute value 1 (cf. [5]). They would, however, enter into expressions for γ–γ scattering.

From [10a] we see that σ_{sc} is just what we would get if there were no γ-ray channels present, i.e. the weak γ-ray channels introduce only higher order corrections to σ_{sc}. The (n, γ) cross section given by [10b], on the other hand, is not yet in a form suitable for calculation. The right-hand side depends on the as yet unknown quantities b_s, c_s, and on all the $\gamma_{\lambda s}$. To see the dependence in detail, we can expand R_{1s},

[11] $$R_{1s} = \sum_\lambda \frac{\gamma_{\lambda 1}\gamma_{\lambda s}}{E_\lambda - E},$$

interchange summations over s and λ in [10b] and so obtain

[12] $$\sigma_{n\gamma} = \frac{4\pi}{k}\frac{1}{1+k^2R_{11}{}^2}\sum_{\lambda\mu}\left\{\frac{\gamma_{\lambda 1}\gamma_{\mu 1}}{(E_\lambda-E)(E_\mu-E)}\sum_s \frac{b_s{}^2}{1+c_s{}^2}\gamma_{\lambda s}\gamma_{\mu s}\right\}.$$

From this equation we see that the vexatious b_s and c_s enter into $\sigma_{n\gamma}$ only in the form $[b_s{}^2/(1+c_s{}^2)]^{\frac{1}{2}}\gamma_{\lambda s}$ which from [4] is $\pm(\frac{1}{2}\Gamma_{\lambda s})^{\frac{1}{2}}$, the sign being that of $\gamma_{\lambda s}$. Hence we can amalgamate $[b_s{}^2/(1+c_s{}^2)]^{\frac{1}{2}}$ with $\gamma_{\lambda s}$ and consider the $\Gamma_{\lambda s}$ as adjustable parameters with physical significance. However, $\sigma_{n\gamma}$ still depends on *all* the $\Gamma_{\lambda s}$; if the sum on s in [12] were independent of λ and μ (this sum could not then be a *negative* constant, because [12] came from [10b], which is positive) we could treat it as a single-level width parameter and [12] would become quite a manageable expression. However, the sum is *not*, in general, independent of λ and μ. We can set an upper limit on its absolute value by Schwartz' inequality:

[13] $$\left|\sum_s \frac{b_s{}^2}{1+c_s{}^2}\gamma_{\lambda s}\gamma_{\mu s}\right| \leqslant \left(\sum_s \frac{b_s{}^2}{1+c_s{}^2}\gamma_{\lambda s}{}^2\right)^{\frac{1}{2}}\left(\sum_s \frac{b_s{}^2}{1+c_s{}^2}\gamma_{\mu s}{}^2\right)^{\frac{1}{2}} = \left(\frac{\Gamma_\lambda}{2}\right)^{\frac{1}{2}}\left(\frac{\Gamma_\mu}{2}\right)^{\frac{1}{2}}$$

where $\Gamma_\lambda = \sum_s \Gamma_{\lambda s}$ is the radiation width of level λ.

Since there are many γ-ray channels into which the level λ can decay, we expect Γ_λ to be independent of λ, and this is indeed supported by experiment (16). Hence [13] becomes

$$[14] \qquad \left| \sum_s \frac{{b_s}^2}{1+{c_s}^2} \gamma_{\lambda s}\gamma_{\mu s} \right| \leqslant \left(\frac{\Gamma_\lambda}{2}\right)^{\frac{1}{2}}\left(\frac{\Gamma_\mu}{2}\right)^{\frac{1}{2}} = \frac{\Gamma}{2} \sim \frac{0.5}{2} \text{ ev.}$$

These considerations, together with the fact that capture processes are unimportant compared to scattering, suggest that the simplest way to make the right-hand side of [12] manageable is to replace the sum on s by a constant, $\frac{1}{2}\Gamma_\gamma$, and so get

$$[15] \qquad \sigma_{n\gamma} = \frac{4\pi}{k} \frac{1}{1+k^2{R_{11}}^2} \frac{\Gamma_\gamma}{2} \left(\sum_\lambda \frac{\gamma_{\lambda 1}}{E_\lambda - E} \right)^2.$$

This is the expression for $\sigma_{n\gamma}$ that we shall use in the numerical calculations. Γ_γ will be treated as a radiation level width whose exact relation to the $\gamma_{\lambda s}$ of [12] is vague but unimportant.

In passing, we may note that [15] and [10*a*] are just the expressions (to first order approximation) one would get for $\sigma_{n\gamma}$ and σ_{sc} from a two-channel R matrix, if in the two-channel case we were to assume $\gamma_{\lambda 2}$ (2 refers to the γ-ray channel) to be independent of λ, and put

$$\frac{\Gamma_\gamma}{2} = \frac{{b_2}^2}{1+{c_2}^2} {\gamma_{\lambda 2}}^2.$$

There is a difference between the two-channel and multi-channel cases, however. In the two-channel formula [15], $\sigma_{n\gamma}$ certainly goes to zero between resonances, while in the multi-channel case [10*b*] it is very unlikely that $\sigma_{n\gamma}$ would ever become zero—for this could happen only if the R_{1s} were all zero, and it would take a very special set of reduced neutron widths to accomplish this.

The Mn data will, then, be fitted by formulas [10*a*] and [15]. Formula [10*a*] can be simplified by noting that in the energy range 0–4 kev., e^{2ika} is practically $1+2ika$, and with this approximation [10*a*] becomes

$$[16] \qquad \sigma_{sc} = 4\pi \frac{(a-R_{11})^2}{1+k^2{R_{11}}^2}.$$

The actual observed total cross section is the sum of two cross sections, due to two R matrices—one, R^- for $J = 2$, and another, R^+ for $J = 3$. One of the set R^+, R^- will be given by a two-level formula, the other by a single-level formula. As was first shown by Wick (23), the total scattering cross section will be an average of the scattering cross sections due to R^+ and R^-. At thermal energies the factor $1+k^2{R_{11}}^2$ in [16] becomes 1 and we may write

$$[17] \qquad \sigma_{sc}(\text{thermal}) = 4\pi(g_+(a-{R_{11}}^+)^2+g_-(a-{R_{11}}^-)^2)$$

where $g_+ = \frac{7}{12}$, $g_- = \frac{5}{12}$ are statistical weight factors.

The coherent scattering between the two spin states (there is no isotopic incoherent scattering because Mn^{55} has only one isotope) is described by the cross section

$$[18] \qquad \sigma_{coh} = 4\pi(g_+(a-{R_{11}}^+)+g_-(a-{R_{11}}^-))^2.$$

The sign of σ_{coh} is defined to be the sign of $a-g_+R_{11}^+-g_-R_{11}^-$ (positive for hard sphere scattering). From [17] and [18] we find that the incoherent scattering cross section is

[19] $$\sigma_{inc} = \sigma_{sc}-\sigma_{coh} = 4\pi(g_+g_-)(R_{11}^+-R_{11}^-)^2.$$

We now proceed to the numerical calculations. With the seven parameters at our disposal (the three E_λ, the three reduced neutron widths γ_n ($\gamma_{\lambda 1}$ in the preceding formulas), and Γ_γ) we hope to fit the Mn curve from thermal energies to about 4 kev., and the following three data (taken from Ref. (17)):

$$\sigma_{sc}\ (0\text{ ev.}) = 2.0\pm0.1\text{ barns},$$

$$\sigma_{coh}\ (0\text{ ev.}) = 1.7\pm0.1(-)\text{ barns},$$

$$\sigma_{n\gamma}(2200\text{ m./s.}) = 13.4\pm0.3\text{ barns}.$$

SPIN ASSIGNMENT

Of the seven parameters referred to in the last section, three can immediately be found: the level positions E_λ. They are, of course, read off from the observed curve to be 337 ev., 1080 ev., and 2360 ev.

A rough idea of the reduced neutron widths is found by fitting the curve in the neighborhood of each resonance. Thus at 300 ev., only the 337 ev. peak is important, so, taking $a = 0.55\times10^{-12}$ cm. (a reasonable value for Mn),

$$\sigma_{total} = 300\text{ barns} = 4\pi\left(0.55-\frac{\gamma_{337}^2}{337-300}\right)^2$$

or $$(\gamma_{337})^2 = 290\times10^{-12}\text{ ev-cm}.$$

Similarly, $$(\gamma_{2360})^2 = 2000\times10^{-12}\text{ ev-cm}.$$

The data in the neighborhood of the 1080 peak are poor, but a reasonable value for $(\gamma_{1080})^2$ is 100. With these approximate values we determine the spin assignment by reasoning as follows:

(*a*) The 337 ev. and 2360 ev. resonances cannot have the same spin, for if they did, σ_{sc} (0 ev.) would be about

$$\sigma_{sc}(0) = \frac{1}{2}4\pi\left(0.55-\frac{290}{337}-\frac{2000}{2360}\right)^2 = 8.3\text{ barns},$$

where we approximate the spin factor ($\frac{7}{12}$ or $\frac{5}{12}$) by $\frac{1}{2}$, (the effect of the 1080 ev. peak is negligible). This is much larger than the observed value of 2 barns.

(*b*) The 1080 ev. and 337 ev. resonances cannot have the same spin, because if they did, their cross section would go to zero somewhere between them—at about 750 ev., say. At this point the total observed cross section would be due to the 2360 ev. resonance alone, and this is about

$$\frac{1}{2}4\pi\left(0.55-\frac{2000}{1610}\right)^2 = 3\text{ barns},$$

which is much less than the observed minimum of 16 barns.

The spin assignment is hence either 2, 3, 3 or 3, 2, 2.

To decide between (2, 3, 3) and (3, 2, 2) we appeal to the measurements of Bernstein *et al.* (3), who measured the capture cross section $\sigma_{n\gamma}$ of polarized

neutrons on polarized Mn^{55}, and found that the antiparallel orientation ($J = 2$) had a little larger cross section than the parallel ($J = 3$). Now, at 2200 m./s. $\sigma_{n\gamma}$ due to the 337 ev. resonance is about

$$\frac{1}{2}\frac{4\pi}{3.49\times10^{-4}}\frac{0.5}{2}\frac{290}{(337)^2} = 11 \text{ barns},$$

while $\sigma_{n\gamma}$ due to the other two is about

$$\frac{1}{2}\frac{4\pi}{3.49\times10^{-4}}\frac{0.5}{2}\left(\frac{100}{1080}+\frac{2000}{2360}\right)^2 = 3.5 \text{ barns}.$$

We see that the 337 ev. peak predominates and so the spin assignment must be $J = 2, 3, 3$. This agrees with Bollinger *et al.* (5), but disagrees with Harris *et al.* (11). The spin assignment determines the peak heights of the various levels, the height of the $J = 2$ peak, for instance, being $g_-(4\pi/k^2)$ (k being the neutron wave number at resonance). The calculated peak heights are 3210, 1410, 650 barns, the observed ones 2000, 240, 520 barns. This is reasonable agreement. (The second peak is so sharp that its full height is almost certainly not observed.)

A FIRST ATTEMPT AT FITTING THE CURVE

The spin assignment is now known ($J = 2, 3, 3$); the neutron reduced widths are about $\gamma_n^2 = (290, 100, 2000)\times10^{-12}$ ev-cm. and Γ_γ is about 0.5 ev. (from a fit to $\sigma_{n\gamma} = 13.4$ at 0.025 ev.). Taking the nuclear radius a to be about 0.55×10^{-12} cm., we can say the following about the curve:

The (n, γ) cross section can be neglected everywhere except at low energies (less than about 10 ev.).

The 0 ev. scattering cross section is determined chiefly by the 337 ev. and 2360 ev. peaks, and to a lesser extent by the 1080 ev. peak. $\sigma_{sc}(0)$ is quite sensitive to the exact values of $(\gamma_{337})^2$ and $(\gamma_{2360})^2$ and, to a lesser extent, of a and $(\gamma_{1080})^2$. The assignment $\gamma_n^2 = 290, 100, 2000$ gives too small a σ_{sc} at 0:

$$4\pi\frac{5}{12}\left(0.55-\frac{290}{337}\right)^2+4\pi\frac{7}{12}\left(0.55-\frac{100}{1080}-\frac{2000}{2360}\right)^2 = 1.6 \text{ barns},$$

while the observed value is 2 barns. In addition, σ_{inc} is too small:

$$\sigma_{inc} = 4\pi\frac{35}{144}\left(\frac{290}{337}-\frac{100}{1080}-\frac{2000}{2360}\right)^2 = 0.02 \text{ barns},$$

while it should be 0.3 barns. However, the sign of the coherent scattering is right:

$$0.55-\frac{5}{12}\frac{290}{337}-\frac{7}{12}\left(\frac{100}{1080}+\frac{2000}{2360}\right) < 0.$$

As we move toward higher energies along the curve, but stay below the 337 ev. peak, the 337 ev. and 2360 ev. peaks remain the most important ones in determining σ_{sc} (and hence σ_{total} because $\sigma_{n\gamma}$ is small). As at 0 ev., the choice $\gamma_n^2 = (290, 100, 2360)\times10^{-12}$ ev-cm. gives too low a total cross section. At 100 ev. we calculate 3.8 barns against the observed 4.7 barns.

Moving again to higher energies, in the immediate neighborhood of the 337 ev. peak our present choice of reduced widths, of course, gives rough agreement. Between the first and second peaks the $J = 2$ and $J = 3$ cross sections are about the same, and for the first time the 1080 ev. peak has become important. At 750 ev. we calculate σ_{total} to be 15.6 barns, while the observed value is 16.0, so our choice of reduced widths gives about the right cross section here.

The 1080 ev. peak is so sharp that the data in its neighborhood are not good; we shall not try to fit them any too well. Since the second and third peaks have the same J, 3, their cross section must be zero somewhere between them, and at this minimum the total cross section is the cross section due to the first peak only. For $(\gamma_{337})^2 = 290$, σ_{total} is about 4.2 barns at this minimum while the observed value is 7.5 barns.

Passing on to the last peak, where, of course, the last level is dominant, $(\gamma_{2360})^2 = 2000$ gives rough agreement with the experimental data, except on the high energy side (>3000 ev.). Here the calculated cross section is too high: at 4000 ev. we calculate 25 barns and observe 16.5. In this energy region the 337 ev. peak contributes a roughly constant cross section of about 2 barns, while the 1080 ev. peak is quite negligible.

ATTEMPTS TO IMPROVE AGREEMENT

To obtain agreement at 0 ev., we must increase either $(\gamma_{337})^2$, $(\gamma_{2360})^2$ (possibly $(\gamma_{1080})^2$), or both, and also increase the difference $R_{11}^{+} - R_{11}^{-}$ at 0 ev. The condition $\sigma_{sc}(0) = 2.0$, and $\sigma_{\text{coh}}(0) = 1.7(-)$ leads by straightforward algebra to the relation

$$\begin{pmatrix} a - R_{11}^{+}(0) \\ a - R_{11}^{-}(0) \end{pmatrix} = \begin{pmatrix} -.242 \\ -.549 \end{pmatrix} \quad \text{or} \quad \begin{pmatrix} -.498 \\ -.191 \end{pmatrix} \times 10^{-12} \text{ cm.}$$

Taking $a = 0.55 \times 10^{-12}$ cm., this means $(\gamma_{337})^2$ must be either 250 or 370. Both of these possibilities give a poor fit to the first peak, as Figs. 1 and 2 show. In these curves, $(\gamma_{1080})^2$ and $(\gamma_{2360})^2$ were determined by insisting that the minimum between the second and third peaks falls at the experimental minimum, 1250 ev. Although when the curves were drawn this seemed justified, further reflection indicated that this was a mistake, because the experimental data around the minimum are not sufficiently reliable to warrant placing this much emphasis on them. Γ_γ was determined by fitting $\sigma_{n\gamma} = 13.4$ at 2200 m./s.

It seems clear that in Fig. 1, $(\gamma_{337})^2$ is too small, $(\gamma_{1080})^2$ too large, and $(\gamma_{2360})^2$ about right, except for the 4000 ev. point. In Fig. 2, $(\gamma_{337})^2$ is too large, $(\gamma_{1080})^2$ possibly a bit big, and $(\gamma_{2360})^2$ definitely small.

In Fig. 1, the nuclear radius was taken to be $a = 0.53$, which does not make much difference to the curve above 200 ev., but improves the low energy fit. We could try to improve Fig. 1 by decreasing $(\gamma_{1080})^2$ to 170, which would give a fit at 750 ev., but also decrease $\sigma_{sc}(0)$ to 1.5, which is too much of a drop, and at the same time leave the fit around 200 ev. poor.

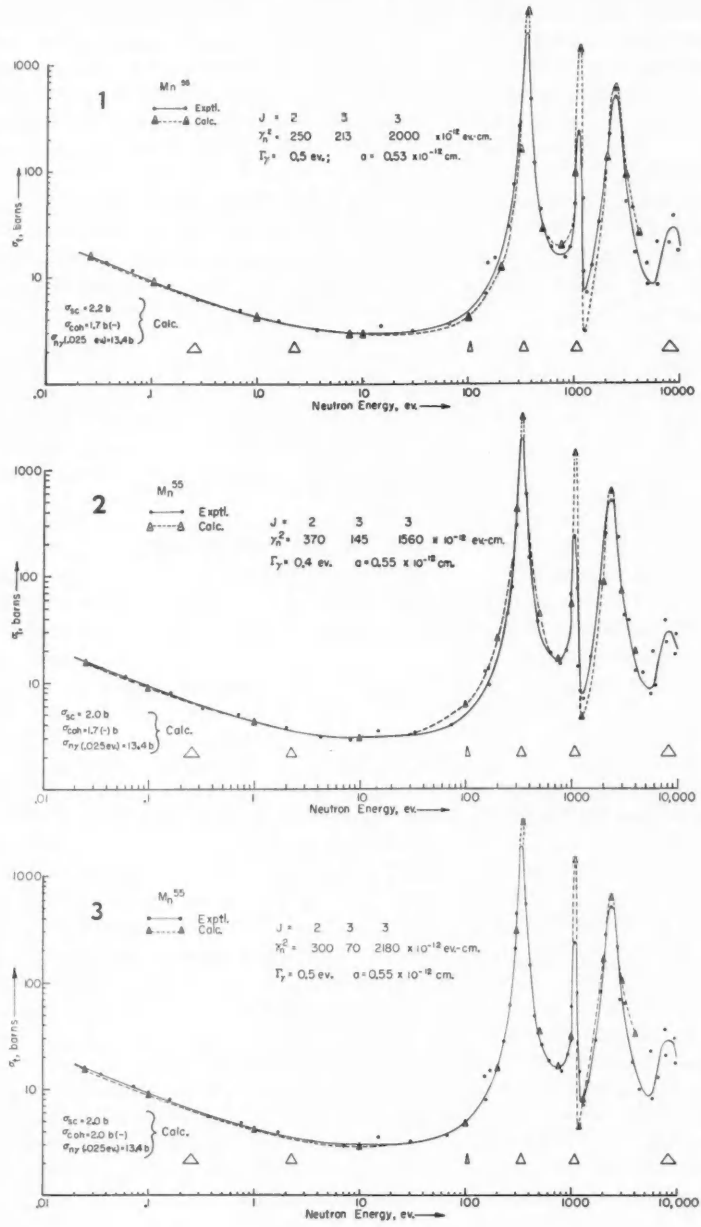
1
Mn 55
Exptl.
Calc.
J = 2 3 3
γn² = 250 213 2000 x10⁻¹² ev-cm.
Γγ = 0.5 ev.; a = 0.53 x10⁻¹² cm.
σsc = 2.2 b
σcoh = 1.7 b(-)
σnγ (.025 ev) = 13.4 b
Calc.
σt, barns
Neutron Energy, ev.
2
Mn 55
Exptl.
Calc.
J = 2 3 3
γn² = 370 145 1560 x 10⁻¹² ev-cm.
Γγ = 0.4 ev. a = 0.55 x 10⁻¹² cm.
σsc = 2.0 b
σcoh = 1.7(-) b
σnγ (.025 ev) = 13.4 b
Calc.
σt, barns
Neutron Energy, ev.
3
Mn 55
Exptl.
Calc.
J = 2 3 3
γn² = 300 70 2180 x 10⁻¹² ev-cm.
Γγ = 0.5 ev. a = 0.55 x 10⁻¹² cm.
σsc = 2.0 b
σcoh = 2.0 b(-)
σnγ (.025 ev) = 13.4 b
Calc.
σt, barns
Neutron Energy, ev.

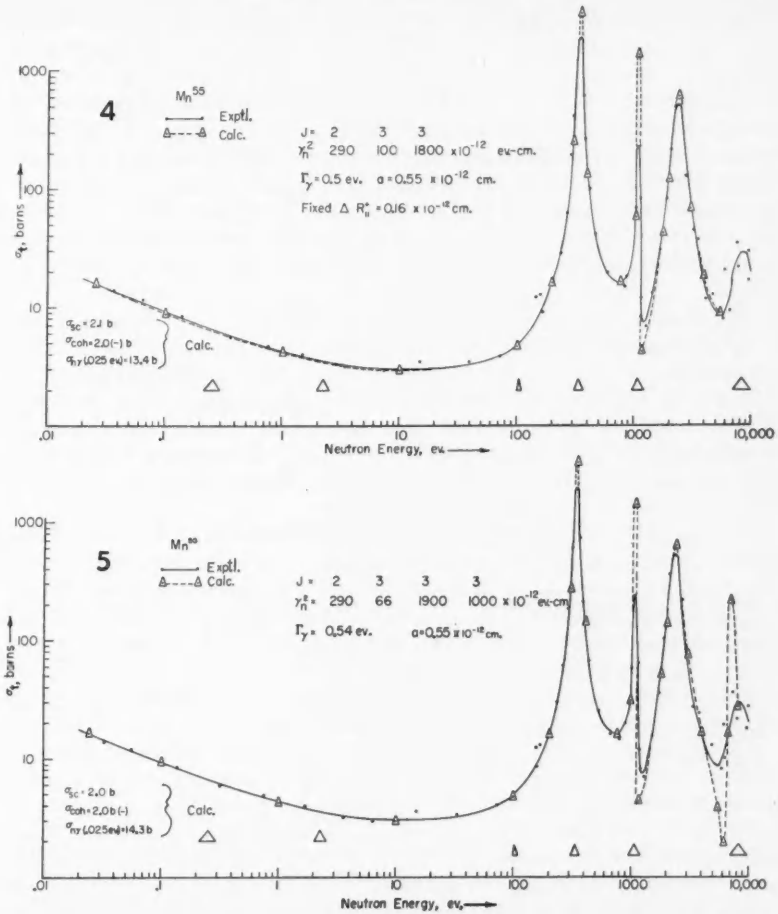

FIGS. 1 to 5. Comparison of the observed and calculated total neutron cross sections σ_t of Mn^{55} as a function of neutron energy. Not all of the experimental points are shown; those appearing are intended only to give a general idea of how much they scatter. The triangles at the bottom give the experimental resolution. Using the parameters indicated, with a being the nuclear radius, the calculated cross sections at 0.025 ev. (neutron velocity 2200 m./s.) are as shown in the bottom left-hand corner. These are to be compared with the experimental values $\sigma_{sc} = 2.0$ barns, $\sigma_{coh} = 1.7$ barns $(-)$, $\sigma_{n\gamma}$ (0.025 ev.) = 13.4 barns.

In the next attempt we abandon our insistence that σ_{coh} be $1.7(-)$, and pick $(\gamma_{337})^2 = 300$, about right to fit the 337 ev. peak alone, but increase $(\gamma_{2360})^2$ to 2180 to get $\sigma_{sc}(0) = 2.0$ and then decrease $(\gamma_{1080})^2$ to get a fit at 750 ev. Γ_γ is determined as usual by fitting $\sigma_{n\gamma} = 13.4$ barns at 2200 m./s. and a is taken to be 0.55×10^{-12} cm. The results (Fig. 3) are not bad, but $\sigma_{coh} = 2.0(-)$ is too high now (though the sign is right) and $(\gamma_{2360})^2 = 2180$ seems large. The 4000 ev. point is now definitely too high.

The large reduced width of the 2360 ev. peak compared to the reduced widths of the first two resonances might lead one to suspect that the last peak is really two or more resonances which have not yet been resolved. However, till more experimental data are available on this point we can use the makeshift of adding a fixed ΔR_{11}^{+}, representing high energy $J = 3$ resonances, to pull down the upper wing of the 2360 ev. peak. This will also raise the points of the low energy side, but not much. Since it is a fixed ΔR_{11}^{+}, we must decrease $(\gamma_{337})^2$ and $(\gamma_{2360})^2$ to get $\sigma_{sc}(0) = 2.0$, then adjust $(\gamma_{1080})^2$ to get agreement at 750 ev. The results are shown in Fig. 4, where we see that the over-all agreement is rather satisfactory, except that σ_{coh} is again too large (2.0(−) instead of 1.7(−)).

The value of $\Delta R_{11}^{+} = 0.16 \times 10^{-12}$ cm. may well not be significant of itself. From the formulas [17] and [18] we see that σ_{sc} and σ_{coh} depend only on the combination $(a - R_{11})$, so that adding a constant ΔR_{11} to R_{11} is equivalent to changing the radius a. Only the difference $(a - \Delta R_{11})$ matters. From this point of view it is sensible to talk about two different equivalent radii a^{+} and a^{-}, corresponding to different fixed ΔR_{11}^{+} and ΔR_{11}^{-}. However, in this work it was not found necessary to use a fixed contribution from distant $J = 2$ resonances.

As a variant on Fig. 4, we try adding a $J = 3$ resonance somewhere above 2360 ev.; this would pull down the 4000 ev. point and have much less effect at 0 ev. than a constant ΔR_{11}^{+} does. There may be a resonance around 7000 ev. with $(\gamma_{7000})^2 = 1000$. We raise $(\gamma_{2360})^2$ to 1900 to make $\sigma_{sc}(0) = 2$ barns, and decrease $(\gamma_{1080})^2$ to 66 to get a fit at 750 ev. We put $a = 0.55$ as usual, but for reasons to be explained later, Γ_γ is raised to make $\sigma_{n\gamma} = 14.3$ at 2200 m./s. instead of 13.4. The result is Fig. 5, where the over-all agreement is seen to be excellent, except above 4000 ev. and for σ_{coh}, which is 2.0(−) instead of 1.7(−).

The reason that in Fig. 5, $\sigma_{n\gamma}$ was taken to be 14.3 at 2200 m./s. instead of 13.4 can be seen from Fig. 6. This is a plot of the experimental low energy cross section against $E^{-\frac{1}{2}}$, where E runs between 1 and 0.02 ev. According to equation [15], this should be a straight line with y-intercept $\sigma_{sc}(0)$ and slope proportional to Γ_γ. However, only the lower part of this is a straight line; the upper part drops away. The straight line part has an intercept of 2.0 barns as it should, but is 0.9 barns above the experimental curve at 2200 m./s. Adjusting Γ_γ to make $\sigma_{n\gamma} = 13.4 + 0.9 = 14.3$ barns at 2200 m./s. (instead of 13.4) hence gives a better fit in the energy region where the experimental curve of Fig. 6 is yet straight.

The reason for the bow in the graph is not clear. A negative energy resonance (either $J = 2$ or $J = 3$) could cause such a fall off by decreasing R_{11} and so decreasing σ_{sc}. However, the decrease would have to be of the order of 1 to 2 barns, and since the total scattering cross section is only 2 barns, this seems improbable. The bow may be due to a crystal effect. In this case the curve should straighten out again as in the curves of Bendt and Ruderman (2).

In considering negative energy resonances one must keep in mind that these decrease $(g_{+}R_{11}^{+} + g_{-}R_{11}^{-})$, and if strong enough could make $(a - g_{+}R_{11}^{+} - g_{-}R_{11}^{-})$ positive at thermal energies, thus destroying agreement with the

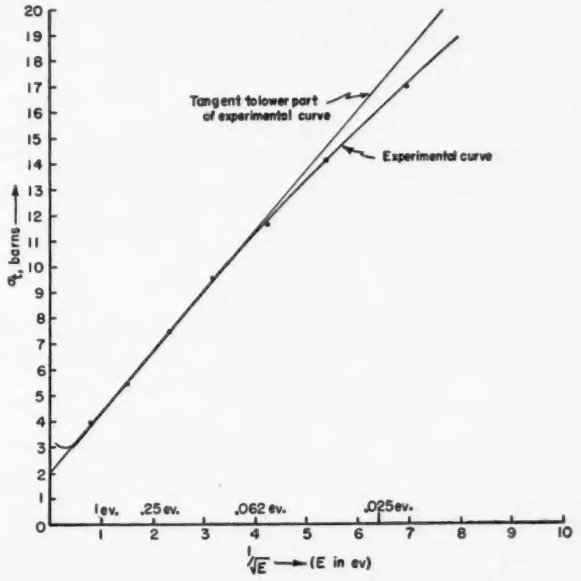

FIG. 6. Low-energy total neutron cross section σ_t of Mn^{55} as a function of $E^{-\frac{1}{2}}$ (i.e. of $1/k$, essentially). As in the other figures, the experimental points shown are intended only to indicate how much these scatter. According to theory (equations [15] and [16] of the text) the curve should be straight; actually only the lower part of it is.

negative sign of σ_{coh}. For instance, using the parameters of Fig. 4, $(a-g_+R_{11}^+-g_-R_{11}^-)$ is -0.4×10^{-12} cm. at thermal energy, so any contemplated negative energy resonance should not change $g_+R_{11}^++g_-R_{11}^-$ by more than 0.4×10^{-12} cm.

CONCLUSION

With no set of parameters were we able both to fit the cross section curve entirely and to account for the value of σ_{coh} accurately. However, rather close agreement was obtained with the parameters of Table I. Upon adding a fixed

TABLE I

RESONANCE PARAMETERS

E_λ, ev.	J	γ_n^2, ev-cm.	Γ_n, ev.
337	2	290×10^{-12}	23
1080	3	75×10^{-12}	11
2360	3	1850×10^{-12}	395

$\Gamma_\gamma = 0.5$ ev., $a = 0.55\times10^{-12}$ cm.

$\Delta R_{11}^+ = 0.16\times10^{-12}$ cm. to represent the contribution of distant, positive energy, $J = 3$ resonances, the experimental curve for the total cross section

and the scattering and absorption cross section at 0 ev. were fitted well. However, the value of the coherent scattering cross section at 0 ev. was not in agreement with experiment (calculated 2.0(−), observed 1.7(−) barns). In the thermal energy region, a not as yet understood effect causes the total cross section curve to deviate from the straight line one would expect. This may well be some crystal effect, in which case we may be misinterpreting the measured coherent cross section of 1.7 barns.

Hence, the R matrix theory can fit the present experimental data quite well, but not perfectly. More comprehensive data on Mn^{55} are required before it can be stated definitely whether the discrepancies are real or not.

ACKNOWLEDGMENT

The author would like to express his gratitude to Professor E. P. Wigner for suggesting this problem and for his continued advice and encouragement during its solution.

REFERENCES

1. Barbre, N. H. and Goldhaber, M. Phys. Rev. 71: 141(A). 1947.
2. Bendt, P. J. and Ruderman, I. W. Phys. Rev. 77: 575. 1950.
3. Bernstein, S., Roberts, L. D., Stanford, C. P., Dobbs, J. W. T., and Stephenson, T. E. Phys. Rev. 94: 1243. 1954.
4. Bollinger, L. M. and Palmer, R. R. ANL-5031. Argonne Natl. Lab., Lemont, Illinois. 1953.
5. Bollinger, L. M., Palmer, R. R., and Dahlberg, D. A. Phys. Rev. 95: 645(A). 1954.
6. Colmer, F. C. W. and Littler, D. J. Proc. Phys. Soc. (London), A, 63: 1175. 1950.
7. Fermi, E. and Marshall, L. Phys. Rev. 71: 666. 1947.
8. Gaerttner, E. R., Yester, M. L., and Albert, R. D. KAPL-1084. Knolls Atomic Power Lab., Schenectady, New York. 1954.
9. Goldhaber, M. and Yalow, A. A. Phys. Rev. 69: 47(A). 1946.
10. Grimeland, B., Hellstrand, E., and Netter, F. Compt. rend. 232: 2089. 1951.
11. Harris, S. P., Hibdon, C. T., and Muehlhause, C. O. Phys. Rev. 80: 1014. 1950.
12. Harris, S. P., Muehlhause, C. O., and Thomas, G. E. Phys. Rev. 79: 11. 1950.
13. Harris, S. P., Rasmussen, S., Schroeder, H., and Thomas, G. ANL-4277. Argonne Natl. Lab., Lemont, Illinois. 1949.
14. Hibdon, C. T., Langsdorf, A., Jr., and Holland, R. E. Phys. Rev. 85: 595. 1952.
15. Hoover, J. I., Jordan, W. H., Moak, C. D., Pardue, L., Pomerance, H., Strong, J. D., and Wollan, E. O. Phys. Rev. 74: 864. 1948.
16. Levin, J. S. and Hughes, D. J. Bull. Am. Phys. Soc. 30: 22. 1955.
17. Neutron cross sections. Atomic Energy Comm. Rept. AECU-2040, with Suppls. 1, 2, 3. Tech. Inform. Div., Dept. of Commerce, Washington, D. C. 1952.
18. Pomerance, H. ORNL-577 and 366. Oak Ridge Natl. Lab., Oak Ridge, Tennessee. 1949.
19. Rainwater, L. J., Havens, W. W., Jr., Wu, C. S., and Dunning, J. R. Phys. Rev. 71: 65. 1947.
20. Seidl, F. G. P., Hughes, D. J., Palevsky, H., Levin, J. S., Kato, W. Y., and Sjostrand, N. G. Phys. Rev. 95: 476. 1954.
21. Shull, C. G. and Wollan, E. O. Phys. Rev. 81: 527. 1951.
22. Teichmann, T. Phys. Rev. 77: 506. 1950.
23. Wick, G. C. Physik. Z. 38: 689. 1937.

THE ν_3 INFRARED BAND OF AMMONIA[1]

By C. Cumming[2]

ABSTRACT

An absorption band in gaseous ammonia at 3 μ is observed at high resolution and attributed to the doubly degenerate fundamental ν_3. The constants $\nu_0 = 3442.9$, $A_0 = A_1 = 6.13$, $A_1\zeta = 0.29$, and $B_1 = 9.75$ cm.$^{-1}$ describe the band. Many of the observed lines are doublets. This doubling is a result of the inversion of the ammonia molecule and the value 1.1 cm.$^{-1}$ is calculated for the inversion doubling of the 0010 state.

INTRODUCTION

The fundamental band of the doubly degenerate ν_3 vibration of gaseous ammonia has been observed in infrared absorption by Barker (1) and recently by Wood, Bell, and Nielsen (12). Neither investigation has led to an analysis of the band. A study of the Raman band has been reported (4) in which an analysis was carried out and the frequency of the band origin, 3444 cm.$^{-1}$, was determined. Because of the comparatively low resolution of the Raman spectrum, due largely to pressure broadening, many of the measured lines were blends; accordingly the results of that analysis are less sure. It therefore seemed desirable to attempt an analysis of the infrared band.

EXPERIMENTAL

The band was observed in absorption using a Pfund-type spectrometer with an Anderson 600 lines/mm. grating and a lead sulphide detector. The practical resolution of the spectrometer at 3 μ was about 0.3 cm.$^{-1}$ when the source of radiation was a Nernst glower. Because of pressure broadening in ammonia, pressures of less than 6 cm. Hg had to be used to take full advantage of the resolution of the spectrometer.

Frequencies corrected to vacuum were found for the ammonia lines by comparison with known frequencies falling at the same grating angle. Certain lines in the 1.4 μ band of water measured by Plyler, Gailar, and Wiggins (8) were used in the 3380–3500 cm.$^{-1}$ region, and the ν_3 band of hydrogen cyanide provided standards between 3300 and 3400 cm.$^{-1}$. The rotational constants B', B'', D', and D'' for the latter band can be calculated very precisely from the results of Rank, Shearer, and Wiggins for $2\nu_3$ (9), and the ν_3 band origin 3311.4_7 was fixed by comparison with Hg 10139.67 and Hg 15295.82. The accuracy of the ammonia frequencies is probably about 0.2 cm.$^{-1}$ and is limited by the interpolations between standards and by a slight nonuniformity in the rotation of the grating.

Unfortunately atmospheric absorptions in the spectrometer obscured the spectrum almost entirely above 3500 cm.$^{-1}$; almost half of the ammonia ν_3 band could therefore not be measured. A number of weak lines below 3300

[1]*Manuscript received August 19, 1955.*
Contribution from the Department of Colloid Science, University of Cambridge, Cambridge, England.
[2]*Present address: Department of Physics, University of British Columbia, Vancouver, British Columbia.*

cm.$^{-1}$ not attributable to ν_3 were observed. It is presumed that these lines belong to the $2\nu_4$ band, but an analysis of these lines was not attempted.

RESULTS AND DISCUSSION

The frequencies of the measured lines are given in Table I. It will be noted that many of the lines are close doublets. This doubling is undoubtedly a

TABLE I

OBSERVED FREQUENCIES IN THE ν_3 INFRARED BAND OF AMMONIA

Frequency (cm.$^{-1}$)	Identification ($J'K'$–$J''K''$)	Frequency (cm.$^{-1}$)	Identification ($J'K'$–$J''K''$)
3493.9$_5$	4,4–3,3	3379.6	4,4–5,5
3493.6		79.2	
78.2	2,1–1,0	73.5$_5$	3,1–4,2
70.8	2,2–1,1	70.0$_5$	4,3–5,4
70.5		69.7	
60.3		67.3	5,5–6,6
58.8		66.9$_5$	
46.0$_5$ w*		60.0$_5$	4,2–5,3
45.0$_5$ w		57.6	5,4–6,5
39.5	1,1–1,0	55.4	6,6–7,7
38.2$_5$	2,1–2,0	54.8$_5$	
37.5$_5$	3,1–3,0	53.5	
35.7$_5$	4,1–4,0	52.7	4,1–5,2
30.0	3,2–3,1	49.5$_5$	
28.8 w		48.5	5,3–6,4
27.0$_5$ w		47.3	
20.0 w	4,3–4,2	45.6	6,5–7,6
19.7 w		45.2	
18.7$_5$ w	5,3–5,2	44.4$_5$	
11.0$_5$	4,4–4,3	43.7	7,7–8,8
07.4 w		43.0$_5$	
07.0 w		39.8$_5$	5,2–6,3
06.4$_5$ w		39.5	
04.6		29.2$_5$	
03.5	2,2–3,3	26.8	
03.1		23.5$_5$	7,5–8,6
00.9		23.2	
3399.2$_5$		22.2$_5$	
94.7$_5$	2,1–3,2	19.2$_5$	
91.7	3,3–4,4	14.0$_5$	
91.3$_5$		13.7	
86.8	2,0–3,1	05.2	
86.4		04.8	
82.8$_5$	3,2–4,3		
82.5$_5$			

*w *indicates a weak absorption.*

splitting due to inversion and will be discussed later. Since an insufficient number of the doublets have been resolved to justify analyses of the separate subbands, the unresolved lines and mean frequencies of doublets are used to calculate molecular constants which would describe the vibrational states in the absence of inversion doubling.

The rotational levels for a symmetric top in an excited state of a degenerate vibration are, according to Teller (11),

$$F_{[v]}(J, K) = B_{[v]}J(J+1)+(A_{[v]}-B_{[v]})K^2 \mp 2A_{[v]}\zeta K,$$

where ζ is the vibrational angular momentum and the other symbols have their

usual significance. The ν_3 band of ammonia corresponds to transitions to such a set of levels from the ground state rotational levels

$$F_0(J, K) = B_0J(J+1)+(A_0-B_0)K^2$$

in accordance with the selection rules $\Delta K = \pm 1$, $\Delta J = 0, \pm 1$. Although there is the further restriction that only the $+l$ levels combine with the ground state for $\Delta K = +1$, only the $-l$ levels for $\Delta K = -1$, the band nevertheless has a fairly complex structure. To facilitate the identification of the observed spectrum, the intensities of the allowed transitions were calculated using the Hönl–London formulae (7) and the known populations of the ground state rotational levels. When the frequencies of the most probable transitions in the infrared band were calculated using the constants* from the Raman band (4), most of the lines in the observed spectrum were readily identified.

The constants ν_0, A_1, A_0, B_1, and $A_1\zeta$ were recalculated making use of the new data. Regrettably the data are not extensive enough to allow a determination of the centrifugal stretching terms $-D_JJ^2(J+1)^2-D_{JK}K^2J(J+1)-D_KK^4$ which would be expected to have an appreciable effect on the spectrum of such a light molecule. In carrying out the analysis, therefore, corrections were applied to the measured frequencies to eliminate centrifugal stretching using the constants calculated by Slawsky and Dennison (10) as modified by Hansler and Oetjen (6). These are $D_J = 8.1\times10^{-4}$, $D_{JK} = -15.5\times10^{-4}$, $D_K = 6.3\times10^{-4}$ cm.$^{-1}$.

Most of the strong lines fall into three series which can be designated ${}^PP(J, K = J)$, ${}^PP(J, K = J-1)$, and ${}^PP(J, K = J-2)$. The frequencies of these lines can be represented by the equations

$${}^PP(J, K = J) = [\nu_0+A_1-2A_1\zeta-B_1]-K[2A_1-2A_1\zeta+B_0-B_1]+K^2[A_1-A_0],$$

$${}^PP(J, K = J-1) = [\nu_0+A_1-2A_1\zeta-B_1-2B_0]-K[2A_1-2A_1\zeta+3B_0-3B_1] +K^2[A_1-A_0],$$

$${}^PP(J, K = J-2) = [\nu_0+A_1-2A_1\zeta+B_1-6B_0]-K[2A_1-2A_1\zeta+5B_0-5B_1] +K^2[A_1-A_0].$$

Since the graphs of these frequencies plotted against K form straight lines, one concludes that A_0-A_1 is small. If $A_0 = A_1$ is assumed, then the intercepts and slopes of these graphs can be used to calculate certain molecular constants. The differences in the slopes give directly $B_0-B_1 = 0.19$, and since $B_0 = 9.94$ is well known (4), $B_1 = 9.75$. The intercepts and slopes allow one to calculate only the combinations $\nu_0-A_1\zeta$ and $A_1 - A_1\zeta$; in order to determine the constants ν_0, A_1, and ζ independently, recourse was had to the frequency interval between the lines of the ${}^SS(J, K = J)$ series of the Raman band (3), which gave

$$4A_1+2A_1\zeta+B_1-B_0 = 24.91.$$

The constants $\nu_0 = 3442.9$, $A_1 = 6.13 = A_0$, and $\zeta = 0.047$ cm.$^{-1}$ were thus found. The spectrum calculated on the basis of these constants is shown below the observed spectrum in Fig. 1.

*$\nu_0 = 3444$, $B_1 = 9.78$, $A_0 = A_1 = 6.24$, $A_1\zeta = 0.28$ cm.$^{-1}$.

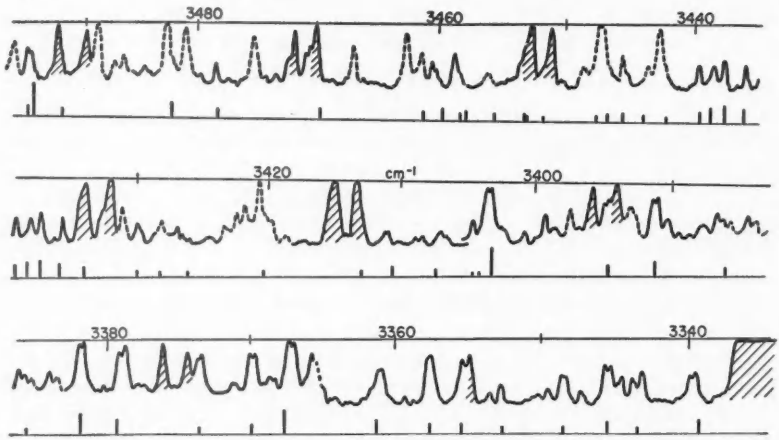

FIG. 1. Tracing of the ν_3 infrared band of ammonia. Superposed are the Q and R branches of ν_1 (shaded area) and atmospheric absorptions (dotted line). The strongest lines in the ν_3 band are plotted under the tracing, with frequencies calculated from the results of the analysis.

The new values of the molecular constants are in substantial agreement with those determined solely from the Raman spectrum; this investigation thus confirms the interpretation of the Raman spectrum. In fact the differences between the new and earlier values can be attributed mainly to the new values for D_J and D_{JK} found by Hansler and Oetjen. The analysis can be criticized for its assumption of $A_0 - A_1 = 0$, since this constant could be as large as ± 0.05 without manifesting a significant curvature in the plots. Evidently an accurate value for A_0 and the moment of inertia of ammonia about the symmetry axis must await more extensive data.

In rotation–vibration transitions from the ground state of ammonia the symmetry selection rule for dipole transitions $- \leftrightarrow +$, and $+ \not\leftrightarrow +$, $- \not\leftrightarrow -$ means that for parallel infrared bands with $\Delta K = 0$ such as ν_1 a doubling equal to the sum of the inversion splittings of the initial and final states should occur; on the other hand, for perpendicular bands with $\Delta K = \pm 1$ such as ν_3 the observed doubling should be the difference. The doubling of lines in the ν_1 band was noted in the early investigation of Dennison and Hardy (5) and can also be seen in Fig. 1; apparently the smaller doubling in the ν_3 band has hitherto escaped detection.

The splitting in the 0010 state can be estimated from the data since the doubling in the ground state is known from the microwave spectrum (2). Fig. 2 is a graph of inversion splittings in the 0010 state for the rotational levels (J, $K = J$), plotted against J. By extrapolating to $J = 0$, one finds the value 1.1 cm.$^{-1}$ for the inversion splitting, which is not markedly different from the corresponding splitting (0.7935) for the ground state (2). Although the splitting due to inversion in ammonia has been evaluated theoretically only for the $v_2 v_2$ series of states, one would expect the splitting to have little depen-

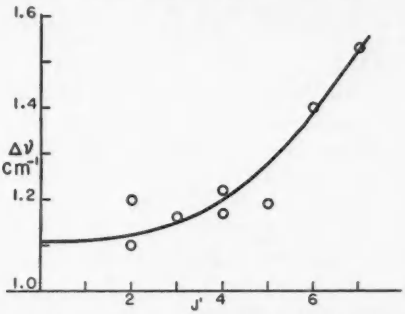

FIG. 2. Determination of the inversion splitting for the 0010 state of ammonia. The graph shows the inversion splittings of the $(J, K = J)$ levels plotted against J.

dence on v_3, since there is at most a second order change in the height of the NH_3 pyramid for this vibration. The large dependence of this doubling on J and K is not so readily understood.

ACKNOWLEDGMENTS

The author wishes to express his gratitude to Dr. N. Sheppard, in whose laboratory the research was carried out, for many helpful discussions. It is a pleasure to acknowledge the financial assistance of a fellowship from the Nuffield Foundation.

REFERENCES

1. BARKER, E. F. Phys. Rev. 55: 657. 1939.
2. BLEANEY, B. and PENROSE, R. P. Proc. Roy. Soc. (London), A, 189: 358. 1947.
3. CUMMING, C. Ph.D. Thesis, University of Toronto, Toronto, Ont. 1952.
4. CUMMING, C. and WELSH, H. L. J. Chem. Phys. 21: 1119. 1953.
5. DENNISON, D. M. and HARDY, J. D. Phys. Rev. 39: 938. 1932.
6. HANSLER, R. L. and OETJEN, R. A. J. Chem. Phys. 21: 1340. 1953.
7. HÖNL, H. and LONDON, F. Z. Physik, 33: 803. 1925.
8. PLYLER, E. K., GAILAR, N. M., and WIGGINS, T. A. J. Research Natl. Bur. Standards, 48: 221. 1952.
9. RANK, D. H., SHEARER, J. N., and WIGGINS, T. A. Phys. Rev. 94: 575. 1954.
10. SLAWSKY, Z. I. and DENNISON, D. M. J. Chem. Phys. 7: 509. 1939.
11. TELLER, E. Handb. u. Jahrb. Chem. Phys. 9, II: 43. 1934.
12. WOOD, D. L., BELL, E. E., and NIELSEN, H. H. Proc. Natl. Acad. Sci. U.S. 36: 497. 1950.

THE FISSION YIELDS OF THE CESIUM ISOTOPES FORMED IN THE THERMAL NEUTRON FISSION OF U^{235} AND THE NEUTRON ABSORPTION CROSS SECTION OF Xe^{135} [1]

By J. A. Petruska,[2] E. A. Melaika, and R. H. Tomlinson

ABSTRACT

The absolute fission yields of the cesium isotopes occurring in the thermal neutron fission of U^{235} have been determined with a mass spectrometer using isotope dilution techniques. Values of 6.59%, 6.41%, and 6.15% have been obtained for the yields of Cs^{133}, Cs^{135}, and Cs^{137} respectively. The neutron absorption cross section of Xe^{135} has also been measured to be 866 times greater than that of B^{10} for a Maxwellian distribution of neutron velocities corresponding to a neutron temperature of 57°C. This ratio gives a thermal neutron absorption cross section of 3.47×10^6 barns for Xe^{135} assuming it is a $1/v$ detector.

INTRODUCTION

Neutron absorption by the fission product isotope Xe^{135} reduces the reactivity of nuclear reactors, particularly when they are operated at high thermal neutron fluxes. Reliable values for the cross section and the fission yield of this isotope are therefore of considerable interest in pile operations. Since the primary yield of Cs^{135} is probably small, the yield of Xe^{135} may be estimated from the cumulative yield of Cs^{135}. The relative yields of the cesium isotopes in U^{235} fission have been obtained from mass spectrometric data by Inghram, Hess, and Reynolds (8) and Wiles, Smith, Horsley, and Thode (14). In the former work the relative yield of the mass 135 isotope appears to be in considerable error owing to the failure of these authors to account adequately for the neutron capture in Xe^{135}. In the more recent work of Wiles *et al.* the relative yield for mass 135 was obtained by measuring the isotopic ratios of fission products formed under conditions where the neutron absorption by Xe^{135} was negligible. Since the large resonance absorption of neutrons by Xe^{135} occurs in the thermal energy region, it was possible to minimize this absorption by shielding the uranium with cadmium during the irradiation.

Absolute fission yields for each of the cesium isotopes may be obtained from these relative yields with the aid of a suitable normalization factor. Katcoff and Rubinson (9) have given a value of 6.62% for the yield of the mass 133 fission chain. On the other hand the yield of this mass chain may be estimated to be 7.25% from the 3.2%[3] yield for I^{131} given by Bartholomew, Brown, Hawkings, Merritt, and Yaffe (1) and the 2.265 value for the ratio of mass 133 to mass 131 given by Thode *et al.* (14). It is therefore of some interest to establish which of the values for the cumulative yield of the mass 133 chain is most reliable since this not only fixes the absolute values of the cesium

[1] *Manuscript received June 9, 1955.*
Contribution from Department of Chemistry, McMaster University, Hamilton, Ontario.
[2] *Holder of Research Council of Ontario Scholarship.*
[3] *Yaffe and Brown have given the value of 3.1% for I^{131} relative to a 6.1% yield of Ba^{140}. The yield of Ba^{140} has recently been given by Yaffe, Thode, Merritt, Hawkings, Brown, and Bartholomew (16) as 6.32% which therefore gives 3.21% for the yield of I^{131}. A further revision of these values causing a 3–4% increase may also be required if a self-shielding correction is applied to the Ba^{140} yield.*

yields but also those of the xenon isotopes whose relative yields in fission products have been determined. The thermal neutron absorption cross section of Xe^{135} has been reported to be 3.5×10^6 barns, but no details of this determination have been released (10).

In the present work the cumulative yield of Cs^{133} has been determined from measurements of the number of cesium atoms produced during a given irradiation and a knowledge of the extent of the U^{235} fission. The number of cesium atoms produced was measured with the mass spectrometer using isotope dilution techniques. The number of U^{235} fissions was calculated from the change in the B^{10}/B^{11} ratio in a simultaneously irradiated boron flux monitor and the known ratio of the neutron fission cross section of U^{235} to the neutron absorption cross section of B^{10}. These data also give a direct determination of the yield of Cs^{137}, but not Cs^{135}, since the neutron flux for this irradiation was large enough that a considerable fraction of the 135 mass chain was lost through neutron absorption by Xe^{135}. To obtain the yield of Cs^{135} relative to Cs^{133} a second sample of natural uranium was irradiated in a thermal column where the neutron flux was sufficiently low that neutron absorption by Xe^{135} was small.

The relative yields from these two samples also made possible an evaluation of the relative neutron absorption cross sections of Xe^{135} and B^{10} since the decrease in the cumulative yield of the 135 mass chain owing to neutron absorption by Xe^{135} may be related to the concomitant change in the B^{10}/B^{11} ratio of the associated flux monitor.

EXPERIMENTAL

Two samples of natural uranium metal were irradiated with thermal neutrons in the N.R.X. (Chalk River) reactor. Sample A weighing 2.966 gm. (a rectangular parallelepiped of approximate dimensions 0.8 cm. $\times$ 0.4 cm. $\times$ 0.5 cm.) along with a quartz container filled with about 1 ml. of BF_3 gas at 0.5 atm. pressure was irradiated with thermal neutrons for a 36-day period. The neutrons were considered to have a Maxwellian distribution of velocities corresponding to a temperature of 57°C. Sample B consisted of several similar samples weighing approximately 20 gm. each. These were simultaneously irradiated for a period of 80 days in the thermal column.

In order to minimize contamination of the fission products by natural isotopes, polyethylene or teflon containers and pipettes were used in the preparation of reagents and the separation of the fission products. The uranium was dissolved in freshly distilled nitric acid and, where isotope dilution was required, known amounts of natural Cs (Cs^{133}) were added to aliquots of this solution. The uranium was separated from the fission products by precipitation of uranium tetroxide from a neutral solution of the nitrate using hydrogen peroxide as precipitant. The supernatant solution containing most of the fission products was concentrated by evaporation and transferred directly to the ion source filament of a 90° sector mass spectrometer. Separation of the fission products from each other was unnecessary since ion emission of cesium occurs at a much lower temperature than any of the other elements which produce ions in this mass region.

The abundances of the boron isotopes in the BF_3 used for a flux monitor were determined with a 180° mass spectrometer. The ratios of the boron isotopes in the unirradiated BF_3 and the irradiated BF_3 were compared directly. Since both samples came from the same supply, the original isotopic composition of the irradiated BF_3 was identical to that of the unirradiated BF_3.

RESULTS AND CONCLUSIONS

Thermal Neutron Fission Yields of the Cesium Isotopes

The observed mass spectrometric ratios for the long-lived and stable isotopes of cesium occurring in the thermal fission of U^{235} as well as values of the ratios obtained after isotope dilution are shown in Table I. The errors shown for the

TABLE I

THE RATIOS OF CESIUM ISOTOPES OCCURRING IN THE THERMAL NEUTRON FISSION OF U^{235} TOGETHER WITH ISOTOPE DILUTION DATA

	Isotope		
	Cs^{133}	Cs^{135}	Cs^{137}
Sample A			
Mass spectrometric ratio*	1.074±0.003	0.768±0.003	1.000
Ratio after isotope dilution			
I. 2.584×10^{15} atoms Cs^{133} added per gram of uranium	1.664	0.768	1.000
II. 3.117×10^{15} atoms Cs^{133} added per gram of uranium	1.789	0.768	1.000
Atoms of fission Cs^{133} per gram of uranium $\times10^{15}$			
I	4.702		
II	4.680		
Average	4.653±0.011†		
Sample B			
Mass spectrometric ratio*	1.072±0.002	1.034±0.002	1.000
Ratio after isotope dilution			
I. 2.013×10^{14} atoms Cs^{133} added per gram of uranium	1.937	1.034	1.000
II. 2.184×10^{14} atoms Cs^{133} added per gram of uranium	2.003	1.034	1.000
Atoms of fission Cs^{133} per gram of uranium $\times10^{14}$			
I	2.488		
II	2.515		
Average	2.50 ±0.01		

**Corrected for 26.6-year half-life of Cs^{137} (15).*
†Corrected for 0.8% contribution of Cs^{133} from fast fission of U^{238}.

mass spectrometric ratios of Sample A are the standard deviations of the observed values from the average for a large number of spectrograms on this single sample. For Sample B the value given represents the average of 11 determinations similar to that of Sample A made on fission products separated from three different samples of uranium. The precision shown for Sample B is the standard deviation of these 11 determinations from the average. Table I

also shows the number of Cs^{133} atoms produced per gram of uranium calculated from the fission product and isotope dilution ratios. The values obtained include Cs^{133} produced by the fast fission of U^{238}. This contribution has been estimated to be 0.8% for Sample A and the final value shown in Table I has been corrected to give only the number of Cs^{133} atoms produced in the thermal neutron fission of U^{235}.

From the number of cesium atoms produced per gram of uranium it is possible to determine the fission yield if the number of fissions per gram is known. This may be calculated if the thermal neutron flux in the uranium is known. The flux associated with Sample A was monitored with BF_3 which showed a ratio of B^{10}/B^{11} before irradiation to that after irradiation of 1.029 ± 0.001. Thus, if the only change in the boron isotope ratio was due to the loss of B^{10} by the $B^{10}(n, \alpha)Li^7$ reaction, then

$$1.029 = \exp {}_5\sigma^{10}\phi t,$$

where ${}_5\sigma^{10}$ = the neutron absorption cross section of B^{10},
ϕ = the neutron flux in the boron,
t = the time of irradiation.

From this relation it may be shown that

[1] $$ {}_5\sigma^{10}\phi t = 0.0286.$$

When the depletion of U^{235} is small, the total number of thermal fissions produced per gram of natural uranium is given by the expression

[2] $$N_f = {}_{92}\sigma_f^{235}\phi' t N_{235},$$

where N_f = the number of thermal fissions of U^{235} per gram of natural uranium,
${}_{92}\sigma_f^{235}$ = the thermal neutron fission cross section of U^{235},
ϕ' = the thermal neutron flux in the uranium,
N_{235} = the number of U^{235} atoms per gram of natural uranium.

In order to evaluate equation [2] with the aid of equation [1], it is necessary to know the relationship between the flux in the boron monitor and the flux in the uranium. The flux reduction in the uranium or the self-shielding correction may be evaluated from the data of Case, Hoffmann, and Placzek (3). These authors have shown that, if an absorbing object is placed in a uniform isotropic neutron bath, the ratio of the average neutron flux within the object to the neutron flux at a distance outside the object is equal to P_0 which is a parameter known as the escape probability. Values of the collision probability, P_c (which is equal to $1-P_0$), have been tabulated for spherical objects where the ratio of the object radius to the absorption mean free path is known. If the object placed in the isotropic neutron bath may scatter as well as absorb neutrons, the escape probability is reduced. Case, Hoffmann, and Placzek (3) have shown, however, that scattering must predominate to a very great extent before the escape probability is materially affected. For natural uranium, where the neutron absorption and scatter cross sections

are approximately equal (10), the effect of scatter may be neglected in the evaluation of the self-shielding correction.

The absorption mean free path of the neutron may be calculated from the relation

[3] $$\lambda = 1/N\sigma_{eff},$$

where λ = the absorption mean free path,

N = the number of atoms per cm.^{3},

σ_{eff} = the effective neutron absorption cross section.

It has been assumed that the neutron absorption cross section of natural uranium varies inversely as the neutron velocity and that the neutron velocity distribution in the reactor was Maxwellian, and therefore the effective neutron absorption cross section of the uranium may be calculated from the relation

$$_{92}\sigma_{eff} = {}_{92}\sigma_{ab}\ \frac{\sqrt{\pi}}{2}\sqrt{\frac{293}{T}},$$

where $_{92}\sigma_{ab}$ = neutron absorption cross section of natural uranium for 2200 m./sec. (neutrons)

= 7.42 barns (10),

T = neutron temperature

= 57°C. for experimental conditions.

Thus the effective neutron absorption cross section of natural uranium is 6.20 barns which when substituted in equation [3] gives:

$$\lambda = \frac{238.07}{0.6023\times10^{24}\times18.7\times6.20\times10^{-24}} = 3.42 \text{ cm.}$$

That is, the absorption mean free path of neutrons having a Maxwellian distribution of velocities corresponding to a neutron temperature of 57°C. is 3.42 cm. in natural uranium. If Sample A weighing 2.966 gm. were spherical in shape, the radius of this sphere would be 0.336 cm., and the ratio of this radius to the mean free path would be 0.0985. From the tables given by Case, Hoffmann, and Placzek (3), a value of 0.070 is obtained for P_c. Since the actual shape of the uranium in Sample A was a rectangular parallelepiped (approximately 0.8 cm.×0.4 cm.×0.5 cm.), the flux reduction would not be as great as that calculated for a sphere. This factor, however, is not very critical unless the surface to volume ratio is much greater than that of a sphere. For example, Case *et al.* (3) have shown that a spheroid with major to minor axis ratio of 5/3 would have a value of P_c equal to 0.98 that of a sphere of equivalent volume. For Sample A therefore this shape factor gives $P_c = 0.068$ and hence the self-shielding correction $P_0 = 0.932$. Calculations show that the accumulation of fission products such as Sm^{149} and Xe^{135} would introduce less than 0.1% increase in this value for the particular irradiation conditions. Equivalent calculations show that the self-shielding correction for the boron flux monitor is negligible. The whole self-shielding correction for the uranium in relation to that

of the boron is therefore applicable providing that the flux in the boron was not reduced by the presence of the uranium. Since the relative positions of the uranium and the boron were not recorded, exact evaluation of this influence can not be calculated. There was, however, no scattering material close to or between the uranium and the boron and hence the flux reduction in the boron was merely the "shadow" cast by the uranium on the boron. It is estimated from the sizes of the uranium, boron, and the irradiation capsule that not more than 10% of the neutrons passing through the boron had passed through the uranium. Since the average flux reduction in the uranium itself as calculated above was 6.8%, the reduction of the flux in the boron resulting from the presence of the uranium would have been less than 1%. The effective flux within the uranium is therefore taken as 0.932 that in the boron, i.e. $\phi' = 0.932\phi$ for Sample A. This relation, together with equations [1] and [2], gives

$$[4] \qquad N_f = 0.932 \times 0.0286 \times \frac{{}_{92}\sigma_f^{235}}{{}_{5}\sigma^{10}} N_{235}.$$

Yaffe *et al.* (16) have given a value of

$${}_{92}\sigma_f^{235}/{}_{5}\sigma^{10} = 0.1456$$

for identical neutron irradiation conditions and

$$N_{235} = \frac{6.023 \times 10^{23} \times 0.00719}{238.07},$$

where the abundance of U^{235} in natural uranium is 0.719% (4). Substitution of these values in equation [4] gives $N_f = 7.06 \times 10^{16}$ thermal neutron fissions per gram of natural uranium in Sample A. From the number of Cs^{133} atoms produced per gram of uranium in Table I a value of 6.59% is obtained for the fission yield of Cs^{133}. In view of the many parameters which have entered the calculation of this fission yield, it is difficult to assess the absolute accuracy of the value. The duplicate isotope dilutions and the mass spectrometry of the cesium isotopes would probably introduce less than 1% error. The largest apparent source of error is in the flux determinations from the change in the boron isotope ratio. The observed change was small and the precision of this value was only ±3.5%. Other sources of error include the self-shielding correction, cross sections, etc., which could lead to a revision of the 6.59% yield if more reliable data and methods of calculation become available.

The yield of Cs^{137} may be obtained from the absolute value of the Cs^{133} yield and the relative yield of Cs^{133} to Cs^{137} for Sample A. However, the extent of neutron absorption by Xe^{135} was sufficiently large for this sample that it is difficult to evaluate the yield of the 135 mass chain. More reliable values of the relative yields of the cesium isotopes can be obtained from the data for Sample B. In this case the correction to the 135 mass ratio for neutron absorption is small compared to that for Sample A and the yield may therefore be estimated with greater accuracy. Wanless (13) has shown that the ratio of the observed yield of Cs^{135} to the cumulative yield of the 135 mass chain is given by equation [5]:

$$[5]\quad \frac{N_{135}}{Y_{135}} = 1-\left[\frac{{}_{54}\sigma^{135}\phi'}{{}_{54}\lambda^{135}+{}_{54}\sigma^{135}\phi'}+\frac{{}_{54}\sigma^{135}\phi'}{t}\left\{\frac{\exp(-Kt)-1}{K^2}+\frac{\exp(-{}_{53}\lambda^{135}t)-1}{{}_{53}\lambda^{135}(K-{}_{53}\lambda^{135})}-\frac{\exp(-Kt)-1}{K(K-{}_{53}\lambda^{135})}\right\}\right]$$

where N_{135} = the observed number of Cs^{135} atoms produced per gram of natural uranium,

Y_{135} = the cumulative yield of the 135 mass chain in atoms per gram of uranium,

${}_{53}\lambda^{135}$ = the decay constant for I^{135} = 0.103 hr.$^{-1}$ (6),

${}_{54}\lambda^{135}$ = the decay constant for Xe^{135} = 0.0752 hr.$^{-1}$ (2),

${}_{54}\sigma^{135}$ = the thermal neutron capture cross section of Xe^{135},

$K = {}_{54}\lambda^{135}+{}_{54}\sigma^{135}\phi'$.

Equation [5] may be approximately represented by equation [6] if the time of irradiation is long compared to the half-life of Xe^{135}.

$$[6]\quad \frac{N_{135}}{Y_{135}} = 1-\frac{{}_{54}\sigma^{135}\phi'}{{}_{54}\lambda^{135}+{}_{54}\sigma^{135}\phi'}.$$

From equation [6] it may be seen that for a sufficiently low value of the flux the observed Cs^{135} yield is equivalent to the cumulative yield of the 135 mass chain. In the case of Sample B this condition is approached and therefore the ratio N_{135}/Y_{135} may be evaluated with accuracy even if considerable error is involved in the values of the parameters required in the solution of equation [6].

The neutron flux was not monitored for Sample B, but the isotope dilution data which give the number of cesium atoms produced may be used with the fission yield established from Sample A to evaluate the flux. Thus if the depletion of U^{235} is small, equation [7] gives the cumulative yield of Cs^{133}:

$$[7]\quad N_{133} = N_{235}\,{}_{92}\sigma_f^{235}\phi' t f_{133},$$

where N_{133} = the number of Cs^{133} atoms produced per gram of uranium,

f_{133} = the fractional fission yield of Cs^{133}.

Equation [7] when rearranged and multiplied by ${}_{54}\sigma^{135}$ gives equation [8]:

$$[8]\quad {}_{54}\sigma^{135}\phi' = \frac{N_{133}}{N_{235}\,t\,f_{133}}\times\frac{{}_{54}\sigma^{135}}{{}_{92}\sigma_f^{235}}.$$

As an approximation the ratio ${}_{54}\sigma^{135}/{}_{92}\sigma_f^{235}$ may be considered independent of neutron velocity distribution and temperature and hence it may be evaluated using ${}_{54}\sigma^{135} = 3.5\times10^6$ barns and ${}_{92}\sigma_f^{235} = 549$ barns (10). With the value of N_{133} for Sample B taken from Table I, f_{133} as determined for Sample A, and t = 1947 hr. equation [8] can be solved:

$${}_{54}\sigma^{135}\phi' = 2.50\times10^{14}\times\frac{238.07}{6.023\times10^{23}\times0.00719\times1947\times0.0659}\times\frac{3.5\times10^6}{549}$$

$$= 0.00068\ \text{hr.}^{-1}$$

Substitution of this value in equation [6] shows that the observed Cs^{135} yield is 99.1% of the cumulative yield of the 135 mass chain for Sample B. It also may be seen that for the irradiation conditions of Sample B, a 10% error in estimating the product ${}_{54}\sigma^{135}\phi'$ will only introduce a 0.1% error in the calculated relative yield. The final value of the relative yield of Cs^{135} shown in Table II has been obtained from the data for Sample B corrected in this

TABLE II

THE RELATIVE AND ABSOLUTE YIELDS OF CESIUM ISOTOPES OCCURRING IN THE THERMAL NEUTRON FISSION OF U^{235}

Isotope	Relative yield	Absolute fission yield	
		This work	Katcoff and Rubinson
Cs^{133}	1.072	6.59	6.62
Cs^{135}	1.043	6.41	6.40
Cs^{137}	1.000	6.15*	6.07*

**Not corrected for delayed neutron emission.*

manner. The corrected relative yields in Table II have been normalized to the measured 6.59% absolute yield of Cs^{133} and shown as absolute thermal neutron fission yields. The yields obtained by Katcoff and Rubinson (9) based on a measured yield of Xe^{133} and the relative yields of Wiles, Smith, Horsley, and Thode are shown in Table II for comparison. The 6.59% yield of Cs^{133} is in excellent agreement with the 6.62% yield obtained by Katcoff and Rubinson (9) and suggests a possible error in the yield of 7.25% obtained from the I^{131} yield and the ratio of the yields of mass 133 and mass 131. This latter ratio has recently been redetermined by Fleming and Thode (5) and the result is substantially the same as that previously published. The existence, however, of the 2.3-day Xe^{133m} isomer not known when the earlier ratio was determined necessitates a small correction to the Xe^{133}/Xe^{131} ratio. It is therefore suggested that the I^{131} yield may be about 2.9% instead of the currently accepted value of 3.2% obtained from the data of Yaffe *et al.* (1) when normalized to a 6.3% yield of Ba^{140}. The difference in the mass 137 yields shown in Table II is largely a result of the different half-lives used to correct for the decay of Cs^{137}. In the present work 26.6 years (15) has been used rather than the previously accepted value of 33 years (14). The absolute yield of Cs^{137} shown in Table II is not the cumulative yield of all isotopes of mass 137 which occur in the thermal neutron fission of U^{235}. Delayed neutron emission by Xe^{137} (with 22.0 sec. half-life of the parent I^{137}) results in a branching of the 137 mass chain. Pappas (11) has estimated the loss to the 137 mass chain to be 0.42% and hence the cumulative yield of isotopes of mass 137 is 6.57% providing no other chain branching processes occur.

The Neutron Absorption Cross Section of Xe^{135}

The value of the neutron absorption cross section of Xe^{135} may be obtained from the measured decrease in the Cs^{135}/Cs^{137} ratio for Sample A compared to the fission yield ratio and the change in the boron isotope ratio of the flux

monitor. The value obtained is therefore independent of the measured absolute fission yields. With equation [5] it is possible to calculate a series of N_{135}/Y_{135} ratios for various values of the product ${}_{54}\sigma^{135}\phi'$. The value of ${}_{54}\sigma^{135}\phi'$ which corresponds to the observed N_{135}/Y_{135} ratio may be used in the evaluation of ${}_{54}\sigma^{135}$.

Unfortunately the 36-day irradiation of Sample A was not continuous. The reactor operated at a constant power output for a total of 650 hr. which in fact represented six separate irradiation periods of 99.8 hr., 111.6 hr., 104.0 hr., 123.8 hr., 139.3 hr., and 71.5 hr. respectively. The periods of irradiation were separated by shut-down periods of 56.0 hr., 48.5 hr., 35.5 hr., 26.0 hr., and 25.5 hr. respectively. The periods between irradiation, however, were sufficiently long compared to the half-life of Xe^{135} that it was possible to consider that each of the six irradiation periods was independent. It was therefore necessary to obtain six calculated values of N_{135}/Y_{135} from equation [5] for an arbitrarily chosen value of ${}_{54}\sigma^{135}\phi'$ corresponding to each of the six irradiation times. These ratios were then weighted in accordance with the fraction of the total irradiation period which they represented and averaged to give a value of N_{135}/Y_{135} corresponding to the chosen value of ${}_{54}\sigma^{135}\phi'$. Graphical representation of N_{135}/Y_{135} for various values of ${}_{54}\sigma^{135}\phi'$ made possible the evaluation of ${}_{54}\sigma^{135}\phi'$ which corresponded to the experimental N_{135}/Y_{135} ratio. The experimental value of N_{135}/Y_{135} for Sample A may be obtained from the product of the observed Cs^{135}/Cs^{137} ratio (Table I) and the fission yield Cs^{137}/Cs^{135} ratio shown in Table II, i.e. $N_{135}/Y_{135} = 0.768/1.043 = 0.736$. This value corresponds to ${}_{54}\sigma^{135}\phi' = 0.0355$ hr.$^{-1}$ which with equation [1] and the relation $\phi' = 0.932\phi$ gives ${}_{54}\sigma^{135}/{}_{5}\sigma^{10} = 866 \pm 40$ for the assumed Maxwellian distribution of neutron velocities corresponding to a neutron temperature of 57°C. This ratio gives an effective neutron absorption cross section of 2.90×10^6 barns for these experimental conditions if the absorption cross section of natural boron is 755 barns (12) and the abundance of B^{10} is 18.83% (7). If it is assumed that the neutron absorption cross section of Xe^{135} varies inversely as the neutron velocity, the neutron absorption cross section of Xe^{135} for 2200 m./sec. neutrons becomes 3.47×10^6 barns, which is in close agreement with the value of 3.5×10^6 barns which was released jointly by the United States, the United Kingdom, and Canada (10).

ACKNOWLEDGMENTS

We wish to thank the Atomic Energy of Canada Limited for arranging the neutron irradiations, Dr. H. G. Thode and Dr. W. H. Fleming for helpful discussion and the isotopic analysis of the BF_3, and Dr. S. A. Kushneriuk for assistance in the calculation of the self-shielding corrections. The financial support of the National Research Council of Canada and the Atomic Energy of Canada Limited is gratefully acknowledged.

REFERENCES

1. Bartholomew, R. M., Brown, F., Hawkings, R. C., Merritt, W. F., and Yaffe, L. Can. J. Chem. 31: 120. 1953.
2. Brown, F. and Yaffe, L. Can. J. Chem. 31: 242. 1953.

3. CASE, K. M., DEHOFFMANN, F., and PLACZEK, G. Introduction to the theory of neutron diffusion. Vol. I. U.S. Government Printing Office, Washington, D.C. 1953.
4. FLEMING, E. H., GHIORSO, A., and CUNNINGHAM, B. B. Phys. Rev. 88: 642. 1952.
5. FLEMING, W. H. and THODE, H. G. Private communication.
6. GLENDENIN, L. E. and METCALF, R. P. Natl. Nuclear Energy Ser. Vol. 9. Paper 140. 1951.
7. INGHRAM, M. G. Phys. Rev. 70: 653. 1946.
8. INGHRAM, M. G., HESS, D. C., and REYNOLDS, J. H. Phys. Rev. 76: 1717. 1949.
9. KATCOFF, S. and RUBINSON, W. Phys. Rev. 91: 1458. 1953.
10. Nuclear Constants for Reactor Studies. Can. J. Phys. 30: 624. 1952.
11. PAPPAS, A. C. Mass. Inst. Technol. Tech. Rept. No. 63. Sept. 15, 1953.
12. RINGO, G. R. Phys. Rev. 87: 785. 1952.
13. WANLESS, R. Ph.D. Thesis, McMaster University, Hamilton, Ont. 1953.
14. WILES, D. R., SMITH, B. W., HORSLEY, R., and THODE, H. G. Can. J. Phys. 31: 419. 1953.
15. WILES, D. M. and TOMLINSON, R. H. Phys. Rev. 99: 188. 1955.
16. YAFFE, L., THODE, H. G., MERRITT, W. F., HAWKINGS, R. C., BROWN, F., and BARTHOLOMEW, R. M. Can. J. Chem. 32: 1017. 1954.

GAUGE-INVARIANT FORMULATION OF QUANTUM ELECTRODYNAMICS[1]

By P. A. M. Dirac

ABSTRACT

Electrodynamics is formulated so as to be manifestly invariant under general gauge transformations, through being built up entirely in terms of gauge-invariant dynamical variables. The quantization of the theory can be carried out by the usual rules and meets with the usual difficulties.

It is found that the gauge-invariant operation of creation of an electron involves the simultaneous creation of an electron and of the Coulomb field around it. The requirement of manifest gauge invariance prevents one from using the concept of an electron separated from its Coulomb field.

GAUGE TRANSFORMATIONS

A gauge transformation of the electromagnetic field changes the potentials $A^\mu(\mu = 0, 1, 2, 3)$ according to the law

[1] $$A^\mu \rightarrow A^\mu + \partial S/\partial x_\mu.$$

In the usual formulation of electrodynamics, one restricts the potentials by the condition

[2] $$\partial A_\mu/\partial x_\mu = 0.$$

Then, in order that the transformation [1] shall preserve this condition, it is necessary that

[3] $$\partial^2 S/\partial x_\mu \, \partial x^\mu = 0,$$

so that the gauge transformations are restricted.

It is possible to do without the condition [2], in which case S can be an arbitrary function of the four x's. One then gets an electrodynamics with general gauge transformations. Such a formulation of electrodynamics has some advantages in that (i) it is simpler, from a certain point of view, as it does not make use of an unnecessary condition, and (ii) it imposes stricter limitations on any alterations one may make when one tries to improve the theory.

It will be shown here how one can develop electrodynamics without the conditions [2], [3] and can quantize it, keeping all the time to a formulation for which the invariance under general gauge transformations is manifest.

THE LAGRANGIAN AND HAMILTONIAN

We must work with the dynamical variables on a space-like three-dimensional surface in space–time and see how they are connected with the dynamical variables on a neighboring surface. These connections constitute the equations of motion. For simplicity we shall here deal only with the flat surfaces $x_0 =$

[1]*Manuscript received August 23, 1955.*
Contribution from St. John's College, Cambridge, England.
This paper formed the subject of two lectures given at the National Research Council at Ottawa on 10 and 12 August, 1955.

constant, corresponding to instants of time. The generalization to arbitrary space-like surfaces can be made without difficulty, but requires elaborate notation.

With the Lagrangian formulation, the variables that we work with are the coordinates and velocities of the field, namely A^0, A^r $(r = 1, 2, 3)$, $\partial A^0/\partial x_0$, $\partial A^r/\partial x_0$, together with suitable variables to describe the electrons. The variables are to be taken at all points of three-dimensional space for a fixed x_0, so they are functions of three parameters x_r.

Let us see how the field variables are affected by a gauge transformation. We have

$$[4] \quad \begin{cases} A^0 \to A^0 + \partial S/\partial x_0, & A^r \to A^r + \partial S/\partial x_r, \\ \partial A^0/\partial x_0 \to \partial A^0/\partial x_0 + \partial^2 S/\partial x_0^2, & \partial A^r/\partial x_0 \to \partial A^r/\partial x_0 + \partial^2 S/\partial x_r\, \partial x_0. \end{cases}$$

If we take S and $\partial S/\partial x_0$ to be zero at all points of three-dimensional space at the time considered, then there is no change in A^0, A^r, and $\partial A^r/\partial x_0$. However, $\partial^2 S/\partial x_0^2$ remains at our disposal, and so we can make an arbitrary change in $\partial A^0/\partial x_0$. This marks an important difference from the usual formulation, in which [3] holds, so that if S and $\partial S/\partial x_0$ vanish then $\partial^2 S/\partial x_0^2$ must also vanish. With the present theory, *the way in which A^0 varies with the time is completely arbitrary, instead of being fixed by the equations of motion and initial conditions.*

The passage from the Lagrangian to the Hamiltonian can be made by standard methods. The work has been done previously (1) and need not be recapitulated, but the main features in it will be mentioned here to show up the differences from the usual theory.

For electrons with spin, described by the four-component wave function ψ, interacting with the electromagnetic field, the Lagrangian is

$$[5] \quad L = \int \{ \Re\, i\hbar\, \bar{\psi}(\psi^0 + \alpha_r \psi^r) + e\, \bar{\psi}(A^0 + \alpha_r A^r)\psi + m\, \bar{\psi}\, \alpha_m\, \psi - \tfrac{1}{4} F_{\mu\nu} F^{\mu\nu} \} d^3x,$$

where $\Re$ means the real part of the term that follows, and the suffix 0 or r added to a field variable such as ψ means its derivative with respect to x_0 or x_r. In the usual theory the last term of the integrand is replaced by

$$[6] \quad -\tfrac{1}{2} A_{\mu\nu} A^{\mu\nu}.$$

The difference of the two terms, integrated over the whole of space–time, vanishes with the help of [2], and so the two Lagrangians give the same equations of motion.

The momenta $B_\mu(x_1 x_2 x_3)$ conjugate to the coordinates $A^\mu(x_1 x_2 x_3)$ are introduced in the usual way, as the coefficients of $\delta A^{\mu 0}$ in the variation of the Lagrangian. Now the Lagrangian [5] does not involve A^{00}, and hence it makes B_0 vanish. The vanishing of B_0 does not produce a difficulty, but merely appears as a supplementary condition in the Hamiltonian scheme of equations. The other components B_r of B are equal to F_{r0}, the components of the electric field.

In the usual theory with the term [6] in the Lagrangian, B_0 does not vanish and the four B's are $B_\mu = -A_\mu{}^0$. These B's are not gauge-invariant quantities, as in the new theory.

The Hamiltonian that follows from the Lagrangian [5] is

$$[7] \quad H = \int \{ -\Re\, i\hbar\, \bar{\psi}\, \alpha_r\, \psi^r - e\, \bar{\psi}\, \alpha_r\, A^r\, \psi - m\, \bar{\psi}\, \alpha_m\, \psi + \tfrac{1}{4}\, F_{rs}\, F^{rs} - \tfrac{1}{2} B_r\, B^r \} d^3x.$$

It is to be used in conjunction with the supplementary conditions

$$[8] \quad B_0 \approx 0,$$

$$[9] \quad B_r{}^r + e\bar{\psi}\psi \approx 0.$$

The second of these is a consequence of the field equations, and since it involves only dynamical coordinates and momenta, it has to be taken into account in the Hamiltonian scheme. The supplementary conditions are all consistent, because their left-hand sides have zero Poisson bracket with one another and with the Hamiltonian.

In the usual theory the last two terms of the integrand in [7] are replaced by

$$[10] \quad \tfrac{1}{2} A_{\mu r}\, A^{\mu r} - \tfrac{1}{2} B_\mu\, B^\mu$$

and a further term must be added to the integrand,

$$[11] \quad -eA^0 \bar{\psi}\psi,$$

representing the potential energy of the electrons. The supplementary condition [8] must be replaced by

$$[12] \quad B_0 - A_r{}^r \approx 0$$

which follows from [2], and the supplementary condition [9] still holds.

An important feature of the new theory is that *the variables A^0, B_0 do not appear in the Hamiltonian* [7]. It follows that these variables are of no physical importance and can be dropped out from the theory. This is a simplification which does not occur in the usual theory, where A^0 and B_0 appear in the terms [11] and [10].

The supplementary conditions can be looked upon as Hamiltonians giving rise to permissible changes in the dynamical variables at one instant of time. In the present case these changes are the gauge transformations.

The supplementary condition [8] merely gives rise to an arbitrary change in A^0 with the other dynamical variables unchanged. This is a gauge transformation [4] with S zero at the time considered, but not $\partial S/\partial x_0$. Such gauge transformations are automatically allowed in the theory when the variables A^0, B_0 are dropped out.

To see the changes produced by the supplementary condition [9], let us work with the general linear combination of [9] at all points of three-dimensional space, say

$$[13] \quad G = \int g(B_r{}^r + e\bar{\psi}\psi) d^3x \approx 0,$$

g being a general function of the three x's. The supplementary condition [13] will make the dynamical variables vary with some parameter τ according to

$$[14] \quad \begin{aligned} dA^r/d\tau &= [A^r, G] = \int g'[A^r, B_s{}^{s'} + e\bar{\psi}'\psi'] d^3x' \\ &= \int g' \delta(x - x')^{r'} d^3x' = -g^r. \end{aligned}$$

With the suffix a denoting one of the four components of ψ,

$$\begin{aligned} d\psi_a/d\tau &= [\psi_a, G] = \int g'[\psi_a, B_s'^{s'} + e\bar{\psi}_b'\psi_b']d^3x' \\ &= -ie\hbar^{-1}\delta_{ab}\int g'\delta(x-x')\psi_b'\, d^3x' \\ &= -ie\hbar^{-1}g\psi_a. \end{aligned} \tag{15}$$

$\bar{\psi}$ will vary with τ according to the conjugate complex equation, and the other dynamical variables will remain unchanged.

With τ going from 0 to 1 say, [14] is just a gauge transformation [4], with g equal to $-S$ at the time considered. Equation [15] shows how ψ changes with this gauge transformation.

THE GAUGE-INVARIANT QUANTITIES

Our problem now is to develop electrodynamics so as to be manifestly invariant under gauge transformations of the type [14], [15]. We can accomplish this by working entirely with gauge-invariant quantities.

A gauge-invariant quantity satisfies the condition that it has zero Poisson bracket with the left-hand side of [13], or of [9] at all points in three-dimensional space. The electric field B_r and the magnetic field F^{rs} at all points are examples of such quantities. Besides these, there is a gauge-invariant quantity involving ψ, which we must now calculate.

Consider the quantity

$$\psi_a^*(x) = \psi_a(x)e^{iC(x)}, \tag{16}$$

where C is a linear function of the A^r over the whole of three-dimensional space, besides being a function of the three x's. Thus C is of the form

$$C(x) = \int c_r(x, x')\, A^r(x')\, d^3x', \tag{17}$$

with $c_r(x, x')$ a number. By a suitable choice of $c_r(x\,x')$ we can make the quantity [16] gauge invariant.

We have

$$[\psi_a^*, G] = [\psi_a, G]e^{iC} + i\psi_a\, e^{iC}\int c_r(x\,x')[A^r(x'), G]\, d^3x'.$$

Using the results [15], [14], this becomes

$$\begin{aligned} [\psi_a^*, G] &= -i\psi_a^*\{e\hbar^{-1}g + \int c_r(x\,x')g'^{r'}d^3x'\} \\ &= -i\psi_a^*\{e\hbar^{-1}g - \int c_r(x\,x')^{r'}g'd^3x'\}. \end{aligned}$$

Thus ψ_a^* is gauge invariant provided $c_r(x\,x')$ satisfies the condition

$$c_r(x\,x')^{r'} = e\hbar^{-1}\,\delta(x-x'). \tag{18}$$

This means that $c_r(x\,x')$, considered as a function of the x''s, is a vector whose divergence vanishes everywhere except at the point $x' = x$, where it has a singularity of the form of a δ function.

Equation [18] has many solutions. One of them is the spherically symmetrical solution

$$c_r(x\,x') = \frac{e}{4\pi\hbar}\,\frac{x_r'-x_r}{|x'-x|^3}. \tag{19}$$

Any other solution differs from this one by a vector whose divergence with respect to x' vanishes everywhere. Such a vector is of the form $\epsilon_{rst}b'^{st'}$, where $b'^{t} = b^{t}(x')$ is some vector function of the x''s, and ϵ_{rst} has the value ± 1 for r, s, t an even or odd permutation of 1, 2, 3 and zero otherwise. With $c_r(x\,x')$ changed in this way, the change in C is

$$\int \epsilon_{rst} b'^{st'} A'^{r} d^3x' = -\int \epsilon_{rst} b'^{t} A'^{rs'} d^3x', \tag{20}$$

which involves only the gauge-invariant quantities $A^{rs}-A^{sr} = F^{sr}$. Thus the various choices of $c_r(x\,x')$ give various ψ^*'s differing from one another by gauge-invariant factors involving the magnetic field.

The variables ψ^* with some choice of $c_r(x\,x')$, together with their conjugate complexes $\bar{\psi}^*$ and the electric and magnetic field quantities, are the only independent gauge-invariant quantities. A gauge-invariant theory should involve only these dynamical variables and functions of them. This means that *whenever ψ occurs, it should be accompanied by a factor e^{iC} which makes it into ψ^*.*

An important gauge-invariant quantity connected with the differentiation of ψ is

$$(i\hbar\psi^{s}+eA^{s}\psi)e^{iC}. \tag{21}$$

To check its gauge invariance, we note that it is equal to

$$i\hbar\psi^{*s}+\psi^{*}(\hbar C^{s}+eA^{s}) = i\hbar\psi^{*s}+\psi^{*}\int\{\hbar c_r(x\,x')^{s}+e\delta_{r}^{s}\delta(x-x')\}A'^{r}\,d^3x'.$$

The coefficient of A'^{r} here is a vector, with respect to the suffix r, whose divergence with respect to the variables x' vanishes, on account of [18]. Thus the integral is like [20] and is gauge invariant. It follows that [21] is gauge invariant.

The gauge invariance of the Hamiltonian [7] now becomes manifest, as it may be written

$$H = \int\{-\Re\bar{\psi}^{*}\alpha_r(i\hbar\psi^{r}+eA^{r}\psi)e^{iC}-m\bar{\psi}^{*}\alpha_m\psi^{*}+\tfrac{1}{4}F^{rs}F^{rs}+\tfrac{1}{2}B_r B_r\}d^3x, \tag{22}$$

involving only quantities like [21] and other gauge-invariants.

QUANTIZATION: GENERAL THEORY

To quantize a dynamical theory, one must make the dynamical variables into linear operators satisfying the appropriate commutation or anticommutation relations, corresponding to their Poisson bracket relations. These linear operators operate on ket vectors, which represent the various physical states.

A convenient way to describe the kets is to refer them all to one standard ket, $|S\rangle$ say, representing some standard state. The ket $|S\rangle$ is defined mathematically by certain linear conditions, say the conditions

$$\kappa_\lambda|S\rangle = 0, \tag{23}$$

the parameter λ being introduced to distinguish the various conditions. The conditions [23] must be consistent, which requires that the commutator or anticommutator of two κ's shall be a linear function of the κ's of the form

$$\int v_\lambda\,\kappa_\lambda\,d\lambda \tag{24}$$

with the coefficients v_λ on the left. Also the conditions [23] must be sufficient to fix $|S\rangle$ completely, except for a numerical factor.

When the standard ket $|S\rangle$ has been chosen, one can express any other ket $|P\rangle$ as the result of some linear operator ϕ applied to $|S\rangle$,

$$|P\rangle = \phi|S\rangle. \tag{25}$$

One may restrict ϕ to be a function of a certain complete set of commuting or anticommuting dynamical variables, in which case ϕ is called a wave function. However it is not necessary to restrict ϕ in this way. In the general case the ϕ corresponding to a certain $|P\rangle$ is not uniquely determined, as any two ϕ's differing by a quantity of the form [24] correspond to the same $|P\rangle$.

If the classical theory contains some supplementary conditions $\beta \approx 0$, these appear in the quantum theory as restrictions on the kets $|P\rangle$ that represent physical states,

$$\beta|P\rangle = 0. \tag{26}$$

The standard ket $|S\rangle$ must satisfy these restrictions,

$$\beta|S\rangle = 0. \tag{27}$$

This means that the operators β must be included in the set of operators κ_λ.

The restriction [26] becomes, with the help of [25],

$$\beta\phi|S\rangle = 0$$

or, from [27],

$$[\beta, \phi]|S\rangle = 0.$$

Thus if we restrict ϕ to involve only quantities that commute with the β's, the ket $\phi|S\rangle$ necessarily satisfies the conditions [26] and so represents a physical state. It is sufficient to consider only such ϕ's to get all physical states.

QUANTIZATION: ELECTRODYNAMICS

In electrodynamics the natural way of choosing the standard ket $|S\rangle$ is to take it to correspond to the vacuum state, for which there are no electrons, positrons, or photons present. A difficulty arises here in that one does not know precisely what mathematical conditions [23] to take for this ket.

The usual procedure is to make a Fourier resolution of the various field quantities ψ, $\bar{\psi}$, B_r, F^{rs} and interpret the various coefficients as emission and absorption operators of electrons, positrons, and photons. One then defines the vacuum state as the state to which the application of any absorption operator gives zero. The objection to this procedure is that the vacuum state defined in this way does not satisfy the equations of motion. If one starts off with this state, after a lapse of time there will be some electrons, positrons, and photons existing, forming what are usually called the vacuum fluctuations of the electromagnetic field. Physically this is not correct. The vacuum state ought to remain unchanged.

The difficulty is the same in the usual formulation of electrodynamics as in the present gauge-invariant formulation. It must mean that the Hamiltonian is wrong in some fundamental way. No better Hamiltonian is known at

present. So we have the situation that we cannot define accurately the vacuum state. We therefore have to work with a standard ket $|S\rangle$ which is ill-defined. One can, however, do many calculations without using the accurate conditions [23] and the successes of quantum electrodynamics are obtained in this way.

Let us ignore the difficulty and suppose we have a standard ket $|S\rangle$ representing the vacuum state. Any other ket can then be expressed as $\phi|S\rangle$, ϕ being some operator. We now take over the Hamiltonian [7] or [22] and the supplementary conditions [9] into the quantum theory. For this purpose we must express all the field quantities in [7] or [22] and [9] in terms of emission and absorption operators and then arrange that in any product containing both emission and absorption operators as factors, the emission operators are all to the left of the absorption operators. This rearrangement causes the Hamiltonian [7] or [22] and the left-hand side of [9] to change by certain infinite quantities, which will be denoted by k_H and $k(x)$. $k(x)$ must be a constant while k_H may also contain terms linear in the A's.

The supplementary conditions now read

$$(B_r{}^r+e\bar{\psi}\psi+k)\phi|S\rangle = 0 \tag{28}$$

for all x. They must be satisfied by the standard ket $|S\rangle$, so

$$(B_r{}^r+e\bar{\psi}\psi+k)|S\rangle = 0. \tag{29}$$

We now see that [28] is satisfied provided ϕ commutes with $B_r{}^r+e\bar{\psi}\psi$, that is, provided ϕ is gauge invariant.

If ϕ involves only the electromagnetic field variables B_r, F^{rs}, the state $\phi|S\rangle$ has only photons and no electrons or positrons. To get a state with one electron, we must take ϕ to be linear in the gauge-invariant operators $\psi_a{}^*(x)$, thus

$$\phi|S\rangle = \int z_a(x)\,\psi_a{}^*(x)\,d^3x\,|S\rangle, \tag{30}$$

where the coefficients $z_a(x)$ may involve $B_r(x')$, $F^{rs}(x')$ for all values of x'. Similarly, to get a state with two electrons we must take ϕ to be quadratic in the ψ^*'s, and so on. For positrons one must replace ψ^* by $\bar{\psi}^*$.

The representation of states in this way is not unique, i.e., corresponding to a given state there are many ϕ's. Without having $|S\rangle$ well-defined one cannot formulate precisely which ϕ's correspond to the same state.

THE ELECTRON EMISSION OPERATOR

The ket

$$\psi_a{}^*(x)|S\rangle = \psi_a(x)e^{iC(x)}|S\rangle \tag{31}$$

represents a state for which there is one electron, situated at the point x. Let us examine the electric field around this electron. We have

$$\begin{aligned} B'_r\,\psi_a{}^*\,|S\rangle &= \psi_a{}^*\,B'_r\,|S\rangle + i\hbar[B'_r,\,\psi_a{}^*]|S\rangle \\ &= \psi_a{}^*\,B'_r\,|S\rangle - \hbar\psi_a{}^*[B'_r,\,C]|S\rangle \\ &= \psi_a{}^*\{B'_r+\hbar\,c_r(x\,x')\}|S\rangle \end{aligned} \tag{32}$$

from [17]. The physical interpretation of this result is that the value of the electric field $B_r(x')$ for the state $\psi_a{}^*|S\rangle$ exceeds its value for the vacuum state

$|S\rangle$ by $\hbar c_r(x\,x')$. If we take the spherically symmetrical solution [19] for $c_r(x\,x')$, the excess electric field is just the Coulomb field of the electron at the point x, with the system of units here used, (the charge on the electron being $+e$). With any other solution for $c_r(x\,x')$, the excess electric field is the Coulomb field plus a field of pure electromagnetic radiation.

We can now see that the operator $\psi^*(x)$ is the operator of creation of an electron *together with its Coulomb field*, or possibly the operator of absorption of a positron *together with its Coulomb field*. It is to be contrasted with the operator $\psi(x)$, which gives the creation or absorption of a bare particle. *A theory that works entirely with gauge-invariant operators has its electrons and positrons always accompanied by Coulomb fields around them*, which is very reasonable from the physical point of view.

By taking various solutions of [18] for $c_r(x\,x')$ one can get the ket [31] to represent the state of one electron at the point x with its Coulomb field and with various possible distributions of photons. However, not all distributions of photons accompanying an electron can be described in this way, but only a certain simple class of them. To get a general photon distribution one must multiply [31] by a function of B_r' and F'^{rs} at all points x'.

One might decide to work always with the spherically symmetrical $c_r(x\,x')$ given by [19]. The convenient way of proceeding is then to resolve the electric field B_r into a part consisting only of transverse waves, B_r^t, whose divergence vanishes, and a part consisting only of longitudinal waves, B_r^l, whose curl vanishes. With the spherically symmetrical $c_r(x\,x')$ it is easily verified that B_r^t commutes with all the ψ^*'s. Thus equation [32] becomes, with x and x' interchanged,

$$B_r^l\,\psi_a'^*\,|S\rangle = \psi_a'^*\left\{B_r^l+\frac{e}{4\pi}\frac{x_r-x_r'}{|x-x'|^3}\right\}|S\rangle. \tag{33}$$

If we could define the vacuum state so as to have no particles, we should expect it to have no longitudinal electric field, so that

$$B_r^l\,|S\rangle = 0. \tag{34}$$

Then [33] reduces to

$$B_r^l\,\psi_a'^*\,|S\rangle = \frac{e}{4\pi}\frac{x_r-x_r'}{|x-x'|^3}\,\psi_a'^*\,|S\rangle. \tag{35}$$

This means that the state $\psi_a'^*|S\rangle$, having an electron located at the point x', is an eigenstate of the longitudinal part of the electric field at all points, the eigenvalues being just the Coulomb field. The result can easily be extended to any distribution of electrons. B_r^l is always equal to the total Coulomb field.

The electric energy term in the Hamiltonian becomes

$$\tfrac{1}{2}\int B_r\,B_r\,d^3x = \tfrac{1}{2}\int(B_r^t\,B_r^t+B_r^l\,B_r^l)\,d^3x, \tag{36}$$

the cross terms vanishing. When this energy operator is applied to a ket $\phi|S\rangle$ representing any distribution of electrons, with no positrons, the above result shows that the longitudinal part $\frac{1}{2}\int B_r^l\,B_r^l\,d^3x$ is just equal to the energy of the Coulomb field of the electrons. This energy may be expressed, in inte-

grated form, as the sum of an interaction energy $e^2/4\pi r$ for each pair of electrons, together with an infinite self-energy for each electron. *The theory now becomes identical with the usual quantum electrodynamics after elimination of the longitudinal electromagnetic waves.*

We can now see the significance of the usual method of elimination of the longitudinal waves. It implies that one looks upon each electron as always surrounded by a spherically symmetrical Coulomb field, and any departures from this field are ascribed to the existence of photons. The method provides us with a definite basis for making calculations, but one can see that it is not always suitable physically.

Suppose for example that we are dealing with a state having an electron moving with a definite velocity in the absence of photons. (Velocity here means average velocity, without the "Zitterbewegung".) It would be reasonable to associate the electron with, not a spherically symmetrical Coulomb field, but a Coulomb field subjected to the Lorentz–Fitzgerald contraction appropriate to its velocity. We should thus take for $c_r(x\,x')$ the solution [19] distorted by the Lorentz–Fitzgerald contraction. With ψ^* so defined and with the coefficients $z_a(x)$ in [30] chosen to give plane waves, we should have the best representation of the one-electron state that is possible with the present imperfect theory. It is an imperfect theory because the ket representing the one-electron state, like that representing the vacuum state, does not satisfy the equations of motion.

THE MOMENTUM

The total momentum M^r has the property that, for any field quantity $\xi(x)$,

$$[\xi, M^r] = \xi^r. \tag{37}$$

It is easily verified that if we take

$$M^r = \int (B_s A^{sr} + \Re i\hbar\bar{\psi}\gamma^r\psi^r)d^3x, \tag{38}$$

it has the desired property, for $\xi = A^s$, B_s, ψ, or $\bar{\psi}$, e.g.,

$$[A^s, M^r] = \int [A^s, B'_t A'^{tr'} + \Re\, i\hbar\, \bar{\psi}'\psi'^{r'}]\, d^3x'$$
$$= \int \delta^s_t\, \delta(x-x')\, A'^{tr'}\, d^3x' = A^{sr}.$$

This property is sufficient to fix M^r except for an arbitrary additive constant. The constant is fixed by the requirement that M^r applied to the vacuum state shall be zero. M^r is then completely determined.

We must check that the expression [38] for M^r is gauge invariant. It may be written

$$M^r = \int (B_s F^{rs} + B_s A^{rs} + \Re i\hbar\bar{\psi}\gamma^r\psi^r)d^3x$$
$$= \int \{B_s F^{rs} + \Re\bar{\psi}^*(i\hbar\psi^r + eA^r\psi)e^{iC}\}d^3x - \int A^r(B_s{}^s + e\bar{\psi}\psi)d^3x. \tag{39}$$

The first of these terms is evidently gauge invariant. The second vanishes with the classical supplementary condition [9]. However, with the extra infinite constant term in the quantum supplementary condition [28] it does not vanish

and a difficulty arises. Evidently some change must be made in the theory, involving a more precise handling of the infinities, so that the second term vanishes also in the quantum theory.

The first term in [39] then gives the total momentum. The part $\int B_r F^{r1}\, d^3x$ just gives the momentum of the electromagnetic field, described by the Poynting vector. The remainder must be the momentum of the electrons.

DISCRETE FARADAY LINES OF FORCE

The equation [18] has a certain discrete type of solution which is of interest. Take

$$[40] \qquad \begin{cases} c_1(x\,x') = -e\hbar^{-1}\epsilon(x_1-x_1')\,\delta(x_2-x_2')\,\delta(x_3-x_3'), \\ c_2(x\,x') = c_3(x\,x') = 0, \end{cases}$$

where the function $\epsilon(x)$ is

$$\epsilon(x) = 1 \text{ for } x > 0$$
$$= 0 \text{ for } x < 0.$$

[40] is a solution of [18] and it gives for C a line integral

$$[41] \qquad C = -e\hbar^{-1}\int_{-\infty}^{x_1} A^1(x_1'\,x_2\,x_3)\,dx_1'.$$

More generally, we may take for C any line integral

$$[42] \qquad C = -e\hbar^{-1}\int_{-\infty}^{x} A^r dx_r'$$

extending from infinity to the electron point x. Such a C will make $\psi^*(x) = \psi(x)e^{ic}$ gauge invariant.

Each choice of C corresponds to a choice of electric field around the electron. The choice [42] corresponds to the electric field being all concentrated in a single Faraday line of force, extending from the electron to infinity. The choice [41], which is more specific, makes the Faraday line of force extend in a straight line in the direction of the negative x_1-axis.

One of the most fundamental unexplained features of present-day physics is the fact that electric charge always occurs in multiples of the electronic charge e. A reasonable attempt at an explanation could be founded on the assumption that quantization of the electromagnetic field results in the electric field being composed of discrete Faraday lines of force, each associated with the charge e, so that there is just one line ending on each charge e. The lines would then be the elementary concept in terms of which the whole theory of electrons and the electromagnetic field would have to be built up. Closed lines would be interpreted as photons and open lines would have their ends interpreted as electrons or positrons.

With such a theory it would be necessary, of course, to depart from the usual expression for the energy of the electric field, given by the last term in the integrand of [7], since this expression would have an infinite value for a

discrete Faraday line of force. We have seen that the Hamiltonian needs modification in any case, and we have here a possible basis for seeking a new one. A representation of the discrete lines of force could be provided by the use of operators $\psi^*(x)$ defined with C of the form [42].

REFERENCE

1. DIRAC, P. A. M. Ann. inst. Henri Poincaré, 13: 1. 1952.

THE FLUCTUATING FIELD MODEL OF FERROMAGNETISM WITH PARTICULAR REFERENCE TO NICKEL[1]

By F. D. Stacey

ABSTRACT

Following Néel's calculations of fluctuations in intermolecular field, a model is suggested in which there is a mutual repulsion of elementary magnets, so that spontaneous magnetization is affected by a process of ordering of the magnets on the lattice sites as well as the ordering in orientation. Specific heat considerations indicate that, if it occurs, the second disordering process is also complete at the Curie point. To explain the observed spontaneous magnetization of nickel it is necessary to assume coupled electron spins and appreciable next-nearest neighbor exchange interactions.

1. INTRODUCTION

Néel (6, 7, 8) showed substantial correlation between the "anomalous" specific heat above the Curie temperature, θ_f, of a ferromagnetic, the difference between this and the paramagnetic Curie temperature θ_p, and the curvature of the $(1/\chi - T)$ graph above θ_f, in terms of fluctuations of the intermolecular field, for which the same parameter was required to explain all the observations. The calculations were based on two alternative models, neither of which bears close resemblance to the accepted structure of a ferromagnetic, but the meaning is clearly that elementary magnets being positive $3d$ holes are considered to have freedom of movement through a sea of $4s$ (conduction) electrons, but at any instant of time to have distinct positions. This approach has been criticized (12), being a contradiction of band theory in general and the collective electron theory of ferromagnetism in particular. Three developments of Néel's theory are needed:

(i) Postulation of a more acceptable model in terms of recognized lattice structure.

(ii) Introduction of band theory of which the success is too great for a serious model to ignore.

(iii) Extension of the theory to explain the marked divergence at low temperatures of present experimental and theoretical spontaneous magnetization curves.

The present paper is an attempt to deal with requirements (i) and (iii) simultaneously, so that some conclusion regarding (ii) can be drawn from its success or failure.

The model considered is a face-centered cubic lattice, of which only a known proportion of the lattice sites are occupied by elementary magnets. The proportion is 0.604 or 0.302 for the cases of the elementary magnets being single or coupled electron spins respectively. The magnets are allowed freedom of spontaneous transfer between lattice sites subject to the conditions that there

[1]*Manuscript received July 14, 1955.*
Contribution from the Department of Physics, University of British Columbia, Vancouver, Canada.

is no double occupation of any lattice site, and that the magnets experience a spin-independent mutual repulsion in addition to exchange interaction. This repulsion may arise electrostatically by virtue of the positive charges associated with the magnets. It is represented by mutual potential energies E_1 and E_2 due to repulsions between pairs of magnets on nearest and next nearest neighboring sites.

A thermal rearrangement of elementary magnets on the lattice sites causes changes in the numbers of nearest neighbors to the magnets and hence in the intermolecular field. The ordered and disordered limits of this thermal rearrangement are considered, to determine the conditions under which the model is sufficient to explain the observed variation in intermolecular field in nickel.

No further consideration is given to Néel's problem of fluctuations, but the model is designed to give fluctuations in intermolecular field by virtue of fluctuating numbers of nearest neighbors.

2. SPONTANEOUS MAGNETIZATION AND INTERMOLECULAR FIELD AS FUNCTIONS OF TEMPERATURE

The quantum-corrected Weiss theory gives values of reduced spontaneous magnetization, σ/σ_0, as a function of reduced temperature, T/θ_f, which are in reasonable agreement with experiment, being closest for uncoupled spins ($s = \frac{1}{2}$). Most tables of comparative values, such as Mott and Jones (4, p. 221), show that the disagreement is greatest at high temperatures, being about 10% at $T/\theta_f = 0.9$. Table I is designed to show that the major disagreement does in fact lie at low temperatures where small differences in σ/σ_0 are critical. It is particularly important to make this comparison since Néel (8, p. 131) showed that the high temperature discrepancy disappears if θ_p is used in T/θ. Table I gives values of intermolecular field which are needed to explain the

TABLE I

TEMPERATURE DEPENDENCE OF INTERMOLECULAR FIELD IN NICKEL

$\frac{T}{\theta}$	$\frac{\sigma}{\sigma_0}$	$\left(\frac{F}{F_\theta}\right)_{s=\frac{1}{2}}$	$\left(\frac{F}{F_\theta}\right)_{s=1}$
0	1.0		0.115*
0.05	0.998_{75}	0.185	0.246_4
0.1	0.996_0	0.312	0.369_8
0.2	0.987_5	0.513	0.593_2
0.3	0.976_6	0.682	0.773_4
0.4	0.958_8	0.807	0.895_3
0.5	0.934	0.904	0.989
0.6	0.892	0.963	1.033
0.7	0.830	1.002	1.055
0.8	0.737	1.025	1.061
0.9	0.582	1.030	1.047
0.95	0.451	1.024	1.034
1.0	0.0	1.0	1.0

**Extrapolated graphically.*

observed spontaneous magnetization of nickel, by the simple, quantum-corrected Weiss theory, with $s = \frac{1}{2}$ and $s = 1$. Experimental values are those

of Weiss and Forrer (15), making use of reductions given by Bozorth (2, p. 720) and Myers and Sucksmith (5). The use of slightly different figures quoted by Mott and Jones (4) shows that the observed variation of intermolecular field is not seriously modified by a different choice of experimental results. Columns 3 and 4 of Table I give intermolecular field, F, in terms of its value F_θ at θ_f, calculated from the appropriate reductions of the Brillouin function:

[1a] $$s = \tfrac{1}{2}: \quad \frac{\sigma}{\sigma_0} = \tanh\left(\frac{F}{kT}\cdot\frac{\sigma}{\sigma_0}\right), \quad F_\theta = k\theta;$$

[1b] $$s = 1: \quad \frac{2-\sqrt{4-3(\sigma/\sigma_0)^2}}{\sigma/\sigma_0} = \tanh\left(\frac{F}{2kT}\cdot\frac{\sigma}{\sigma_0}\right), \qquad F_\theta = \frac{3}{2}k\theta.$$

The first observation from Table I is that the problem is not essentially different with $s = \frac{1}{2}$ and $s = 1$, although its explanation in terms of ordering processes is only possible with $s = 1$.

3. NUMBERS OF NEAREST AND NEXT-NEAREST NEIGHBORS

The face-centered cubic structure may be divided into four completely equivalent sublattices. In any unit cell they are represented by the cell corners and each opposite pair of cube faces. Each lattice site has 12 nearest neighbors, of which there are four on each of the other three sublattices, and six next-nearest neighbors, all on its own sublattice. We may find expressions for the average number of nearest and next-nearest magnetic neighbors for n magnets disposed on four sublattices each with $\frac{1}{4}N$ sites, and occupied by w, x, y, z magnets respectively, so that

[2] $$w+x+y+z = n.$$

The average number of nearest neighbors to each magnet on the w sublattice is

$$4\frac{x}{N/4}+4\frac{y}{N/4}+4\frac{z}{N/4} = \frac{16}{N}(x+y+z).$$

Giving this the weight w/n for the w magnets and adding similar expressions for magnets on the other sublattices we find the average number of occupied neighboring sites for each elementary magnet:

$$\eta = \frac{32}{Nn}(wx+wy+wz+xy+xz+yz).$$

A similar argument gives the average number of next-nearest neighbors:

$$\eta' = \frac{24}{Nn}(w^2+x^2+y^2+z^2).$$

These may be combined through equation [2] to give

$$\frac{\eta}{16}+\frac{\eta'}{24} = \frac{n}{N}.$$

We are interested in finding the maximum allowable ranges of variation of η and η' with values 0.604 and 0.302 for n/N, corresponding to $s = \frac{1}{2}$ and $s = 1$ respectively in nickel. $\eta_{\max}$ is realized when $w = x = y = z = \frac{1}{4}n$ (com-

plete disorder) and $\eta_{\min}$ is found by filling first one sublattice and then another, and so on until the required number of elementary magnets have been used (ordered state). We first make an assumption, which is reconsidered for the calculation in §4, that there is no process of ordering within each sublattice, but simply a rearrangement of elementary magnets between them. This yields:

	$s = \frac{1}{2}$	$s = 1$
Ordered state:	$\eta = 7.3$	$\eta = 3.6$
	$\eta' = 3.6$	$\eta' = 1.8$
Disordered state:	$\eta = 6.1$	$\eta = 1.4$
	$\eta' = 5.4$	$\eta' = 5.2$

Although it is a substantial approximation which detracts from the point of the present approach, we may consider the intermolecular field at each magnet to be that due to interaction with the average number of nearest neighbors:

$$F = \eta J_1 + \eta' J_2$$

where J_1 and J_2 are nearest and next-nearest neighbor exchange interactions. Using the value of F/F_θ extrapolated to 0°K. and the above values of η and η' we find, assuming the variation of F in Table I to be due to changes in η and η', the following relations between J_1 and J_2:

$s = \frac{1}{2}$: $J_2 \leqslant -1.04\, J_1$
$s = 1$: $J_2 \leqslant -0.2\, J_1$ (equality signs if disorder is complete at θ_f).

In fact this approximation requires negative next-nearest neighbor interaction, being impossibly large for $s = \frac{1}{2}$. The same difficulty regarding $s = \frac{1}{2}$ is found in the more exact approach which can be made in the limiting case of low temperatures.

4. THE APPROACH TO ABSOLUTE SATURATION AT 0°K.

Plotted on a σ/σ_0 vs. T/θ_f curve, experimental results can be fitted to the Bloch law (1):

$$1 - \sigma/\sigma_0 = C(T/\theta)^{3/2}$$

up to about $T/\theta = 0.3$. This fact is remarkable in view of the approximations made in its derivation which restrict the range of validity almost to immeasurably low temperatures, so that the experimental and theoretical laws must be regarded as independent. This view has been expressed by Néel (9) as an interpretation of the formula developed by Schafroth (11) giving important higher powers of (T/θ). The same implication can be made from the earlier less complete formula of Opechowski (10). Table I gives an alternative method of viewing the experimental values which does not indicate a $T^{3/2}$ law, since this law would put $F = 0$ at the 0°K. extrapolation. It thus appears that insensitivity of the (σ/σ_0) vs. (T/θ) curve to the exact function of (T/θ) tends to mask the nature of their interdependence.

The limiting intermolecular field at 0°K. on the four-sublattice model is readily calculable and may be compared with that at the Curie point. If $s = \frac{1}{2}$, then $n/N = 0.604$ (Bohr magnetons per atom), so that at complete order every elementary magnet has at least four others as nearest neighbors as compared with the disordered average 7.3. This makes the wide range of observed values of F (Table I) impossible to explain without assuming an unacceptably large negative value of J_2. Further considerations are therefore restricted to coupled spins, $s = 1$, $n/N = 0.302$.

In the ordered state we may regard the w sublattice as being filled, leaving $0.052N$ magnets for the x sublattice. Assuming that these are uniformly spread throughout the structure, each providing a nearest neighbor for four w magnets, none of which has two nearest neighbors, then there are $(0.25N - 4\times 0.052N) = 0.046N$ w magnets with no nearest neighbors, experiencing only the weak field of next-nearest neighbor interactions. It is reasonable to expect that $J_1 \gg J_2$, whence we may assume that at low temperatures almost all of the observed value of $(1-\sigma/\sigma_0)$ is accounted for by such magnets, since they have the highest probability of being antiparallel to the domain direction. Multiplying the values of $(1-\sigma/\sigma_0)$ by 0.302/0.046 to find the corresponding values for the $0.046N$ magnets alone and substituting these into equation [1*b*] we can obtain a graphical extrapolation $F_0/F_\theta = 0.08$ for these magnets alone. Since it is a reasonable approximation to consider the field at the Curie temperature to be that due to the average number of nearest neighbors in the disordered state we may put

$$\frac{6J_2}{3\cdot 6J_1 + 1\cdot 8J_2} = 0\cdot 08,$$

whence

[3] $$J_2 = 0.04\, J_1.$$

5. SPECIFIC HEAT CONTRIBUTION OF THE SECOND ORDERING PROCESS

The parameters E_1, E_2 have been introduced without restriction as to magnitude, which must however be similar to the exchange energies to spread the process of ordering of elementary magnets on the lattice sites over the same temperature range as the alignment process. The calculations of Néel (8), substituting θ_p for θ_f in T/θ, can be extended to show that this change roughly cancels the excess of (F/F_θ) over unity in the range $0.5 < T/\theta < 1.0$, so that to a first approximation we may regard disorder as being complete by about $T/\theta = 0.5$. It is however necessary to examine the process to establish the absence (at high temperatures) of an ordering "tail" which could give a specific heat contribution and add to $(\theta_p - \theta_f)$. The examination as made is subject to Néel's fluctuation correction, being a consideration of free energy above the Curie point.

Use is made of the requirement that the free energy F of the system must be a minimum, where

[4] $$F = E - KT \ln A.$$

E is the energy, which if spontaneous magnetization, even locally, is zero, reduces to

$$E = \frac{n}{2}(\eta E_1 + \eta' E_2) = \frac{8n^2}{N} E_1 - \frac{(8E_1 - 12E_2)}{N} (w^2 + x^2 + y^2 + z^2)$$

by neglecting all terms not connected with the ordering. A is the number of arrangements of the system with the distribution w, x, y, z of magnets and is easily shown to be given by

$$\ln A = -\frac{N}{4} \sum \left\{ \left(1 - \frac{4w}{N}\right) \ln\left(1 - \frac{4w}{N}\right) + \frac{4w}{N} \ln\left(\frac{4w}{N}\right) \right\}.$$

Differentiation of F with respect to changes of the type $\Delta x = -\Delta w$, $\Delta y = 0 = \Delta z$ and equating ΔF to zero for equilibrium at any temperature yields three equations connecting w, x, y, z, which with equation [2] may be used to find E. Numerical calculations show a λ-point discontinuity in dE/dT due to this process, and that the system approaches complete disorder catastrophically at a critical temperature in a manner similar to the more simple two-sublattice model. The peak value of excess specific heat is about $0.8R$ which specific heat measurements (13) show to be far greater than any observed anomaly above θ_f in nickel. It is therefore concluded that disorder is complete at θ_f, and that E_1 is of the order $\frac{1}{2}J_1$.

It must be remembered that this approach is not statistical and is subject to the Néel fluctuation correction.

6. CONCLUSION

Tables comparing experimental values of reduced spontaneous magnetization, σ/σ_0, as a function of reduced temperature, T/θ, with values calculated from the quantum-corrected Weiss theory are misleading in the respect that they indicate the important disagreement to be at the higher temperatures.

Table I gives the values of intermolecular field which are needed to explain the observed variation of σ/σ_0 in nickel, assuming correctness of the Weiss approach in all respects except invariability of the field constant. It shows that at 0°K. this constant extrapolates to 1/10th of its Curie point value. This is a significant disagreement with the $T^{3/2}$ law, generally regarded to hold at low temperatures, which would require the Weiss field constant to extrapolate to zero. The disagreement is not apparent from a direct consideration of the values of σ/σ_0.

The postulated model of wandering elementary magnets, discretely located at the lattice sites of a face-centered cubic structure, and subject to a spin-independent mutual repulsion as well as a larger exchange interaction, is found capable of explaining the 10:1 variation in field constant provided that:

(i) 0.302 coupled spins per lattice site are assumed,

(ii) next-nearest neighbors exchange energy is 4% of that for nearest neighbors.

The concept of an ordering process which may occur in pure metals, as a consequence of the non-integral Bohr magneton numbers which are observed experimentally, is more general than the ordering of alloys as considered by Goldman (3) and Smoluchowski. It follows more closely the approach proposed by Van Vleck and Hurwitz (14), who point out that some measure of

compromise with collective electron theory is made necessary by neutron diffraction results.

Such a compromise must come through a modification of the assumption that the elementary magnets occupy discrete lattice sites. It simplifies the problem to assume instead that they have probability distributions over the lattice sites with unequal probabilities of occupying each of the four sublattices of the face-centered cubic structure. The intermolecular field will then be an average over all lattice sites of the field which a discretely located magnet would experience, weighted according to the probability of occupation of the sites. This leads to the conclusion of §3 that next-nearest neighbor exchange interaction is negative with a value one fifth that for nearest neighbors.

Calculations for the two sublattices of body-centered iron are simpler, but in this case it is difficult to decide how the spins are coupled, being in excess of two per atom unless a 10% orbital contribution is allowed, in which case all lattice sites are occupied and the simple ordering process visualized here cannot appear.

REFERENCES

1. BLOCH, F. Z. Physik, 61: 206. 1930.
2. BOZORTH, R. M. Ferromagnetism. D. Van Nostrand Company, Inc., New York. 1951.
3. GOLDMAN, J. E. J. Appl. Phys. 20: 1131. 1949.
4. MOTT, N. F. and JONES, H. The theory of the properties of metals and alloys. Oxford University Press, London. 1936.
5. MYERS, H. P. and SUCKSMITH, W. Proc. Roy. Soc. (London), A, 207: 427. 1951.
6. NÉEL, L. Ann. phys. 18: 5. 1932.
7. NÉEL, L. J. phys. radium, 5: 104. 1934.
8. NÉEL, L. Le magnetism II. Inst. intern. cooperation intellectuelle. Strasbourg Conference. p. 65. 1940.
9. NÉEL, L. J. phys. radium, 15: 74S. 1954.
10. OPECHOWSKI, W. Physica, 4: 715. 1937.
11. SCHAFROTH, M. R. Proc. Phys. Soc. (London), A, 67: 33. 1954.
12. STONER, E. C. Repts. Progr. in Phys. 11: 43. 1947.
13. SYKES, C. and WILKINSON, H. Proc. Phys. Soc. (London), 50: 834. 1938.
14. VAN VLECK, J. H. Revs. Mod. Phys. 25: 220. 1953.
15. WEISS, P. and FORRER, R. Ann. phys. 5: 153. 1926; 12: 279. 1929.

LONG RANGE FORCES BETWEEN HYDROGEN MOLECULES[1]

By F. R. Britton and D. T. W. Bean

ABSTRACT

Long range forces between two hydrogen molecules are calculated by using methods developed by Massey and Buckingham. Several terms omitted by them and a corrected numerical factor greatly change results for the van der Waals energy but do not affect their results for the static quadrupole–quadrupole energy. By using seven approximate ground state H_2 wave functions information is obtained regarding the dependence of the van der Waals energy on the choice of wave function. The value of this energy averaged over all orientations of the molecular axes is found to be approximately $-11.0\,R^{-6}$ atomic units, a result in close agreement with semiempirical values.

INTRODUCTION

Massey and Buckingham (7) have calculated the static quadrupole–quadrupole and the dynamic dipole–dipole (van der Waals) interaction energies between two hydrogen molecules, but in making their calculation they omitted several terms that have a large effect on the results obtained for the van der Waals energy. These terms are included in the present treatment and a numerical factor has been corrected.

The methods used by Massey and Buckingham are outlined in order to show where the present treatment differs from the original one and to facilitate reading. The original treatment is referred to by numbering in the form M.B. 1.

METHODS

The Hasse variational method is applied to the function $\Psi(1+\lambda v)$, where Ψ is a wave function for two non-interacting molecules, λ is a parameter, and v is the molecular interaction potential. To a second order of approximation the minimized interaction energy is given by M.B. 9 as

$$[1] \qquad \epsilon_v = \frac{1}{a}\left[\int \Psi^* v \Psi d\tau - \frac{2m\{\int \Psi^* v^2 \Psi d\tau - (1/a)(\int \Psi^* v \Psi d\tau)^2\}^2}{\hbar^2 \int \Psi^* \sum_i (\nabla_i v)^2 \Psi d\tau}\right],$$

where $a = \int \Psi^* \Psi \, d\tau$ and $i = 1, 2, 3, 4$ are electron coordinates.

An alternative second order perturbation treatment gives M.B. 10 as

$$[2] \qquad \epsilon_p = \frac{1}{a}\left[\int \Psi^* v \Psi d\tau + \frac{1}{E_0}\left\{\int \Psi^* v^2 \Psi d\tau - \frac{1}{a}(\int \Psi^* v \Psi d\tau)^2 + \sum_{s \neq 0} \frac{E_s |\int \Psi_s^* v \Psi d\tau|^2}{E_0(E_0 - E_s)}\right\}\right],$$

where E_0 is the ground state energy and E_s that of another state of the non-interacting binary molecular system.

Electrons 1, 2 are assigned to molecule A and electrons 3, 4 to molecule B. The vector joining the mass centers of the molecules is $\mathbf{R}$; $\mathbf{d}_A$ and $\mathbf{d}_B$ join the nuclei of molecules A and B respectively; $\mathbf{r}_1$, $\mathbf{r}_2$ are position vectors of electrons

[1]*Manuscript received June 22, 1955.*
Contribution from Department of Mathematics, Hamilton College, McMaster University, Hamilton, Ontario.

in molecule A and $\mathbf{r}_3, \mathbf{r}_4$ position vectors of electrons in molecule B. The molecular axes are inclined to R at angles $\alpha = (\mathbf{d}_A, \mathbf{R})$, $\beta = (\mathbf{d}_B, \mathbf{R})$ and θ is the angle between the projections of $\mathbf{d}_A$ and $\mathbf{d}_B$ on a plane perpendicular to $\mathbf{R}$.

$$[3] \qquad \Psi = \psi(\mathbf{r}_1, \mathbf{r}_2)\, \psi(\mathbf{r}_3, \mathbf{r}_4),$$

where ψ is a normalized ground state H_2 wave function. $d_A = d_B = d_0$, where d_0 is the equilibrium internuclear distance in H_2.

Only the terms in the asymptotic expansion of v involving R^{-5} and R^{-3} are required, and these are labelled v_1 and v_2. v_1 gives the static quadrupole–quadrupole energy, varying as R^{-5}, when used in place of v in the first integral of [1] or [2]. The van der Waals energy, varying as R^{-6}, is given when v is replaced by v_2 in those integrals in [1] and [2] that involve v^2 and in $\sum_i (\nabla_i v)^2$ in [1]. The final summation term is neglected in the calculation of van der Waals energy from [2]. All other integrals in [1] and [2] are zero to the order R^{-6}.

THE VAN DER WAALS ENERGY*

$$[4] \qquad v_2 = \frac{1}{R^3} \sum_p \sum_q e_p e_q [3(\mathbf{r}_p \cdot \mathbf{R}_0)(\mathbf{r}_q \cdot \mathbf{R}_0) - (\mathbf{r}_p \cdot \mathbf{r}_q)],$$

where $p = 1, 2$ and $q = 3, 4$ for electrons; $\mathbf{r}_p = \pm \frac{1}{2}\mathbf{d}_A$, $\mathbf{r}_q = \pm \frac{1}{2}\mathbf{d}_B$ for nuclei; $\mathbf{R}_0 = \mathbf{R}/R$; $e_p = e_q = -e$ for electrons and $e_p = e_q = e$ for nuclei.

Symmetry properties of ground state H_2 wave functions are used after squaring [4] and after squaring $\nabla_i v_2$ to give expressions for use in [1] and [2] as follows:

$$\begin{aligned}[5] \qquad (v_2)_e^2 = \frac{4e^4}{R^6}[&(\mathbf{r}_1 \cdot \mathbf{r}_3)^2 + (\mathbf{r}_1 \cdot \mathbf{r}_3)(\mathbf{r}_1 \cdot \mathbf{r}_4) + (\mathbf{r}_1 \cdot \mathbf{r}_3)(\mathbf{r}_2 \cdot \mathbf{r}_3) + (\mathbf{r}_1 \cdot \mathbf{r}_3)(\mathbf{r}_2 \cdot \mathbf{r}_4) \\ &+ 9\{(\mathbf{r}_1 \cdot \mathbf{R}_0)^2 (\mathbf{r}_3 \cdot \mathbf{R}_0)^2 + (\mathbf{r}_1 \cdot \mathbf{R}_0)(\mathbf{r}_2 \cdot \mathbf{R}_0)(\mathbf{r}_3 \cdot \mathbf{R}_0)^2 \\ &+ (\mathbf{r}_3 \cdot \mathbf{R}_0)(\mathbf{r}_4 \cdot \mathbf{R}_0)(\mathbf{r}_1 \cdot \mathbf{R}_0)^2 + (\mathbf{r}_1 \cdot \mathbf{R}_0)(\mathbf{r}_2 \cdot \mathbf{R}_0)(\mathbf{r}_3 \cdot \mathbf{R}_0)(\mathbf{r}_4 \cdot \mathbf{R}_0)\} \\ &- 6\{(\mathbf{r}_1 \cdot \mathbf{r}_3)(\mathbf{r}_1 \cdot \mathbf{R}_0)(\mathbf{r}_3 \cdot \mathbf{R}_0) + (\mathbf{r}_1 \cdot \mathbf{r}_3)(\mathbf{r}_1 \cdot \mathbf{R}_0)(\mathbf{r}_4 \cdot \mathbf{R}_0) \\ &+ (\mathbf{r}_1 \cdot \mathbf{r}_3)(\mathbf{r}_2 \cdot \mathbf{R}_0)(\mathbf{r}_3 \cdot \mathbf{R}_0) + (\mathbf{r}_1 \cdot \mathbf{r}_3)(\mathbf{r}_2 \cdot \mathbf{R}_0)(\mathbf{r}_4 \cdot \mathbf{R}_0)\}], \end{aligned}$$

and

$$\begin{aligned}[6] \qquad \sum_i (\nabla_i v_2)_e^2 = \frac{4e^4}{R^6}[&2r_1^2 + 2(\mathbf{r}_1 \cdot \mathbf{r}_2) + 3(\mathbf{r}_1 \cdot \mathbf{R}_0)^2 + 3(\mathbf{r}_3 \cdot \mathbf{R}_0)^2 + 3(\mathbf{r}_1 \cdot \mathbf{R}_0)(\mathbf{r}_2 \cdot \mathbf{R}_0) \\ &+ 3(\mathbf{r}_3 \cdot \mathbf{R}_0)(\mathbf{r}_4 \cdot \mathbf{R}_0)]. \end{aligned}$$

If molecular symmetry properties are used before squaring [4] and $\nabla_i v_2$,

**The form [4] is used for v_2 in order to compare our revised results with those given by Massey and Buckingham. The development is made somewhat easier by using the Cartesian form*

$$v_2 = \frac{1}{R^3} \sum_p \sum_q e_p e_q (2z_p z_q - x_p x_q - y_p y_q),$$

where the z axes are in the direction $\mathbf{R}$*, and transforming coordinates for v_2^2 by rotation of the z axes to axes along the molecular axes.*

only those terms given by M.B. 14 remain, three terms of [5] and three terms instead of the six in [6].

Using the notation

$$\langle f\rangle_A = \iint [\psi(\mathbf{r}_1, \mathbf{r}_2)]^2 f\, d\tau_1 d\tau_2,$$

$$\langle f\rangle_B = \iint [\psi(\mathbf{r}_3, \mathbf{r}_4)]^2 f\, d\tau_3 d\tau_4,$$

$$\langle\langle f\rangle\rangle = \iiiint [\psi(\mathbf{r}_1, \mathbf{r}_2)\ \psi(\mathbf{r}_3, \mathbf{r}_4)]^2 f\, d\tau_1 d\tau_2 d\tau_3 d\tau_4,$$

and cosine formulae of spherical trigonometry it can be shown that

$$\langle \mathbf{r}_1\cdot\mathbf{r}_2\rangle_A = \langle \mathbf{r}_1\cdot\mathbf{r}_2 \cos(\mathbf{r}_1, \mathbf{d}_A)\cos(\mathbf{r}_2, \mathbf{d}_A)\rangle_A = X,$$

$$\langle r_1^2\rangle_A = \langle r_1^2\cos^2(\mathbf{r}_1, \mathbf{d}_A)\rangle_A + \langle r_1^2\sin^2(\mathbf{r}_1, \mathbf{d}_A)\rangle_A = C+S,$$

$$\langle (\mathbf{r}_1\cdot\mathbf{R}_0)(\mathbf{r}_2\cdot\mathbf{R}_0)\rangle_A = X\cos^2\alpha,$$

$$\langle (\mathbf{r}_3\cdot\mathbf{R}_0)(\mathbf{r}_4\cdot\mathbf{R}_0)\rangle_B = X\cos^2\beta,$$

$$\langle (\mathbf{r}_1\cdot\mathbf{R}_0)^2\rangle_A = \tfrac{1}{2}S + (C-\tfrac{1}{2}S)\cos^2\alpha,$$

$$\langle (\mathbf{r}_3\cdot\mathbf{R}_0)^2\rangle_B = \tfrac{1}{2}S + (C-\tfrac{1}{2}S)\cos^2\beta,$$

[7]
$$\langle\langle (\mathbf{r}_1\cdot\mathbf{r}_3)^2\rangle\rangle = (C-\tfrac{1}{2}S)^2\cos^2(\mathbf{d}_A, \mathbf{d}_B) + S(C+\tfrac{1}{4}S),$$

$$\langle\langle (\mathbf{r}_1\cdot\mathbf{r}_3)(\mathbf{r}_2\cdot\mathbf{r}_4)\rangle\rangle = X^2\cos^2(\mathbf{d}_A, \mathbf{d}_B),$$

$$\langle\langle (\mathbf{r}_1\cdot\mathbf{r}_3)(\mathbf{r}_2\cdot\mathbf{r}_3)\rangle\rangle = X^2\{(C-\tfrac{1}{2}S)\cos^2(\mathbf{d}_A, \mathbf{d}_B) + \tfrac{1}{2}S\},$$

$$\langle\langle (\mathbf{r}_1\cdot\mathbf{r}_3)(\mathbf{r}_1\cdot\mathbf{R}_0)(\mathbf{r}_3\cdot\mathbf{R}_0)\rangle\rangle = \tfrac{1}{4}S^2 + \tfrac{1}{2}S(C-\tfrac{1}{2}S)(\cos^2\alpha+\cos^2\beta) + (C-\tfrac{1}{2}S)^2\cos\alpha\cos\beta\cos(\mathbf{d}_A, \mathbf{d}_B),$$

$$\langle\langle (\mathbf{r}_1\cdot\mathbf{r}_3)(\mathbf{r}_1\cdot\mathbf{R}_0)(\mathbf{r}_4\cdot\mathbf{R}_0)\rangle\rangle = X\{\tfrac{1}{2}S\cos^2\beta + (C-\tfrac{1}{2}S)\cos\alpha\cos\beta\cos(\mathbf{d}_A, \mathbf{d}_B)\},$$

$$\langle\langle (\mathbf{r}_1\cdot\mathbf{r}_3)(\mathbf{r}_2\cdot\mathbf{R}_0)(\mathbf{r}_3\cdot\mathbf{R}_0)\rangle\rangle = X\{\tfrac{1}{2}S\cos^2\alpha + (C-\tfrac{1}{2}S)\cos\alpha\cos\beta\cos(\mathbf{d}_A, \mathbf{d}_B)\},$$

$$\langle\langle (\mathbf{r}_1\cdot\mathbf{r}_3)(\mathbf{r}_2\cdot\mathbf{R}_0)(\mathbf{r}_4\cdot\mathbf{R}_0)\rangle\rangle = X^2\cos\alpha\cos\beta\cos(\mathbf{d}_A, \mathbf{d}_B).$$

From [5], [6], and [7]

[8]
$$\langle\langle (v_2)^2\rangle\rangle = \frac{4e^4}{R^6}[S(X+C+S)+\tfrac{3}{2}S(X+C-\tfrac{1}{2}S)(\cos^2\alpha+\cos^2\beta) + (X+C-\tfrac{1}{2}S)^2(\sin\alpha\sin\beta\cos\theta - 2\cos\alpha\cos\beta)^2],$$

and

[9]
$$\langle\langle \textstyle\sum_i (\nabla_i v_2)^2\rangle\rangle = \frac{4e^4}{R^6}[(X+C-\tfrac{1}{2}S)\{2+3(\cos^2\alpha+\cos^2\beta)\}+6S].$$

The integral X does not appear in the Massey and Buckingham treatment, and the factor 3 in [9] replaces a factor 6 in M.B. 23.

From [1], [2], [8], and [9] the van der Waals and quadrupole–quadrupole energies are given by

[10]
$$\epsilon_v = -\frac{e^2}{a_0}\left(\frac{a_0}{R}\right)^6 \frac{c_1\{f(\alpha,\beta,\theta)\}^2}{h(\alpha,\beta)} + \frac{e^2}{a_0}\left(\frac{a_0}{R}\right)^5 c_2\, g(\alpha,\beta,\theta),$$

$$\epsilon_p = -\frac{e^2}{a_0}\left(\frac{a_0}{R}\right)^6 c_1'\, f(\alpha,\beta,\theta) + \frac{e^2}{a_0}\left(\frac{a_0}{R}\right)^5 c_2\, g(\alpha,\beta,\theta),$$

where

$$f(\alpha,\beta,\theta) = 1 + M(\cos^2\alpha+\cos^2\beta) + N(\sin\alpha\sin\beta\cos\theta - 2\cos\alpha\cos\beta)^2,$$

$$h(\alpha,\beta) = 1 + L(\cos^2\alpha+\cos^2\beta),$$

$$g(\alpha,\beta,\theta) = 1 + 17\cos^2\alpha\cos^2\beta - 4\sin 2\alpha\sin 2\beta\cos\theta - 5(\cos^2\alpha+\cos^2\beta) + 2\sin^2\alpha\sin^2\beta\cos^2\theta,$$

$$L = \frac{3(X+C-\frac{1}{2}S)}{2X+2C+5S}, \quad M = \frac{3(X+C-\frac{1}{2}S)}{2(X+C+S)}, \quad N = \frac{(X+C-\frac{1}{2}S)^2}{S(X+C+S)},$$

$$c_1 = \frac{8S^2(X+C+S)^2}{2X+2C+5S}, \quad c_1' = \frac{4S(X+C+S)}{E_0}, \quad c_2 = 3(C-\tfrac{1}{2}S-\tfrac{1}{4}d^2)^2.$$

Compared with M.B. 33, which corresponds to [10], the functions $g(\alpha, \beta, \theta)$ and c_2 are unaltered. They define the R^{-5} static quadrupole–quadrupole energy and details of their derivation are given by Massey and Buckingham. The large sinusoidal variation of this energy with orientation of the molecular axes is illustrated by M.B. Figs. 2A and 2B. Averaged over all orientations this energy vanishes so that for gas kinetic phenomena in which symmetry properties permit this energy to be neglected the van der Waals R^{-6} dynamic dipole–dipole energy is of predominant importance provided that R is sufficiently large to neglect the R^{-8} dynamic dipole–quadrupole energy.

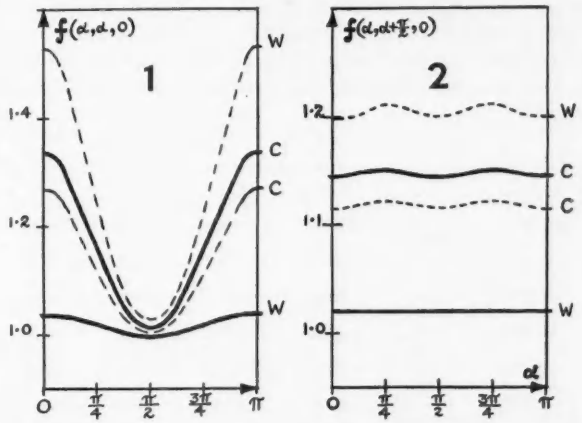

FIGS. 1 and 2. Variation of $f(\alpha, \beta, \theta)$ with orientation of molecular axes as given by the Coulson (C) and Wang (W) functions compared with that given by M.B. Figs 2A and 2B which is shown by broken curves. (Note that the labelling, $\theta = 0°$ and $\theta = 90°$, should be interchanged in M.B. Fig. 2B.)

Massey and Buckingham used the Coulson (1) and Wang (9) functions for H_2 in their calculations. In [10] as compared with M.B. 33 the function $X+C$ replaces C in all constants except c_2, and L is reduced by a factor $\frac{1}{2}$. The effect of these revisions on values of $f(\alpha, \beta, \theta)$ is illustrated by Figs. 1 and 2 in which Massey and Buckingham values are shown by dotted curves. $X = 0$ for the Coulson function and the differences in values of $f(\alpha, \beta, \theta)$ are due to our calculations being made for values of constants given by Coulson instead of for those used by Massey and Buckingham which are not carried to as many figures. $X \neq 0$ for the Wang function and our values of $f(\alpha, \beta, \theta)$ are much lower and vary much less with orientation of molecular axes.

For the Coulson function the additional factor $\frac{1}{2}$ in L does not change the character of the variation of the van der Waals energy, $E_{v.d.w.}$, with orientation

but its value averaged over all orientations, $\bar{E}_{\text{v.d.w.}}$, as given by ϵ_g in [10] is $-15.7\ R^{-6}$ instead of $-15.0\ R^{-6}$ as given by Massey and Buckingham. (Atomic units are used here and following.)

For the Wang function our revisions produce large changes. $E_{\text{v.d.w.}}$ varies very little with orientation and ϵ_g gives $\bar{E}_{\text{v.d.w.}} = -11.3\ R^{-6}$ instead of $-15.9\ R^{-6}$, the additional factor of $\frac{1}{2}$ in L that tends to increase the magnitude of $E_{\text{v.d.w.}}$ being more than compensated for by $X \neq 0$.

Because the Coulson and Wang functions give greatly differing values of $\bar{E}_{\text{v.d.w.}}$ and differing amounts of variation of $E_{\text{v.d.w.}}$ with orientation, calculations were made for five other functions in order to investigate the dependence of van der Waals energy on the function used to approximate the ground state energy of H_2 (i.e., $\frac{1}{2}E_0$). The Heitler–London (3), Gurnee–Magee (2), Rosen (8), and the two Weinbaum (10) functions were used. All seven functions are given in an appendix together with formulae for the constants X, C, and S that appear in [10]. Numerical values of these constants and of c_1 and c_1' are given in Table I. Atomic units are used and functions are referred to in tables and graphs as follows: Heitler–London (HL), Wang (W), Gurnee–Magee (GM), Rosen (R), Weinbaum Wang-ionic (WWI), Weinbaum Rosen-ionic (WRI), and Coulson (C).

TABLE I

Functions	HL	W	GM	R	WWI	WRI	C
X	−0.3793	−0.3360 (0)	−0.2764	−0.1768	−0.2097	−0.1492	0 (0)
S	2.0804	1.5341 (1.534)	1.4971	1.5386	1.4789	1.4706	1.5744 (1.594)
$X+C-\frac{1}{2}S$	0.0393	0.0316 (0.364)	0.0286	0.0235	0.1439	0.1050	0.2534 (0.200)
L	0.0094	0.0102 (0.220)	0.0095	0.0076	0.0471	0.0349	0.0764 (0.120)
M	0.0187	0.0203 (0.203)	0.0187	0.0151	0.0914	0.0682	0.145 (0.116)
N	0.00024	0.00035 (0.032)	0.00024	0.00015	0.0059	0.0032	0.0156 (0.0097)
c_1	27.52	11.055 (13.7)	10.355	11.095	10.656	10.228	13.62 (13.7)
c_1'	11.78	6.26 (7.01)	5.96	6.25	6.09	5.90	7.25 (7.03)

M. B. values are given in parentheses.

Values of $E_{\text{v.d.w.}}$ given by the variational method are more reliable than those given by the perturbation method because of the neglect of summation terms in [2], and variational values will be considered hereafter.

The dependence of $E_{\text{v.d.w.}}$ on the relative orientation of the molecular axes is illustrated by Fig. 3 and again by Figs. 4 and 5 from which the Heitler–London and Coulson results are excluded. Figs. 3 and 4 are for the orientation that gives extreme variation of $E_{\text{v.d.w.}}$, $\alpha = \beta, \theta = 0$. The perturbation method gives similar but smaller dependence on orientation. The values of $\bar{E}_{\text{v.d.w.}}$ given in Table II were calculated analytically and range from $-28.1\ R^{-6}$ for the Heitler–London function to $-10.5\ R^{-6}$ for the Gurnee–Magee function. A good approximate value of $\bar{E}_{\text{v.d.w.}}$ is obtained by evaluating $c_1 f(\frac{1}{4}\pi, \frac{1}{4}\pi, 0)$.

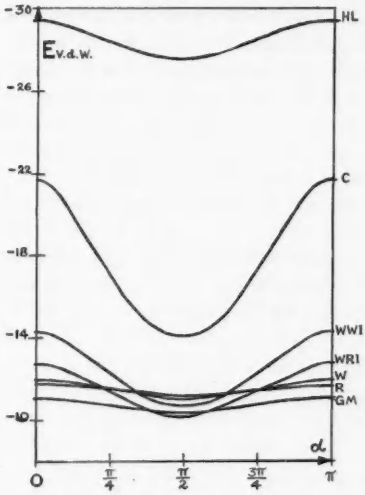

FIG. 3. Variation of $E_{v.d.w.}$ with orientation of the molecular axes for $\alpha = \beta$, $\theta = 0$. Units are atomic.

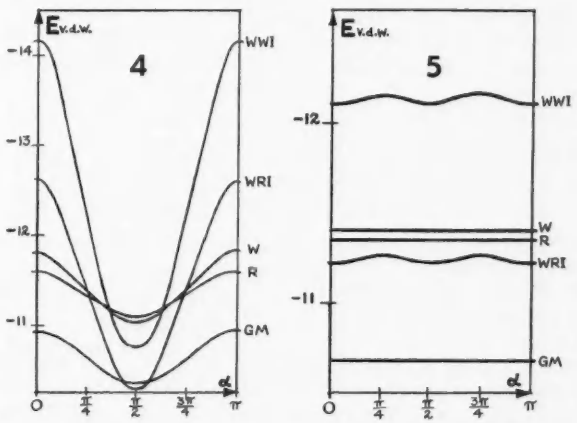

FIGS. 4 and 5. Variation of $E_{v.d.w.}$ with orientation of the molecular axes for $\alpha = \beta$, $\theta = 0$ and for $\beta = \alpha + \frac{1}{2}\pi$, $\theta = 0$. Units are atomic.

DISCUSSION OF RESULTS

Hartree atomic units are used in the following discussion.

The Heitler–London, Wang, and Gurnee–Magee functions for the ground state of a H_2 molecule are of the same form (see Appendix). In the case of the first two of these functions the 1*s* orbitals are centered at the two molecular nuclei but in the case of the latter function the 1*s* orbitals are centered at two

points on the molecular axis each of which is offset a distance x from a nucleus towards the center of the molecule. Data available for the Gurnee–Magee function did not permit exact determination of x, internuclear separation d, or screening parameter z for the position of minimum energy. Calculations were made with small variations from the approximate values $x_0 = 0.065$, $d_0 = 1.425$, $z_0 = 1.179$ and gave small changes in $E_{\text{v.d.w.}}$ with values numerically smaller than those given by the Wang function.

Each of these functions gives very little variation of $E_{\text{v.d.w.}}$ with orientation (see Fig. 3) but the Heitler–London function gives a much larger value of $|\bar{E}_{\text{v.d.w.}}|$ than the other functions (see Table II). However, Hirschfelder and Kincaid (4) have shown that the Heitler–London function does not satisfy the virial theorem of quantum mechanics and so values of $E_{\text{v.d.w.}}$ given by it cannot be reliable.

TABLE II

Function	d_0	z_0	E_0	$\bar{E}_{\text{v.d.w.}}$	
				Pert.	Var.
HL	1.518	1	2.232	−11.78	−28.1
W	1.406	1.166	2.278	−6.25	−11.3
				−(8.11)	−(15.9)
GM	1.425	1.179	2.308	−6.04	−10.5
R	1.416	1.170	2.297	−6.31	−11.2
WWI	1.417	1.193	2.296	−6.48	−11.7
WRI	1.416	1.190	2.303	−6.18	−11.0
C	1.40		2.266	−8.03	−15.7
				−(7.62)	−(15.0)
Observed	1.40		2.351		

The Wang function can be considered to be of Gurnee–Magee type with $x = 0$, and both functions satisfy the virial theorem. For such functions $E_{\text{v.d.w.}}$ depends on z_0 and the equilibrium position separation of orbital centers (see the appendix and [10]), and, by using data given by Gurnee and Magee, it can be shown that $|\bar{E}_{\text{v.d.w.}}|$ has a maximum value for an orbital center separation of about 1.40 at the equilibrium position. For the Wang function the equilibrium center separation is also d_0 and is slightly larger than 1.40, so that this function gives a value of $|\bar{E}_{\text{v.d.w.}}|$ very near to the maximum given by functions of Gurnee–Magee–Wang type that satisfy the virial theorem. This value is 11.3 R^{-6}.

The Wang function gives a value of d_0 only a little larger than the observed value but takes no account of polarization and ionic effects which tend to increase the concentration of electron density towards the center of the molecule and therefore to reduce values of $|E_{\text{v.d.w.}}|$. The effect of adding terms that approximate polarization is seen in results obtained for the Rosen function. The greater concentration of electron density towards the center of the molecule produces less variation of $E_{\text{v.d.w.}}$ with orientation (see Fig. 4). Both d_0 and z_0 are larger than for the Wang function and whilst the increase in d_0 tends to increase values of $E_{\text{v.d.w.}}$ the increase in z_0 has the opposite effect.

$|\bar{E}_{\text{v.d.w.}}| = 11.2\ R^{-6}$, a little smaller than the value given by the Wang function. The effect of adding weighted ionic terms, as in the Weinbaum Wang-ionic function, is to produce greatly increased variation of $E_{\text{v.d.w.}}$ with orientation (see Fig. 4). Both z_0 and d_0 are larger than for the Rosen or Wang functions and $|\bar{E}_{\text{v.d.w.}}| = 11.7\ R^{-6}$. The Weinbaum Rosen-ionic function includes both polarization and less heavily weighted ionic terms. d_0 is the same as for the Rosen function but z_0 is a little larger. The variation of $E_{\text{v.d.w.}}$ with orientation is smaller than that given by the Wang-ionic function (see Fig. 4) and $|\bar{E}_{\text{v.d.w.}}| = 11.0\ R^{-6}$.

The molecular orbital Coulson function gives greater variation of $E_{\text{v.d.w.}}$ with orientation than any other function considered (see Fig. 3). $|\bar{E}_{\text{v.d.w.}}| = 15.7\ R^{-6}$. This function uses a value of d_0 that differs very little from the observed value and the constant used in exponential factors (see Appendix) is derived from the James and Coolidge function (5). However, the Coulson function does not take account of the electron interaction terms that were shown to be so important by James and Coolidge. Molecular orbital functions of the form $\phi(1)\ \phi(2)$ give $X = 0$. They are not well suited to represent ground state functions of homonuclear molecules and the poor value of E_0 obtained by using an almost exact value of d_0 and four constants determined by the self-consistent field method indicates a poor representation of electron density. Values of $E_{\text{v.d.w.}}$ given by this function cannot be reliable.

The results given by the Coulson, Heitler–London, and Weinbaum Wang-ionic functions will not be considered further, the latter results being dismissed because the Rosen-ionic function can be expected to give a better approximation to the true wave function.

Of the remaining functions, that of Wang gives the best d_0 and poorest E_0 whilst that of Gurnee–Magee gives the poorest d_0 and best E_0. The former has insufficient electron density towards the center of the molecule and the latter probably too much. Therefore $|\bar{E}_{\text{v.d.w.}}|$ probably lies between $11.3\ R^{-6}$ and $10.5\ R^{-6}$.

The Weinbaum Rosen-ionic function gives E_0 slightly smaller than the Gurnee–Magee and a much improved $d_0 = 1.416$. This function can be expected to give the best approximation to the true electron density distribution of any of the simple functions considered and hence the best description of the variation of $E_{\text{v.d.w.}}$ with orientation and the best value of $\bar{E}_{\text{v.d.w.}}$. The maximum variation from the mean is about 10% which is much less than that given by the Coulson function and also much less than that given by Massey and Buckingham. The one-parameter Wang function appears to give a fairly good value of $\bar{E}_{\text{v.d.w.}}$ but insufficient variation of $E_{\text{v.d.w.}}$ with orientation.

From the above considerations it appears that $\bar{E}_{\text{v.d.w.}} = -11.0\ R^{-6}$ approximately.

COMPARISON WITH EXPERIMENT

The most reliable semiempirical calculation of $\bar{E}_{\text{v.d.w.}}$ is probably that made by Margenau (6) who based his calculation on oscillator strengths and their associated energies that had been determined empirically by Wolf and Herz-

feld (11), who fitted the experimental index of refraction of H_2 as a function of frequency very accurately by a two-term dispersion formula. Margenau's two-term value is $\bar{E}_{\text{v.d.w.}} = -10.9\,R^{-6}$, which is in good agreement with our value for $\bar{E}_{\text{v.d.w.}}$.

ACKNOWLEDGMENTS

From correspondence with H. S. W. Massey and R. A. Buckingham regarding revised values of $\bar{E}_{\text{v.d.w.}}$ obtained by using the Wang and Coulson functions for H_2, it was discovered that B. C. Carlson had conveyed to them results obtained by making the same revisions as ours in a letter dated January 8, 1950. Using the variational treatment and the Wang function he found that $E_{\text{v.d.w.}}$ varied very little with orientation and obtained the value $-11.3\,R^{-6}$ for $\bar{E}_{\text{v.d.w.}}$, results that agree with ours but that have not been published.

The authors wish to thank the Ontario Research Foundation for financial assistance given in the course of this project.

APPENDIX

H_2 WAVE FUNCTIONS AND FORMULAE FOR CONSTANTS

Molecular nuclei are labelled A, B and electrons 1, 2. r_{Ai}, r_{Bi} are vectors to $i = 1$ or 2 from A and B respectively. The equilibrium separation of nuclei is d. Prolate spheroidal coordinates are defined by

$$\lambda_i = (r_{Ai}+r_{Bi})/d, \quad \mu_i = (r_{Ai}-r_{Bi})/d, \quad \phi_i = \text{azimuthal angle},$$

and were used to derive formulae for constants. Atomic units are used with normalized $1s$ hydrogen-like orbitals of the form

$$a(i) = (z^3/\pi)^{\frac{1}{2}} \exp(-zr_{Ai}).$$

The following functions appear in constants:

$$\Delta = (1+s+\tfrac{1}{3}s^2)e^{-s},$$

$$P = (1+s+\tfrac{2}{5}s^2+\tfrac{1}{15}s^3)e^{-s},$$

$$Q = (1+s+\tfrac{9}{20}s^2+\tfrac{7}{60}s^3+\tfrac{1}{60}s^4)e^{-s},$$

$$G = (1+s+\tfrac{53}{126}s^2+\tfrac{11}{126}s^3+\tfrac{1}{210}s^4-\tfrac{2}{945}s^5-\tfrac{1}{1890}s^6)e^{-s},$$

$$H = (1+s+\tfrac{45}{84}s^2+\tfrac{17}{84}s^3+\tfrac{19}{336}s^4+\tfrac{19}{1680}s^5+\tfrac{1}{720}s^6)e^{-s},$$

$$Q-P = \Delta s^2/20, \; s = zd.$$

The Heitler-London, Wang, and Gurnee–Magee Functions (3, 9, and 2)

$$\psi(1,2) = N\{a(1)b(2)+a(2)b(1)\},$$

$$N^{-2} = 2(1+\Delta^2),$$

$$X = -N^2s^2/2z^2,$$

$$C = (2N^2/z^2)(1+\tfrac{1}{4}s^2+\Delta Q),$$

$$S = (4N^2/z^2)(1+\Delta P),$$

$$X+C-\tfrac{1}{2}S = N^2\Delta^2s^2/10z^2.$$

For the Heitler–London function $z = 1$, $d = 1.518$.
For the Wang function $z = 1.166$, $d = 1.406$.

For the Gurnee–Magee function $z = 1.179$, $d = 1.295$ were used, with d the distance between the centers of $1s$ orbitals for an equilibrium internuclear distance 1.425 and $x = 0.065$ in the case of this function.

The Rosen Function (*8*)

$$\psi(1,2) = N\{U_A(1)U_B(2)+U_A(2)U_B(1)\},$$

where

$$U_A(i) = a(i)\{1+\tfrac{1}{2}d\omega(1+\lambda_i\mu_i)\},$$
$$U_B(i) = b(i)\{1+\tfrac{1}{2}d\omega(1-\lambda_i\mu_i)\},$$
$$z = 1.170, \quad d = 1.416, \quad \omega = 0.12.$$

$$N^{-2} = 2\left\{\left(1+\frac{\omega^2}{z^2}\right)^2+F^2\right\}, \quad F = \left(1+\omega d+\frac{\omega^2 d^2}{5}\right)\Delta-\frac{\omega^2}{z^2}P,$$

$$X = -2N^2\left\{\frac{d}{2}\left(1+\frac{\omega^2}{z^2}\right)-\frac{2\omega}{z^2}\right\}^2,$$

$$C = \frac{2N^2}{z^2}\left[\left(1+\frac{\omega^2}{z^2}\right)\left(1+\frac{s^2}{4}-2\omega d+\frac{\omega^2 d^2}{4}+\frac{9\omega^2}{2z^2}\right)+F\left\{(1+\omega d)Q-\frac{9\omega^2}{2z^2}G\right\}\right],$$

$$S = \frac{4N^2}{z^2}\left[\left(1+\frac{\omega^2}{z^2}\right)\left(1+\frac{3\omega^2}{2z^2}\right)+F\left\{\left(1+\frac{\omega d}{2}\right)^2 P+\frac{1}{8}\omega^2 d^2 Q-\frac{3\omega^2}{2z^2}H\right\}\right],$$

$$X+C-\frac{S}{2} = \frac{2N^2}{z^2}\left[\left(1+\frac{\omega^2}{z^2}\right)\frac{3\omega^2}{z^2}-\frac{4\omega^2}{z^2}\right.$$
$$\left.+F\left\{\left(1+\frac{\omega d}{2}\right)^2\frac{\Delta s^2}{20}-\frac{3}{8}\omega^2 d^2 Q-\frac{3\omega^2}{2z^2}(3G-H)\right\}\right].$$

The Weinbaum Functions (*10*)

(i) $\psi(1,2) = N(\psi_W+k\psi_I)$, $k = 1/3.9$, $d = 1.417$, where ψ_W is the unnormalized Wang function and

$$\psi_I = a(1)a(2)+b(1)b(2).$$
$$z = 1.193 \text{ for all } 1s \text{ orbitals.}$$
$$N^{-2} = 2\{(1+k^2)(1+\Delta^2)+4k\Delta\},$$
$$X = N^2\{X_W+2kX_{WI}+k^2X_I\},$$

where X_W, C_W, and S_W are the X, C, and S functions as given for the Wang function without the normalizing factor N^2. C, S, and $X+C-\frac{1}{2}S$ are given similarly.

$$X_{WI} = 0,$$
$$C_{WI} = (2/z^2)\{(1+\tfrac{1}{4}s^2)\Delta+Q\},$$
$$S_{WI} = (4/z^2)(\Delta+P),$$
$$(X+C-\tfrac{1}{2}S)_{WI} = 3\Delta s^2/5z^2,$$
$$X_I = s^2/2z^2,$$
$$C_I = (2/z^2)(1+\tfrac{1}{4}s^2+\Delta Q),$$
$$S_I = (4/z^2)(1+\Delta P),$$
$$(X+C-\tfrac{1}{2}S)_I = (s^2/z^2)(1+\tfrac{1}{10}\Delta^2).$$

(ii) $\psi(1,2) = N(\psi_R + k\psi_I)$, $k = 1/5.7$, $d = 1.416$, $\omega = 0.0833$, where ψ_R is the unnormalized Rosen function and $z = 1.190$ for all $1s$ orbitals.

$$N^{-2} = 2\left[\left(1+\frac{\omega^2}{z^2}\right)^2 + \left\{\left(1+\frac{\omega d}{2}\right)^2\Delta - \omega^2 d^2 P\right\}^2 + k^2(1+\Delta^2) + 4k\Delta\left(1+\frac{\omega d}{2}\right)\right].$$

X, C, and S are as given for (i) with the Wang function replaced by the Rosen function and

$$\begin{aligned} X_{RI} &= (2\omega/z^2)(d - 2\omega/z^2)Q, \\ C_{RI} &= (2/z^2)(1+\tfrac{1}{2}\omega d)\{(1+\tfrac{1}{4}s^2 - \omega d)\Delta + Q\}, \\ S_{RI} &= (4/z^2)(1+\tfrac{1}{2}\omega d)(\Delta + P), \\ (X + C - \tfrac{1}{2}S)_{RI} &= (2/z^2)\{(1+\tfrac{1}{2}\omega d)(\tfrac{3}{10}s^2 - \omega d)\Delta + (\omega d - 2\omega^2/z^2)Q\}. \end{aligned}$$

The Coulson Function (1)

$$\psi(1,2) = \phi(1)\phi(2), \qquad d = 1.40,$$

where

$$\phi(1) = 0.87758e^{-0.75\lambda_1}(1 + 0.27787\mu_1 - 0.12863\lambda_1 + 0.012503\lambda_1^2 - 0.039589\lambda_1\mu_1^2).$$

The following reduction formulae were used in the calculation of constants, numerical values of which are given in Table I:

$$\int_{-1}^{1} \mu^n d\mu = \frac{2}{n+1}\,\delta_{n\ \text{even}}$$

$$\int_1^\infty e^{-s\lambda}\lambda^n d\lambda = \frac{1}{s}e^{-s} + \frac{n}{s}\int_1^\infty e^{-s\lambda}\lambda^{n-1}d\lambda.$$

REFERENCES

1. COULSON, C. A. Proc. Cambridge Phil. Soc. 34: 204. 1938.
2. GURNEE, E. F. and MAGEE, J. L. J. Chem. Phys. 18: 142. 1950.
3. HEITLER, W. and LONDON, F. Z. Physik, 44: 455. 1927.
4. HIRSCHFELDER, J. O. and KINCAID, J. Phys. Rev. 52: 658. 1937. See also Ref. 2 and HIRSCHFELDER, J. O. and LINNETT, J. W. J. Chem. Phys. 18: 130. 1950.
5. JAMES, H. M. and COOLIDGE, A. S. J. Chem. Phys. 1: 825. 1933.
6. MARGENAU, H. Phys. Rev. 64: 131. 1943.
7. MASSEY, H. S. W. and BUCKINGHAM, R. A. Proc. Roy. Irish Acad. 45: 31. 1938.
8. ROSEN, N. Phys. Rev. 38: 2099. 1931.
9. WANG, S. C. Phys. Rev. 31: 579. 1928.
10. WEINBAUM, S. J. Chem. Phys. 1: 593. 1933.
11. WOLF, K. L. and HERZFELD, K. F. Handbuch der physik. Vol. 20. Verlag von Julius Springer, Berlin. 1928.

FIELD THEORETICAL DESCRIPTION OF THE SUPERCONDUCTING STATE[1]

By Robert E. Pugh

ABSTRACT

The superconducting state is described in terms of the electronic plasma in interaction with the electromagnetic potentials. The interaction of the plasma with itself and with the lattice is represented by a potential energy determined such that the equations of motion are self-consistent. The resulting non-linear field equations are solved in the linear approximation. There exist four independent modes of vibration of the field variables corresponding to the plasma oscillations, and one longitudinal and two transverse oscillations of the electromagnetic potentials. The contribution of these modes to the specific heat is discussed.

I. INTRODUCTION

In this work an attempt is made to describe the phenomenon of superconductivity by representing the so-called "superconducting electrons" as a classical charged fluid. It will be shown that the hydrodynamic equations describing the fluid are consistent with London's phenomenological equations (3). Since as yet the behavior of the specific heat of a superconducting metal below its transition temperature has not been satisfactorily explained, we shall try to describe this phenomenon in terms of the energies of the wave motions of the electric and magnetic field potentials. We shall begin our discussion by reviewing briefly some of the experimental facts associated with the phenomenon of superconductivity.

A. The Experimental Facts

In 1911, Kamerlingh Onnes (5) discovered that at a certain very low temperature, T_c, the resistance of certain conductors dropped sharply to zero, indicating that no electric field could be maintained inside this 'superconductor'. Kamerlingh Onnes further discovered that this phenomenon of superconductivity was destroyed by the application of a sufficiently strong magnetic field, $H_c(T)$.

Considering the superconductor to be a perfect conductor (infinite conductivity), then it follows from Maxwell's equations that the magnetic field inside a superconductor is constant ($\dot{B} = 0$). One would then expect that if a superconducting metal were placed in a magnetic field and then cooled below its transition temperature, the magnetic field would be 'frozen in'. It was found, however, by Meissner (4) in 1933 that when the metal became superconducting the field in the neighborhood of the specimen increased, thus showing that the field inside the superconductor was pushed out, leaving no magnetic field inside. It was also shown that when a superconductor initially in zero field is placed in a magnetic field, the field inside the superconductor remains zero. Hence one concludes that this process is a reversible one and that the magnetic field may therefore be treated as a thermodynamic variable.

[1]*Manuscript received May 19, 1955.*
Contribution from the Department of Physics, University of British Columbia, Vancouver, British Columbia. The author is a holder of a National Research Council Bursary, 1954–55.

Treating the magnetic field H as a thermodynamic variable of the state of the superconductor, one can easily derive from the first and second laws of thermodynamics that the difference between the specific heat in the superconducting state and the specific heat in the normal state is

$$C_s - C_n = \frac{T}{8\pi}\frac{d^2H_c}{dT^2}.$$

The specific heat at constant volume in the normal state at low temperature can be represented by

$$C_n = \alpha T + 464.4(T/\theta)^3.$$

The T^3 term, which is hereafter denoted by C_L, is attributed to the lattice vibrations according to the well-known Debye theory of specific heats. The linear term has been shown (6) to result from the application of Fermi–Dirac statistics to a free electron gas, and is hence usually referred to as the normal electronic specific heat and is designated by C_n^{el}.

It is generally found that at the transition temperature T_c, where the change from normal to superconducting states takes place, the specific heat as a function of temperature is discontinuous (see Fig. 1). It is seen from Fig. 1 that

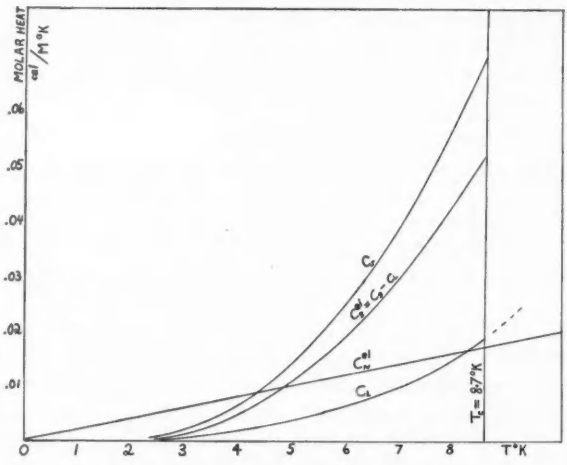

FIG. 1. Molar heat capacities of niobium.

the specific heat in the superconducting state, C_s, is greater than the lattice contribution, C_L, at all points, but not always greater than the normal electronic specific heat. Hence it is generally assumed that the lattice vibrations still contribute to the specific heat in the superconducting state, whereas the normally conducting electrons do not contribute. Since the difference $C_s - C_L$ cannot be accounted for by C_n^{el}, this difference is called the superconducting electronic specific heat, and is designated by C_s^{el}. Experimental measurements

of C_s^{el} generally indicate that it follows a T^3 law. Recent work on the specific heat of superconducting niobium (1) shows that in this case C_s^{el} rises much faster than any T^3 dependence. We shall later discuss the contribution of various modes of vibration to the superconducting specific heat, and will give a possible reason for this deviation from a T^3 dependence.

B. The Present State of the Theory of Superconductivity

There exists at present no atomistic theory of superconductivity. One can, however, specify some of the conditions that a successful theory of superconductivity must fulfill. It must

(i) agree with the phenomenological theory (London's equations),

(ii) give the transition temperature and the critical magnetic field, and

(iii) give the isotope effect ($M^{\frac{1}{2}} T_c = \text{const.}$).

Taking the usual view that superconductivity is caused by the conduction electrons, and is not a property of the lattice, one can say that a successful approach towards the problem has been made if one can explain the origin of a large gap in the energy levels of the conduction electrons near the surface of the Fermi sphere. In fact, if electrons were Bose particles, one could construct a fairly reasonable model of the superconductor, in which the existence of the critical magnetic field is explained in terms of the Zeeman effect field which would tend to close the gap between the ground state and the first excited state of the electrons in a superconductor of reasonable dimensions. This effect comes out in the right order of magnitude in the approximation in which the interaction between the electrons themselves and between the electrons and the lattice is neglected. Such a model is unfortunately of little use in the case of a Fermi gas of electrons, since the level density near the surface of the Fermi sphere is so large that the magnetic field needed to make neighboring energy levels coincide by Zeeman effect is extremely small (10^{-3} oersteds). It can therefore be only by taking into account the interaction between electrons themselves, and between the electrons and lattice vibrations, that one can hope to obtain a successful start towards an atomistic theory of superconductivity. The very existence of the isotope effect indicates that the width of the energy gap at the surface of the Fermi sphere depends essentially on the interactions between the electrons and the lattice vibrations.

It is beyond the scope of the present work to try to describe the mechanism which sets up the superconducting state, which is presumably due to the interaction of electrons among themselves and with the lattice ions. It will be assumed that this interaction leads to a rigid ground state for the electrons, i.e., most of the electrons must be in their lowest states, and the probability that they can rise to states of higher energy must be small.

In the following, the electronic description of the superconductor will be characterized by a system of continuous electric charges which interact with the electromagnetic field which they themselves produce. In other words, the electronic behavior is characterized by a system of simultaneous differential equations consisting of Maxwell's equations and the classical hydrodynamic equations for a continuous fluid.

II. THE LAGRANGIAN FORMULATION OF THE SUPERCONDUCTING STATE AND THE RESULTING EQUATIONS OF MOTION

We shall try the following Lagrangian density:*

$$[1] \qquad L = -\rho\dot{\phi} - \tfrac{1}{2}\rho v^2 + \frac{1}{8\pi}(\epsilon E^2 - H^2) - \frac{1}{8\pi}\left(\frac{\epsilon}{c}\dot{\Phi} + \nabla\cdot\mathbf{A}\right)^2 - \frac{e}{m}\rho_1\Phi_1$$

where $\mathbf{H}$ is the magnetic field, $\mathbf{E}$ the electric field, Φ and $\mathbf{A}$ the electric and magnetic vector potentials respectively, ϵ the dielectric constant, and $\mathbf{v}$ (defined by equation [2] below) the velocity of the fluid. ϕ is the velocity potential, and ρ is the mass density of the fluid. The first two terms are the usual classical hydrodynamic terms for a free continuous fluid of density ρ; by themselves, they give upon independent variation with respect to ρ and ϕ the equation of continuity and the Bernoulli equation for a continuous fluid. The last three terms are the electromagnetic terms which give, by themselves, upon variation with respect to $\mathbf{A}$ and Φ, Maxwell's equations. There is, however, one important difference: the usual term $(e/m)\rho\Phi$ has been replaced by $(e/m)\rho_1\Phi_1$, where ρ_1 and Φ_1 are the deviations from the average density ρ_0 and the average potential Φ_0 respectively. This means that the background of positive lattice charge effectively cancels out the Coulomb interaction† of the fluid leaving only the interaction between the net electric charge density $(e/m)\rho_1$, and the net electric field potential Φ_1. ρ and Φ are imagined to be written as $\rho = \rho_0+\rho_1$ and $\Phi = \Phi_0+\Phi_1$.

In addition we define the following:

$$[2] \qquad \mathbf{v} = \nabla\phi - \frac{e}{mc}\mathbf{A},$$

$$[3] \qquad \mathbf{H} = \operatorname{curl}\mathbf{A},$$

$$[4] \qquad \mathbf{E} = -\nabla\Phi - \frac{1}{c}\dot{\mathbf{A}}.$$

The choice [2] has been made to satisfy identically London's equation

$$[2a] \qquad \operatorname{curl}\Lambda\mathbf{j}_s = -\frac{1}{c}\mathbf{H} \text{ where } \Lambda\mathbf{j}_s = \frac{m}{e}\mathbf{v},$$

while [3] and [4] are the usual expressions for the electric and magnetic fields in terms of the potentials Φ and $\mathbf{A}$.

We will now assume that the density of the fluid is almost constant and that variations in density are small, i.e., we assume that in the expansion $\rho = \rho_0+\rho_1$, the deviation ρ_1 is much smaller than ρ_0, and that ρ_0 is constant. This assumption, with the previous assumption that the positive lattice charge effectively cancels out the electric field due to the electrons, makes it reasonable to assume that ϕ, $\mathbf{A}$, and Φ_1 are small, so that second order terms in them can be neglected.

**This Lagrangian is chosen for simplicity; one can try another Lagrangian which is derived from analogy with the classical Schroedinger field, but it turns out that this more complicated type of Lagrangian leads to the same solutions if one demands that London's first equation be satisfied. The treatment of this type of Lagrangian is outlined in Appendix A.*

†This is shown to be true in Appendix A.

By independent variation of the Lagrangian density with respect to ϕ, ρ, Φ, and $\mathbf{A}$, we get the following equations of motion:

$$\dot{\rho}_1+\rho_0\nabla^2\phi-\frac{e}{mc}\rho_0\nabla\cdot\mathbf{A}=0, \tag{5}$$

$$\dot{\phi}+\frac{e}{m}\Phi_1=0, \tag{6}$$

$$\nabla^2\mathbf{A}-\frac{\epsilon}{c^2}\ddot{\mathbf{A}}+\frac{4\pi e}{mc}\rho_0\left(\nabla\phi-\frac{e}{mc}\mathbf{A}\right)=0, \tag{7}$$

$$\nabla^2\Phi_1-\frac{\epsilon}{c^2}\ddot{\Phi}+\frac{4\pi e}{m\epsilon}\rho_1=0, \tag{8}$$

neglecting second order terms. Equation [5] is the usual equation of continuity expressing the law of conservation of matter. Equation [6] is Bernoulli's equation for the conservation of energy in the case that the kinetic energy of the fluid is negligible. Equations [7] and [8] are the usual electromagnetic field equations. London's first equation follows directly from equation [6]. We have

$$\frac{\partial\Lambda\mathbf{j}_E}{\partial t}=\frac{\partial(m/e)\mathbf{v}}{\partial t}=\frac{m}{e}\nabla\dot{\phi}-\frac{1}{c}\dot{\mathbf{A}}=-\nabla\Phi-\frac{1}{c}\dot{\mathbf{A}}=\mathbf{E} \tag{6a}$$

which is London's first equation.

The equations [5] to [8] may be solved for ρ_1 as follows: differentiate [5] with respect to time and substitute $\dot{\phi}$ from [6]. Making use of the Lorentz condition $\nabla\cdot\mathbf{A}=-(\epsilon/c)\dot{\Phi}$, equation [5] becomes:

$$\ddot{\rho}_1+\frac{4\pi e^2}{m^2\epsilon}\rho_0\rho_1=0. \tag{9}$$

Hence

$$\rho_1=f(\mathbf{r})\exp(i\omega_0 t)$$

where

$$\omega_0{}^2=\frac{4\pi e^2}{m^2\epsilon}\rho_0 \tag{10}$$

and $f(\mathbf{r})$ is, as far as equation [9] is concerned, an arbitrary function of the co-ordinates. However, in order to solve the rest of the equations, we must know the explicit form of $f(\mathbf{r})$. It turns out that if $f(\mathbf{r})$ is taken to be a constant, the Lorentz condition cannot be satisfied. In Appendix A, where a more general Lagrangian is considered, $f(\mathbf{r})$ is shown to be of the form $\exp(i\mathbf{K}_0\cdot\mathbf{r})$ where $\mathbf{K}_0$ is a vector whose magnitude depends on the coefficient of a term which does not appear in the Lagrangian used above. It is therefore convenient to take

$$f(\mathbf{r})=\text{const.}\exp(i\mathbf{K}_0\cdot\mathbf{r}) \tag{11}$$

where for this discussion $\mathbf{K}_0$ can be taken to be any arbitrary non-zero vector. Hence we have:

$$\rho_1=\text{const.}\exp(i\mathbf{K}_0\cdot\mathbf{r}+i\omega_0 t). \tag{12}$$

We may now solve equation [8] for Φ_1. We get:

$$[13] \qquad \Phi_1 = \text{const.}\exp(i\mathbf{K}\cdot\mathbf{r}+i\omega t)+\frac{4\pi e}{m\epsilon[K_0^2-(\epsilon/c^2)\omega_0^2]}\rho_1$$

where

$$[14] \qquad K^2 = \epsilon\omega^2/c^2.$$

For brevity we put $\Phi_1' = \text{const.}\exp(i\mathbf{K}\cdot\mathbf{r}+i\omega t)$ and $\alpha = 4\pi e/[m\epsilon\{K_0^2-(\epsilon/c^2)\omega_0^2\}]$. Equations [5] and [6] yield the following solution for ϕ:

$$[15] \qquad \phi = \frac{e\alpha}{m\omega_0^2}\dot{\rho}_1+\frac{e}{m\omega^2}\dot{\Phi}_1'+\phi'$$

where ϕ' is a general solution of $\dot{\phi}' = 0$ and $\nabla^2\phi' = 0$. Finally equation [7] yields:

$$[16] \qquad \mathbf{A} = \frac{mc}{e}\nabla\phi'+\frac{c}{\omega^2}\nabla\dot{\Phi}_1'+\frac{\epsilon\alpha}{cK_0^2}\nabla\dot{\rho}_1+\mathbf{A}_0\exp(i\mathbf{K}_1\cdot\mathbf{r}+i\omega_1 t)$$

where $\mathbf{A}_0$ is a constant vector, and

$$[17] \qquad \omega_1^2 = \frac{c^2K_1^2}{\epsilon}+\omega_0^2.$$

It is seen from [13] and [16] that the Lorentz condition is satisfied provided that $\mathbf{A}_0\cdot\mathbf{K}_1 = 0$, i.e. provided that the vector potential

$$[18] \qquad \mathbf{A}' = \mathbf{A}_0\exp(i\mathbf{K}_1\cdot\mathbf{r}+i\omega_1 t)$$

is a transverse wave.

It should be pointed out that the magnetic vector potential $\mathbf{A}$ given by [16] has a very unusual feature: *it has a longitudinal component*, $(c/\omega^2)\nabla\dot{\Phi}_1'$.

We see from the above that the solutions are constructed from four independent modes of oscillation: ρ_1, Φ_1', and the two components of $\mathbf{A}'$ which are orthogonal to its propagation vector $\mathbf{K}_1$. ρ_1 has a fixed frequency, ω_0, given by [10], and an arbitrary propagation vector, $\mathbf{K}_0$. Φ_1' has a frequency, ω, and a propagation vector, $\mathbf{K}$, which are related by

$$\omega^2 = c^2K^2/\epsilon.$$

$\mathbf{A}'$ has a frequency ω_1, and a propagation vector $\mathbf{K}_1$, related by

$$\omega_1^2 = (c^2K_1^2/\epsilon)+\omega_0^2.$$

It is shown in Section III that, for thermodynamic considerations, ω_0^2 is negligible compared with $c^2K_1^2/\epsilon$. The contribution of these four modes of oscillation to the specific heat of the system is considered below.

Equation [10] is the clue to a possible explanation of the high specific heats of superconductors. It states simply that the frequency of the classical charged fluid representing the superconducting electrons, i.e., the frequency of the so-called plasma oscillations, is a constant. We could then imagine the following model. In the normal state, the conducting electrons are essentially free, as shown by the existence of C_n^{el}. At some critical temperature the electrons, under the influence of the lattice ions, vibrate with some fixed frequency

which is a subharmonic of the maximum lattice frequency, i.e. a subharmonic of the upper limit of the Debye spectrum of lattice frequencies. Let us assume that this plasma frequency is of order of magnitude $kT_c/h \sim 10^{10}$ to 10^{11}. This frequency results in an extremely large dielectric constant as was pointed out by Ginsburg (2). For example, if we take the "number of superconducting electrons" per unit volume ρ_0/m to be 5×10^{21}, then from equation [10] we have

$$\epsilon = \frac{4\pi e^2}{m^2\omega_0^2}\rho_0 \sim 10^8 \text{ to } 10^{10}.$$

This large dielectric constant plays a very important role in the behavior of the superconductor. Such a large ϵ means a very small velocity of light ($c/\sqrt{\epsilon} \sim 10^5$ cm./sec.). Now the smaller the velocity of light, the larger is the momentum p associated with black body radiation of given energy E. Hence, since the number of photons which can have energy between E and $E+dE$ is proportional to p^2dp, there are more photons with energy E when ϵ is large than when ϵ is small. In fact, the number of photons of given energy is proportional to $\epsilon^{3/2}$. Because of the greatly increased number of photons present, a much greater expenditure of energy will be required to raise the temperature of the superconductor. This means a larger specific heat in the superconducting state than in the normal state. This subject is treated quantitatively in the next section.

III. SPECIFIC HEAT

From the solutions for the equations of motion given in Section II, we see that there are four independent modes of vibration in the superconductor. They are:

(1) the plasma oscillation,
(2) the electric field potential oscillation Φ_1',
(3) and (4) the two independent modes of vibration due to $\mathbf{A}'$. There are two modes because $\mathbf{A}'$ is a transverse wave and hence there are two independent mutually orthogonal oscillations each perpendicular to the direction of propagation of the wave.

In thermal equilibrium, each of these modes will contribute separately to the total energy of the system. We will first show that the contribution of the plasma oscillations to the specific heat of the system is negligible and then proceed to calculate the contribution of the other three modes of vibration.

(1) *Plasma Contribution*

It was shown in Section II that the density of the continuous charged fluid representing the superconducting electrons was of the form

$$\rho = \rho_0+\rho_1 = \rho_0+\text{const. } \exp(i\mathbf{K}_0\cdot\mathbf{r}+i\omega_0 t).$$

We define the energy of such an oscillation as $E_0 = \hbar\omega_0$ and the momentum as $\mathbf{P}_0 = \hbar\mathbf{K}_0$. Then the total energy per unit volume due to the plasma oscillation is

$$E_{0\text{tot}} = \frac{4\pi}{(2\pi\hbar)^3}\int_0^{P_{0\max}} \frac{E_0 P_0^2 dP_0}{e^{E_0/kT}-1}$$

where $P_{0\max}$ is the maximum momentum associated with the plasma oscillations, k is Boltzmann's constant, and T is the temperature. Because E_0 is independent of P_0, the size of $E_{0\text{tot}}$ will be determined entirely by E_0 and $P_{0\max}$. Since we know nothing about the size of $P_{0\max}$, the best we can do is to assume some upper limit for it. We will assume that

$$P_{0\max} = \frac{\sqrt{\epsilon}}{c} E_0 = \frac{\hbar}{c}\left(\frac{4\pi e^2 \rho_0}{m^2}\right)^{\frac{1}{2}};$$

presumably it would be much smaller than this. We therefore have:

$$E_{0\text{tot}} = \frac{4\pi P_{0\max}^3 E_0}{3(2\pi\hbar)^3 (e^{E_0/kT}-1)}.$$

We will now assume for the sake of the following order of magnitude calculation that $P_{0\max}$ and E_0 are temperature independent. In general, of course, they will not be independent of temperature, but taking this into account would not change the results obtained below by more than a small factor.

The contribution of the plasma oscillations to the specific heat is then

$$c_v = \frac{dE_{0\text{tot}}}{dT} = \frac{4\pi k P_{0\max}^3}{3(2\pi\hbar)^3} \cdot \frac{x^2 e^x}{(e^x-1)^2}$$

where $x = E_0/kT$. The expression $x^2e^x/(e^x-1)^2$ is a monotonic decreasing function, having its largest value (for positive x) at $x = 0$, at which point it is unity. It follows then that C_v has its largest value when $E_0 \ll kT$; i.e.,

$$C_{v\max} = \frac{4\pi k P_{0\max}^3}{3(2\pi\hbar)^3}.$$

Taking the "number of superconducting electrons" per unit volume, ρ_0/m, to be about 5×10^{21}, we get:

$$C_{v\max} \cong 5.5\times10^{-3} \text{ erg/cc. °K.}$$

Since measured values (1) of the specific heat in niobium and other superconducting metals are about 10^4 ergs/cc. °K., we conclude that the contribution from the plasma oscillations to the specific heat is negligible.

(2) *Electric Field Potential Contribution*

We saw in Section II that the electric field potential Φ could be expressed as

$$\Phi = \Phi_0 + \Phi_1 = \Phi_0 + \text{const.} \exp(i\mathbf{K}\cdot\mathbf{r} + i\omega t) + \alpha\rho_1$$

with $K^2 = \epsilon\omega^2/c^2$. The contribution of the oscillation ρ_1 to the energy of the system has been taken into account in III (1). We will now consider the contribution of the mode of vibration represented by Φ_1'. We define the energy and momentum of this oscillation in the usual fashion by $E = \hbar\omega$ and $\mathbf{P} = \hbar\mathbf{K}$, respectively, and we define the total energy per unit volume of such oscillations by

$$[19] \qquad E'_{\text{tot}} = \frac{4\pi}{(2\pi\hbar)^3}\int_0^\infty \frac{E(P)P^2dP}{e^{E/kT}-1} = \frac{4\pi^5 k^4}{15(2\pi\hbar c)^3}\epsilon^{3/2}T^4.$$

(3) *Contribution of the Magnetic Potential*

From equation [16] we see that the magnetic vector potential $\mathbf{A}$ can be expressed as the sum of the waves grad ρ_1, grad $\dot{\Phi}_1'$, and the complimentary function $\mathbf{A}' = \mathbf{A}_0 \exp(i\mathbf{K}_1 \cdot \mathbf{r} + i\omega_1 t)$. ($\phi'$, being independent of time, is not a wave motion.) The wave represented by $\mathbf{A}'$ can be treated in the same way as that represented by Φ_1'. We define the energy and momentum of the $\mathbf{A}'$ wave as $E_1 = \hbar\omega_1$, and $\mathbf{P}_1 = \hbar\mathbf{K}_1$ respectively. Equation [17] gives

$$E_1^2 = (c^2 P_1^2/\epsilon) + E_0^2$$

where $E_0 = \hbar\omega_0$. Hence the total energy of the A' wave is given by

$$[20] \quad E_{1\text{tot}} = 2 \cdot \frac{4\pi}{(2\pi\hbar)^3} \int_0^\infty \frac{E_1(P_1) P_1^2 dP_1}{e^{E_1/kT} - 1} = \frac{8\pi\epsilon^{3/2}}{(2\pi\hbar c)^3} \int_{E_0}^\infty \frac{(E_1^2 - E_0^2)^{\frac{1}{2}} E_1^2 dE_1}{e^{E_1/kT} - 1}.$$

The factor of two appearing in front of the integral in equation [20] comes from the fact that $\mathbf{A}'$ has two possible polarizations, i.e., two independent directions for $\mathbf{A}_0$ perpendicular to the propagation vector $\mathbf{K}_1$. Equation [20] is simplified a little by putting $u = E_1/kT$ and $u_0 = E_0/kT$, and by denoting by I the integral

$$I(u_0) = \int_{u_0}^\infty \frac{(1 - (u_0/u)^2)^{\frac{1}{2}} u^3 du}{e^u - 1}.$$

Then

$$E_{1\text{tot}} = \frac{8\pi\epsilon^{3/2} k^4 T^4}{(2\pi\hbar c)^3} I(u_0).$$

It will be shown below that the specific heat due to the energy of the Φ_1' wave as given by equation [19] is of the same order of magnitude as experimentally measured values if the dielectric constant is taken to be about 10^{10}. With this ϵ and with the number of superconducting electrons taken to be 5×10^{21}/cc., we get $u_0 = 0.05$. Hence a very good approximation is made to I by taking $u_0 = 0.00$, in which case $I = \pi^4/15$. We therefore have for the total energy of the Φ_1' and $\mathbf{A}'$ waves,

$$[21] \quad E_{\text{tot}} = E_{\text{tot}}' + E_{1\text{tot}} = \frac{4\pi^5 k^4 \epsilon^{3/2} T^4}{5(2\pi\hbar c)^3}.$$

Considering the dielectric constant to be a function of temperature, we get for the specific heat contribution from these waves:

$$[22] \quad C_v = \frac{dE_{\text{tot}}}{dT} = aT^3 \left(\epsilon^{3/2} + \tfrac{1}{4} T \frac{d\epsilon^{3/2}}{dT} \right)$$

where

$$a = \frac{16\pi^5 k^4}{5(2\pi\hbar c)^3} = 4.38 \times 10^{-14} \text{ erg/(deg.)}^4\text{cc.}$$

Figure 2 shows a plot of C_v^{el}/aT^3 versus T calculated from the experimental data for niobium (1). This graph shows quite clearly that C_v^{el} does not obey a T^3 law in niobium.

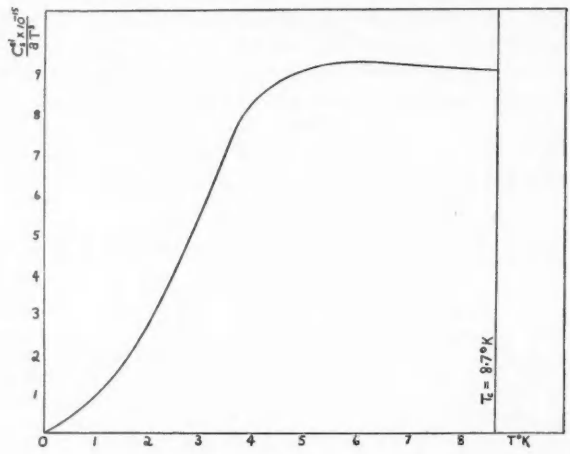

FIG. 2. Variation of C_s^{el} from a T^3 law.

Since we cannot expect to find the functional dependence of the dielectric constant on the temperature from this present theory, we must content outselves with finding what function will give the closest fit between the experimental and theoretical specific heat curves. By a process of trial and error, a curve of ϵ versus T was found which could be used to construct the curve in Fig. 2 by the relation

$$\frac{C_s^{el}}{aT^3} = \epsilon^{3/2} + \tfrac{1}{4} T \frac{d\epsilon^{3/2}}{dT}.$$

It was found that this empirical curve of $\epsilon^{3/2}$ versus T could be described quite accurately by the function

[23] $$\epsilon^{3/2} = \epsilon_0^{3/2} \frac{T_c}{T} \exp\left(\frac{-T_c}{T}\right)$$

where $\epsilon_0^{3/2} = 16.4 \times 10^{15}$ for niobium.

Hence we can write

[24] $$C_s^{el} = a\epsilon_0^{3/2} T_c T^2 e^{-T_c/T}\left(3 + \frac{T_c}{T}\right)$$

$$= 1.625 \times 10^3 T^2 e^{-8.7/T}\left(3 + \frac{8.7}{T}\right) \text{ for niobium.}$$

Table I shows a comparison of C_s^{el} calculated from [24] with the experimental values (1) of C_s^{el}. It should be noted that the experimental values listed for $T < 2.5°K$. are extrapolations and not measurements. Hence the large differences in the first four entries are not significant.

TABLE I

T, °K.	C_s^{el}, ergs/°K. cc.		% difference
	Experimental	Theoretical	
0.5	20	0.00030	
1.0	70	3.23	
1.5	230	97.4	
2.0	700	616	
2.5	1900	2021	+5.9
3.0	4.56×10^3	4.74×10^3	+3.8
3.5	9.25×10^3	9.12×10^3	−1.4
4.0	1.601×10^4	1.528×10^4	−4.8
4.5	2.458×10^4	2.350×10^4	−4.4
5.0	3.48×10^4	3.38×10^4	−2.9
5.5	4.69×10^4	4.64×10^4	−1.1
6.0	6.12×10^4	6.10×10^4	−0.3
6.5	7.75×10^4	7.78×10^4	+0.4
7.0	9.59×10^4	9.74×10^4	+1.5
7.5	11.7×10^4	11.9×10^4	+1.7
8.0	14.2×10^4	14.3×10^4	+0.7
8.5	17.0×10^4	17.0×10^4	0.0
8.7	18.1×10^4	18.1×10^4	0.0

IV. CONCLUSIONS

Demanding that London's phenomenological equations be consistent with the hydrodynamic description of a classical charged fluid has led us to find that solutions of the equations of motion contain four independent modes of oscillation. One of these, the plasma oscillation, does not contribute appreciably to the specific heat of the system. The other three oscillations, the one electric potential oscillation and the two magnetic vector potential oscillations, have been shown to contribute appreciably to the specific heat provided that the dielectric constant is, as was suggested by Ginsburg, of the order of 10^{10}.

Whether or not this is the correct interpretation of the high specific heat in superconducting metals can only be ascertained by an experiment* determining the dielectric constant in superconductors.

ACKNOWLEDGMENT

I wish to thank Professor F. A. Kaempffer for suggesting the research problem and for his advice and encouragement throughout the performance of this work.

I am grateful to the National Research Council of Canada for the donation of a Bursary (1954–55) in support of the research.

APPENDIX A

In analogy with the classical Schroedinger field we could start with the Lagrangian density:

$$[1'] \quad L = -\rho\dot{\phi} - \frac{\hbar^2}{8m^2}\rho\left(\frac{\nabla\rho}{\rho}\right)^2 - \tfrac{1}{2}\rho v^2 + \frac{1}{8\pi}(\epsilon E^2 - H^2) - \frac{1}{8\pi}\left(\frac{\epsilon}{c}\dot{\Phi} + \nabla\cdot\mathbf{A}\right) + U(\rho, \Phi)$$

*Ginsburg (2) mentions that an experiment has been performed by Galkin and Besugly which indicates that the dielectric constant of tin is about 5×10^9. The author, however, has been unable to find the paper referred to by Ginsburg.

where $U(\rho, \Phi)$ is some energy density which is to be determined. By independent variation with respect to ϕ, ρ, $\mathbf{A}$, and Φ, we get the equations of motion:

$$[5'] \qquad \dot{\rho}+\nabla\cdot(\rho\mathbf{v}) = 0,$$

$$[6'] \qquad \dot{\phi}+\tfrac{1}{2}v^2+\frac{\hbar^2}{4m^2}\left\{\frac{1}{2}\left(\frac{\nabla\rho}{\rho}\right)^2-\frac{1}{\rho}\nabla^2\rho\right\} = \frac{\partial U}{\partial\rho},$$

$$[7'] \qquad \nabla^2\mathbf{A}-\frac{\epsilon}{c^2}\ddot{\mathbf{A}}+\frac{4\pi e}{mc}\rho\mathbf{v} = 0,$$

$$[8'] \qquad \nabla^2\Phi-\frac{\epsilon}{c^2}\ddot{\Phi} = \frac{4\pi}{\epsilon}\frac{\partial U}{\partial\Phi}.$$

Making the expansions:

$$\rho = \rho_0+\rho_1,$$

$$\Phi = \Phi_0+\Phi_1,$$

$$U(\rho, \Phi) = U(\rho_0, \Phi_0)+A_1\Phi_1+B_1\rho_1+C_1\rho_1\Phi_1+\tfrac{1}{2}A_2\Phi_1^2+\tfrac{1}{2}B_2\rho_1^2,$$

where

$$A_1 = \left(\frac{\partial U}{\partial\Phi}\right)_{\rho_0,\Phi_0}, \qquad A_2 = \left(\frac{\partial^2 U}{\partial\Phi^2}\right)_{\rho_0,\Phi_0},$$

$$B_1 = \left(\frac{\partial U}{\partial\rho}\right)_{\rho_0,\Phi_0}, \qquad B_2 = \left(\frac{\partial^2 U}{\partial\rho^2}\right)_{\rho_0,\Phi_0},$$

$$C_1 = \left(\frac{\partial^2 U}{\partial\rho\partial\Phi}\right)_{\rho_0,\Phi_0},$$

and

$$\frac{\partial U}{\partial\Phi} = A_1+A_2\Phi_1+C_1\rho_1+\ldots,$$

$$\frac{\partial U}{\partial\rho} = B_1+B_2\rho_1+C_1\Phi_1+\ldots,$$

and assuming that $\mathbf{A}$ and ϕ are small such that second order terms in them may be neglected, we find that in order to satisfy the zero order equations we must have $A_1 = B_1 = 0$. Hence the first order equations of motion become:

$$[5''] \qquad \dot{\rho}_1+\rho_0\nabla^2\phi-\frac{e}{mc}\rho_0\nabla\cdot\mathbf{A} = 0,$$

$$[6''] \qquad \dot{\phi}-\frac{\hbar^2}{4m^2\rho_0}\nabla^2\rho_1 = B_2\rho_1+C_1\Phi_1,$$

$$[7''] \qquad \nabla^2\mathbf{A}-\frac{\epsilon}{c^2}\ddot{\mathbf{A}}+\frac{4\pi e}{mc}\rho_0\nabla\phi-\frac{4\pi e^2}{m^2c^2}\rho_0\mathbf{A} = 0,$$

$$[8''] \qquad \nabla^2\Phi_1-\frac{\epsilon}{c^2}\ddot{\Phi}_1 = \frac{4\pi}{\epsilon}(A_2\Phi_1+C_1\rho_1).$$

We can determine A_2 and C_1 as follows: take the divergence of [7''] and demand that the Lorentz condition $\nabla\cdot\mathbf{A} = -(\epsilon/c)\dot{\Phi}$ holds. We get

[7″a] $$\nabla^2\dot{\Phi}_1-\frac{\epsilon}{c^2}\dddot{\Phi}_1-\frac{4\pi e}{m\epsilon}\rho_0\nabla^2\phi-\frac{4\pi e^2}{m^2c^2}\rho_0\dot{\Phi}_1=0.$$

Substituting $\nabla^2\phi$ from [5″] we get

[7″b] $$\nabla^2\dot{\Phi}_1-\frac{\epsilon}{c^2}\dddot{\Phi}_1=-\frac{4\pi e}{m\epsilon}\dot{\rho}_1.$$

Differentiating equation [8″] with respect to t, we get

[8″b] $$\nabla^2\dot{\Phi}_1-\frac{\epsilon}{c^2}\dddot{\Phi}_1=\frac{4\pi}{\epsilon}(A_2\dot{\Phi}_1+C_1\dot{\rho}_1).$$

Comparison of equations [7″b] and [8″b] shows that $A_2=0$ and $C_1=-e/m$. Therefore

$$\frac{\partial U}{\partial\Phi}=-\frac{e}{m}\rho_1+\ldots+\text{nigher order terms},$$

and

$$\frac{\partial U}{\partial\rho}=-\frac{e}{m}\Phi_1+B_2\rho_1+\ldots+\text{higher order terms}.$$

Hence

$$U(\rho,\Phi)=U(\rho_0,\Phi_0)-\frac{e}{m}\rho_1\Phi_1+\frac{B_2}{2}{\rho_1}^2+\ldots+\text{higher order terms}.$$

The absence of any terms in U like $(e/m)\rho_1\Phi_0$ or $(e/m)\rho_0\Phi_1$ means that there is no Coulomb interaction between the electrons on the average. This means essentially that the interaction with the positive lattice charges cancels the interaction with the average negative electron charges represented by ρ_0 and Φ_0. Using these coefficients, the equations of motion become

[5b] $$\dot{\rho}_1+\rho_0\nabla^2\phi-\frac{e}{mc}\rho_0\nabla\cdot\mathbf{A}=0,$$

[6b] $$\dot{\phi}-\frac{\hbar^2}{4m^2\rho_0}\nabla^2\rho_1+\frac{e}{m}\Phi_1=B_2\rho_1,$$

[7b] $$\nabla^2\mathbf{A}-\frac{\epsilon}{c^2}\ddot{\mathbf{A}}+\frac{4\pi e}{mc}\rho_0\nabla\phi-\frac{4\pi e^2}{m^2c^2}\rho_0\mathbf{A}=0,$$

[8b] $$\nabla^2\Phi_1-\frac{\epsilon}{c^2}\ddot{\Phi}_1+\frac{4\pi e}{m\epsilon}\rho_1=0.$$

We will now demand that London's first equation is satisfied. Taking the gradient of all terms in equation [6b] we have

$$\frac{m}{e}\nabla\dot{\phi}+\nabla\Phi_1=\frac{m}{e}\nabla\left(B_2\rho_1+\frac{\hbar^2}{4m^2\rho_0}\nabla^2\rho_1\right),$$

or

$$\frac{\partial\Lambda\mathbf{j}_E}{\partial t}-\mathbf{E}=\frac{m}{e}\nabla\left(B_2\rho_1+\frac{\hbar^2}{4m^2\rho_0}\nabla^2\rho_1\right)=0.$$

Hence

$$\nabla\left(B_2\rho_1+\frac{\hbar^2}{4m^2\rho_0}\nabla^2\rho_1\right)=0$$

or $$\nabla^2\rho_1+\frac{4m^2\rho_0B_2}{\hbar^2}\rho_1 = C = \text{const.}$$

The solution of the above equation is:

[12a] $$\rho_1 = g(t)\exp(i\mathbf{K}_0\cdot\mathbf{r})+\frac{C}{K_0^2} \quad \text{where} \quad K_0^2 = \frac{4m^2\rho_0B_2}{\hbar^2}.$$

If we demand that the spatial average of ρ_1 is zero, then it follows immediately from [12a] that the constant C must be zero. Hence we have:

[12b] $$\rho_1 = g(t)\exp(i\mathbf{K}_0\cdot\mathbf{r}).$$

Proceeding as before we can now construct the solutions to the equations of motion.

REFERENCES

1. Brown, A., Zemansky, M. W., and Boorse, H. A. Phys. Rev. 92: 52. 1953.
2. Ginsburg, W. L. Fortschr. Physik, Band 1, Heft 3/4: 101. 1953.
3. London, F. Superfluids. Vol. 1, Pt. B. John Wiley & Sons, Inc., New York. 1950.
4. Meissner, W. and Ochsenfeld, R. Naturwiss. 21: 785. 1933.
5. Onnes, H. K. Communs. Phys. Lab. Univ. Leiden, Suppl. No. 34*b*. 1913.
6. Sommerfeld, A. Z. Physik, 47: 1. 1928.

THE ABSOLUTE FISSION YIELDS OF TWENTY-EIGHT MASS CHAINS IN THE THERMAL NEUTRON FISSION OF U^{235} [1]

By J. A. Petruska,[2] H. G. Thode, and R. H. Tomlinson

ABSTRACT

Twenty-eight absolute fission yields totalling 78% of the heavy and 16% of the light fragments have been determined using the mass spectrometer and isotope dilution techniques. The precision of the values obtained is in most cases better than 2% and the absolute accuracy is estimated to be about 3%. Fine structure in the mass–yield curve is discussed in terms of structural preference and various chain branching mechanisms.

INTRODUCTION

Early radiochemical determinations of fission yields established the asymmetric character of the mass–yield curve for the thermal neutron fission of U^{235}. However, widely divergent values for the yield of the same mass chain were often obtained and, therefore, a smooth curve of best fit was drawn through a plot of the mass–yield data such that the sum of the yields would total 100%. This work was largely carried out as part of the Manhattan Project and has been summarized by Coryell and Sugarman (4). Thode and Graham (23) and Macnamara, Collins, and Thode (16), who reported abnormally high yields for Kr^{84}, Xe^{133}, and Xe^{134}, were the first to establish the existence of irregularity or "fine structure" in the mass–yield curve. Glendenin (7, 8) attempted to explain the high yields of the 133 and 134 mass chains by assuming that nuclei with 83 neutrons (formed either as primary fragments or as secondary products by the emission of a neutron from a primary fragment) would have a high probability of "boiling off" a prompt neutron to form the more stable 82 neutron configuration. This mechanism was shown to partially account for the high yields of masses 133 and 134; but Wiles, Smith, Horsley, and Thode (27) have shown that this mechanism fails to completely account for the observed fine structure. Wiles (25) and Wiles *et al.* (27) have therefore postulated that, in addition to the Glendenin mechanism, high yields must result from an actual structural preference for isotopes with 82 neutrons in the primary fission act. Glendenin, Steinberg, Inghram, and Hess (11) reached a similar conclusion after observing a high yield of Mo^{100}, the complementary fragment to the 134 mass chain.

The more recent radiochemical yields determined by Pappas (20) seem to indicate that fine structure in the mass–yield curve is the rule rather than the exception. He has also extended the Glendenin hypothesis of neutron "boil-off" to include nuclei with 83, 85, 87, and 89 neutrons in order to explain the yields obtained by him for isotopes in the heavy mass region.

It is difficult to establish from the currently published radiochemical yields whether fine structure in the mass–yield curve is widespread. The existence of

[1]*Manuscript received July 4, 1955.*
Contribution of Chemistry Department, Hamilton College, McMaster University, Hamilton, Ontario.
[2]*Holder of Research Council of Ontario Scholarship.*

numerous fission yield values suggests that many are indeed accurate, but it is often difficult to distinguish these from the less accurate values. In this regard, the 6.62% yield of Xe^{133} obtained by Katcoff and Rubinson (15) and the 6.32% yield of Ba^{140} obtained by Yaffe, Thode, Merritt, Hawkings, Brown, and Bartholomew (29) are perhaps outstanding. The yields of Ba^{139}, Ba^{140}, Sr^{89}, Sr^{91}, and Mo^{99} have also been determined with considerable precision by Reed and Turkevich (22). However, these yields are too few to establish the details of the fine structure in the mass–yield curve.

Relative fission yields obtained with the mass spectrometer are themselves usually precise to within a few per cent, but have required normalization to some radiochemical yield before their significance in relation to the over-all mass–yield curve could be established. In the present work, normalization of relative mass spectrometric yields has been achieved without reference to any radiochemical yields. Twenty-eight absolute fission yields have been determined with the mass spectrometer using isotope dilution techniques. The yields of the 28 mass chains have been directly related by evaluating the number of atoms of a given isotope from the respective isotope dilutions. These values together with the measured number of fissions give absolute fission yields. The number of fissions was calculated from the change in the B^{10}/B^{11} ratio in a simultaneously irradiated boron flux monitor and the known cross section for neutron fission of U^{235} relative to the neutron absorption cross section of B^{10}. Yields have been determined for four isotopes of krypton, two of rubidium, and two of strontium in the light mass region and four of xenon, three of cesium, two of cerium, six of neodymium, and five of samarium in the heavy mass region.

EXPERIMENTAL

A piece of natural uranium metal weighing 2.966 gm. (approximate dimensions 0.8 cm. × 0.5 cm. × 0.4 cm.) and a BF_3 flux monitor were irradiated with thermal neutrons in the NRX (Chalk River) reactor. Details of the irradiation, separation of the fission products, and evaluation of the neutron flux have been described in a previous paper (21). The fission products, after separation from the uranium, were deposited on the source filament of a 90° sector type mass spectrometer. Chemical separation of the various fission product elements from each other was not necessary since each gives positive ions which may be distinguished from those of the other elements. Rubidium and cesium yield ions at relatively low temperatures of the source filament. At slightly higher filament temperatures the mass spectra of these elements disappear and the strontium mass spectrum is observed. At higher temperatures lanthanum, praseodymium, and neodymium appear as singly charged monoxide ions. As the filament temperature is increased still further samarium appears, chiefly as singly charged metal ions but also to some extent as metal oxide ions. As the filament temperature is further increased, the spectra of these elements gradually disappear and the spectrum of cerium monoxide ions develops. It has not yet been possible to measure the isotopic ratios of the cerium isotopes without correcting the Ce^{144} ratio for the presence of Nd^{144}. This correction however can be obtained since the amount of Nd^{143} may be measured relative to the

combined Ce^{144} and Nd^{144}. With the value of the ratio of Nd^{143} to Nd^{144} obtained at lower filament temperatures it is therefore possible to subtract the contribution of the Nd^{144} and obtain the ratio of Ce^{144} to the other cerium isotopes. The measurement of the ratios of the neodymium and samarium isotopes has been described in a previous paper (17).

In spite of precautions to prevent contamination of the fission products with stable isotopes, significant amounts of natural rubidium and strontium were found to be present in the determination of the mass spectrometric ratios of these fission products. In the case of strontium, the contamination correction could be evaluated from the amounts of Sr^{86} and Sr^{87} present since these isotopes do not have significant yields in fission. On the other hand, with rubidium it was necessary to determine the amount of contamination by means of a blank. The procedure for this technique has been described by Wiles, Smith, Horsley, and Thode (27). It was further found by means of isotope dilution studies that essentially all of the contaminating rubidium and strontium was originally present in the uranium rather than in the chemical reagents used to separate the fission products.

Xenon and krypton isotope ratios were not measured as part of this work since they had previously been reported by Wanless and Thode (24). In addition, isotope dilution was not required for these elements or for cerium since the relative yields of each could be normalized through measured yields. With regard to the krypton isotopes, the yields of masses 83, 84, and 86 were obtained relative to the 10.27-year Kr^{85} and the yield of the mass 85 chain was determined from Rb^{85}. Similarly, the xenon isotope ratios were determined relative to 5.27-day Xe^{133} and the yield of the 133 mass chain obtained from Cs^{133}. The yields of the cerium isotopes were obtained in a similar manner from their ratio to 282-day Ce^{144} and the measured yield of Nd^{144}.

RESULTS

The mass spectrometric data for the elements rubidium, strontium, neodymium, and samarium are shown in Tables I to IV respectively. The observed rubidium and strontium ratios were corrected for contamination by stable isotopes originally present in the uranium used. This correction was estimated by adding known amounts of uranium from the same original supply to the sample and redetermining the above ratios (see Tables I and II). For strontium the corrected value determined in this way was identical to that obtained when one assumed that all the Sr^{86} in the fission product was stable contamination and then made the appropriate correction to the Sr^{88} assuming the natural abundances of Sr^{88} and Sr^{86}. The Rb^{85} has been further corrected for the fraction of the 85 mass chain which had not yet decayed from Kr^{85}. This correction has been made assuming that 0.29 is the branching ratio for the 10.27-year Kr^{85} isomer (1). Since this value requires that 77.5% of the mass 85 chain pass directly to rubidium, the ultimate yield of Rb^{85}, after allowing for the fraction of Kr^{85} which decays in 2.5 years, is relatively insensitive to the exact value of the branching ratio.

TABLE I

THE RATIOS OF THE RUBIDIUM ISOTOPES PRODUCED IN THE THERMAL NEUTRON FISSION OF U^{235} TOGETHER WITH ISOTOPE DILUTION DATA

	Isotope	
	85	87
Mass spectrometric ratio	0.437±0.001	1.000
Ratio after dilution with natural rubidium		
1. 3.587×10^{15} atoms per gram of uranium	1.207±0.003	1.000
2. 4.313×10^{15} atoms per gram of uranium	1.308±0.003	1.000
Atoms of rubidium per gram of uranium* $\times10^{14}$		
1.	7.847	17.96
2.	7.716	17.66
Average	7.782±0.07	17.81±0.15
Ratio after dilution with unirradiated uranium (1 part irradiated : 1.81 parts unirradiated)	0.459±0.001	1.000
Number of atoms of fission rubidium per gram of uranium $\times10^{14}$		
Corrected for natural contamination*	7.518	17.70
Corrected for chain branching†	9.270	17.70
Corrected for fast fission‡	9.19±0.08	17.56±0.15

Assuming 72.15% Rb^{85} and 27.85% Rb^{87} in natural rubidium (19).
†Assuming 0.29 for fraction of mass 85 chain passing through the 10.27-year Kr^{85} isomer (1) and 2.55 years between irradiation and separation of the rubidium from the krypton.
‡Assuming 0.8% of each rubidium isotope formed by fast fission of U^{235}.

TABLE II

THE RATIOS OF STRONTIUM ISOTOPES PRODUCED IN THE THERMAL NEUTRON FISSION OF U^{235} TOGETHER WITH ISOTOPE DILUTION DATA

	Isotope		
	86	88	90
Mass spectrometric ratio	0.0100±0.0003	0.740±0.007	1.000
Ratio after dilution with natural strontium*			
1. 2.395×10^{15} atoms Sr^{88} per gram of uranium	—	1.376±0.014	1.000
2. 2.825×10^{15} atoms Sr^{88} per gram of uranium	—	1.464±0.011	1.000
Atoms of strontium per gram of uranium $\times10^{15}$			
1.	—	2.788	3.768
2.	—	2.889	3.905
Average	—	2.838±0.050	3.846±0.070
Ratio after dilution with unirradiated uranium (1 part irradiated : 1.81 parts unirradiated)	0.0241±0.0008	0.858±0.012	1.000
Number of atoms of fission strontium per gram of uranium $\times10^{15}$			
Corrected for stable contamination*	—	2.516	3.846
Corrected for decay of Sr^{90}†	—	2.516	4.091
Corrected for fast fission‡	—	2.496±0.050	4.058±0.070

Assuming 82.56% Sr^{88} and 9.86% Sr^{86} in natural strontium (18).
†Assuming 27.7-year half-life for Sr^{90} (28) and 2.48 years from time of irradiation to time of mass spectrometric analysis.
‡Assuming 0.8% of each strontium isotope formed by fast fission of U^{235}.

TABLE III

MASS SPECTROMETRIC AND ISOTOPE DILUTION DATA FOR Nd^{143} PRODUCED IN THE THERMAL NEUTRON FISSION OF U^{235}

	Isotope	
	142	143
Mass spectrometric ratio	0	1.000
Ratio after dilution with natural neodymium		
1. 1.428×10^{16} atoms per gram of uranium	0.664±0.003	1.000
2. 1.775×10^{16} atoms per gram of uranium	0.761±0.002	1.000
Atoms of fission Nd^{143} per gram of uranium*† $\times10^{15}$		
1.	—	4.061
2.	—	4.132
Average	—	4.096±0.036

Assuming 27.1% Nd^{142} and 12.2% Nd^{143} in natural neodymium (14).
†Corrected for 0.8% contribution from fast fission of U^{238}.

TABLE IV

MASS SPECTROMETRIC AND ISOTOPE DILUTION DATA FOR Sm^{149} PRODUCED IN THE THERMAL NEUTRON FISSION OF U^{235}

	Isotope		
	148	149	150
Mass spectrometric ratio	0	1.000	0.255±0.003
Ratio after dilution with natural samarium			
1. 3.350×10^{15} atoms per gram of uranium	0.478±0.004	1.000	
2. 3.963×10^{15} atoms per gram of uranium	0.516±0.005	1.000	
Atoms of fission Sm^{149} per gram of uranium*†‡ $\times10^{14}$			
1.	—	8.120	—
2.	—	7.894	—
Average	—	8.01±0.11	—

Assuming 11.2% Sm^{148} and 13.8% Sm^{149} in natural samarium (13).
†Since all Sm^{150} in fission products is formed by the $Sm^{149}(n, \gamma)Sm^{150}$ reaction, the total yield of $Sm^{149} = Sm^{149}+Sm^{150} = 1.255$ times the actual number of Sm^{149} atoms present at time of analysis.
‡Corrected for 0.8% contribution from fast fission of U^{238}.

The number of atoms of Nd^{143} and Sm^{149} produced per gram of irradiated uranium is evaluated from the mass spectrometric data in Tables III and IV respectively. The final values shown for these isotopes as well as those for rubidium and strontium isotopes have been reduced by 0.8% to allow for contributions from the fast fission of U^{238}. The 0.8% correction would not be expected to apply uniformly to all yields since the mass–yield curve for U^{238} is different from that of U^{235} but, in view of the small magnitude of this correction, the error introduced on this account should be small.

The ratios of the cerium isotopes are shown in Table V. Since the fission products were 2.5 years old at the time of analysis, most of the 282-day Ce^{144} had decayed to the final product Nd^{144}. The correction for this loss to the Ce^{144} ratio is therefore large and increases the uncertainty of the yields of the 140 and 142 mass chains relative to the 144 mass chain.

TABLE V

RELATIVE ABUNDANCES OF THE CERIUM ISOTOPES FORMED IN THE THERMAL NEUTRON FISSION OF U^{235}

Isotope	Mass spectrometric ratio	Corrected for decay of Ce^{144}*
140	1.05	1.17
142	1.00	1.12
144	0.101	1.00

**Assuming 282-day half-life of Ce^{144}.*

The relative yields of the isotopes of krypton and xenon taken from the data of Wanless and Thode (24) and the neodymium and samarium isotope ratios from the data of Melaika, Parker, Petruska, and Tomlinson (17) are shown in Table VI. The ratios of the neodymium and samarium isotopes were determined

TABLE VI

RELATIVE YIELDS OF XENON, KRYPTON, NEODYMIUM, AND SAMARIUM IN THE THERMAL NEUTRON FISSION OF U^{235}

Krypton (24)		Xenon (24)		Neodymium (17)		Samarium (17)	
Isotope	Relative yield	Isotope	Relative yield	Isotope	Relative yield	Isotope	Relative yield
83	1.000	131	1.000	143	1.000	147	2.10
84	1.839	132	1.496	144	0.930	149	1.00
85	2.387	134	2.750	145	0.665	151	0.398
86	3.715	136	2.207	146	0.505	152	0.251
				148	0.281	154	0.068
				150	0.110		

for the particular irradiation reported in this work. However, the values given in Table VI, which include other determinations, are therefore more reliable.

Tables I, II, III, and IV show the number of atoms present per gram of uranium for each of several isotopes. In order to obtain absolute fission yields for these isotopes, it is necessary to know the number of fissions per gram of uranium. This determination, which required correction for self-shielding of the uranium, has been described in detail in a previous paper (21). The value obtained was 7.06×10^{16} fissions per gram of uranium. The fission yields of Rb^{85}, Rb^{87}, Sr^{88}, Sr^{90}, Nd^{143}, and Sm^{149} given in Tables VII and VIII are based on this value and on the number of fission product atoms per gram of uranium for the isotopes given in Tables I, II, III, and IV. The yields of Cs^{133}, Cs^{135}, and Cs^{137} were determined for this particular irradiation and the details are given in a previous paper (21). The yields of Nd^{144}, Nd^{145}, Nd^{146}, Nd^{148}, Nd^{150}, Sm^{147}, Sm^{151}, Sm^{152}, Sm^{154} shown in Table VIII are based on the measured absolute yields of Nd^{143} and Sm^{149} together with the relative yields shown in Table VI. The yields of Ce^{140} and Ce^{142} are obtained from the relative yields given in Table V normalized to the yield of the 144 mass chain given by Nd^{144}. The yields of Kr^{83}, Kr^{84}, and Kr^{86} given in Table VII are based on the relative yields given in Table VI and normalized to the measured yield of Rb^{85}. The

TABLE VII

ABSOLUTE FISSION YIELDS OF LIGHT FRAGMENTS FORMED IN THE THERMAL NEUTRON FISSION OF U^{235}

Mass chain	Element	Yield		Mass chain	Element	Yield	
		This work	Literature			This work	Literature
72–80	—	—	0.15 (4)	96	Zr	—	6.26 (11)
81	Se	—	0.13 (9)	97	Mo	—	6.03 (11)
82	—	—	0.26 (4)	98	Mo	—	6.00 (11)
83	Kr	0.545	—	99	Mo	—	6.00 (26)†
84	Kr	1.00	—	100	Mo	—	6.56 (11)
85	Rb (Kr)	1.30	—	101	Mo	—	5.6 (26)
86	Kr	2.02	—	102	Mo	—	4.1 (26)
87	Rb	2.49	—	103	—	—	3.1 (4)
88	Sr	3.53	—	104	—	—	2.0 (4)
89	Sr	—	4.78 (22)	105	Mo	—	1.35 (26)
90	Sr	5.74	—	106	Ru	—	0.52 (10)
91	Zr	—	5.60 (11)*	107–117	—	—	0.4 (4)
92	Zr	—	5.73 (11)				
93	Zr	—	6.12 (11)	Summation of yields:		This work	16.62
94	Zr	—	6.28 (11)			Literature	83.40
95	Mo	—	6.35 (11)*			Total	100.0

Arbitrarily normalized.
†*Normalized to 6.3% yield for* Ba^{140}.

TABLE VIII

ABSOLUTE FISSION YIELDS OF HEAVY FRAGMENTS FORMED IN THE THERMAL NEUTRON FISSION OF U^{235}

Mass chain	Element	Yield		Mass chain	Element	Yield	
		This work	Literature			This work	Literature
117–129	—	—	1.8(4)	145	Nd	3.86	—
130	Sb	—	2.1 (20)	146	Nd	2.93	—
131	Xe	2.92	—	147	Sm	2.38	—
132	Xe	4.37	—	148	Nd	1.63	—
133	Cs (Xe)	6.59	—	149	Sm	1.13	—
134	Xe	8.03	—	150	Nd	0.64	—
135	Cs	6.41	—	151	Sm	0.45	—
136	Xe	6.44	—	152	Sm	0.28$_5$	—
137	Cs	6.15	—	153	—	—	0.15 (4)
138	—	—	~6.4	154	Sm	0.077	—
139	Ba	—	6.4 (22)	155–162	—	—	0.06 (4)
140	Ce	6.33	—				
141	Ce	—	5.9 (3), 6.4 (12)	Summation of yields:		This work	77.84
						Literature	22.8
142	Ce	6.03	—			Total	100.64
143	Nd	5.80	—				
144	Nd	5.39	—				

absolute yields of Xe^{131}, Xe^{132}, Xe^{134}, and Xe^{136} shown in Table VIII have been obtained from the relative yields shown in Table VI normalized to the measured yield of Cs^{133}. This normalization also requires the ratio of the 133 mass chain to the 131 mass chain. The Xe^{133}/Xe^{131} ratio has recently been redetermined and is given the value 2.26 ± 0.02 (5).

In Table VII selected radiochemical yields of mass less than 117 are shown in addition to the yields obtained in this work. The mass spectrometric yields

of the zirconium and molybdenum isotopes (11) have been arbitrarily normalized so that the yields in this table total 100%. The yields of the heavy fragments shown in Table VIII also include radiochemical values for those mass chains where values were not obtained in this work. The data shown in Table VII have been plotted in Fig. 1 and the data from Table VIII plotted in Fig. 2. Fig. 3 shows Fig. 1 folded over on Fig. 2 in order to facilitate comparison of the two.

DISCUSSION

The mass spectrometric precision of the relative yields of the isotopes for each element is in most cases better than 1%. The yields of Ce^{142} and Ce^{140}, however, relative to Ce^{144} may be in error by as much as 5% as a result of the large correction for radioactive decay of Ce^{144}. The yield of Sm^{147} is likewise subject to a similar error because of the holdup from its precursor Pm^{147}. The precision of the values for the number of fission atoms per gram of uranium obtained from the duplicate isotope dilutions for each of the elements was $\pm 1\%$. It is expected therefore that the relative yield of each fission chain obtained for the elements rubidium, strontium, cesium, neodymium, and samarium is accurate to within $\pm 2\%$. The ratio of Xe^{133}/Xe^{131} used in the normalization of the relative xenon abundances to that of the Cs^{133} yield has been determined with a precision of better than 1%. The xenon yields are therefore considered to be well within the $\pm 2\%$ limit relating the cesium yields to those of the isotopes of the other elements. The krypton abundances

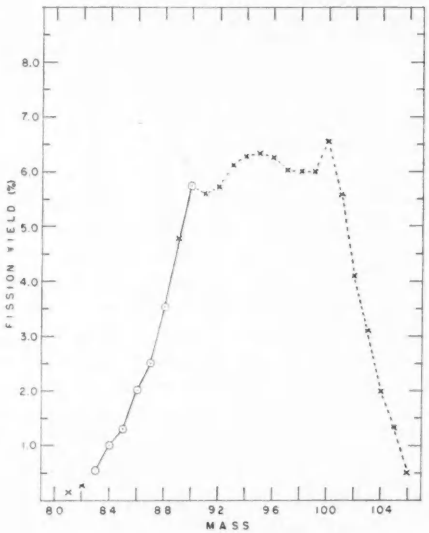

FIG. 1. Yields of light fragments formed in the thermal neutron fission of U^{235}.
⊙ Values obtained in this work.
× Literature values.

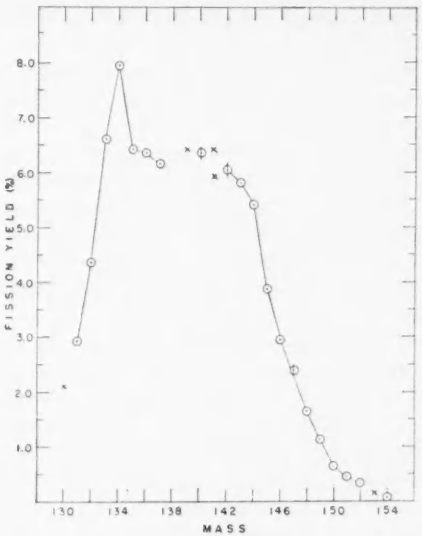

FIG. 2. Yields of heavy fragments formed in the thermal neutron fission of U^{235}.
⊙ Values obtained in this work.
× Literature values.

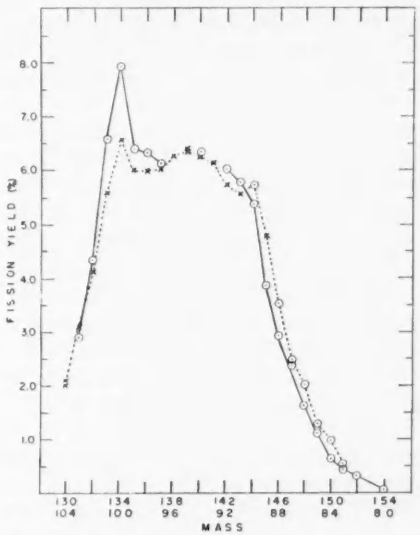

FIG. 3. Comparison of yields obtained for light and heavy fragments in the thermal neutron fission of U^{235}.
⊙ Values obtained in this work.
× Literature values.
- - Mass–yield curve for light fragments.
— Mass–yield curve for heavy fragments.

have been normalized through the relative yield of Kr^{85} and the measured yield of Rb^{85}. Whereas the yield of the mass 85 chain measured from Rb^{85} is not strongly dependent on the branching ratio to the Kr^{85} isomers, the yields of the krypton isotopes relative to that of the mass 85 chain, obtained by correcting the measured Kr^{85} yield, may be subject to considerable error on this account. Independent isotope dilutions of krypton and xenon (2), however, confirm the normalization of the krypton isotopes and hence the value of the branching ratio. Thus the relative yields of all the mass chains determined in this work are expected to be within $\pm 2\%$ except the yields of masses 140, 142, and 147. In Figs. 1 and 2 all yields determined in this work have been indicated by circles and relative precision indicated by a line through the circle where the uncertainty exceeds the circle diameter.

The absolute fission yields are dependent not only on the number of atoms of each isotope produced per gram of uranium but also on the value used for the total number of fissions. The absolute accuracy of the number of fissions per gram of uranium is dependent on several factors which have been discussed in a previous paper (21) and which by themselves place a minimum probable error of $\pm 3.5\%$. It will be noted, however, that if the value for the number of fission atoms per gram of uranium is in error all the measured yields will be affected in the same manner. Several radiochemical yields have recently been determined with considerable precision, and where these values are available, excellent confirmation with the present yields is found. Thus the value of 6.62% yield for the mass 133 chain obtained by Katcoff and Rubinson (15) is in excellent agreement with the value of 6.59% obtained in this work. Also Reed and Turkevich (22) have given a value of 6.3% and Yaffe *et al.* (29) 6.32% for the yield of Ba^{140}, both of which confirm the Ce^{140} yield of 6.33% determined in this work. The yield obtained by Yaffe *et al.*, however, should probably be increased by some 3–4% to account for a self-shielding correction as discussed in a previous paper (21). The resultant value of about 6.55% is probably more reliable for the yield of this mass chain since only 5% accuracy is claimed in this work for the yields of the 140 and 142 mass chains.

A further indication of the accuracy of the absolute yields may be obtained by consideration of their sum. In the heavy mass region 77.58% of the fission yields have been determined. Only three mass chains with significant yields have not been measured. Using the best literature values for these yields a total between 100 and 101% is obtained (see Table VIII). It is therefore estimated that the absolute fission yields reported in Tables VII and VIII are accurate to $\pm 3\%$.

The fission yields determined in the present work indicate only minor fine structure other than that in the mass region 132–137. It may be noted in Fig. 1, however, that yields of the even masses 84 and 86 appear high in comparison with the yields of the odd masses 83, 85, and 87. Also in the heavy mass region (Fig. 2) it appears that the yield of mass 144 is relatively high. In view of the uncertainty of the 147 yield little significance can be attached to its deviation from the smooth curve through other mass yields in this region. Fig. 1, how-

ever, shows further fine structure if the fission yields taken from the literature are included.

In order to discuss the values obtained for the various fission yields, it is important to review the four processes which may affect the observed cumulative fission yields.

1. Structural preference in the fission act for isotopes of a given mass and charge.
2. Neutron emission from the primary fission fragment.
3. Delayed neutron emission from fission products which have undergone one or more β decay processes.
4. Neutron capture by fission products.

Any structural preference in binary fission must result in equal yields of complementary fragments, and hence if both fragments de-excite by the loss of the same number of neutrons, the observed fission yields must be identical. The asymmetry of the over-all fission yield curve is, of course, a general manifestation of structural preference. The other three processes, which all result in chain branching, affect the fission yield resulting from one fission fragment but do not affect the yield of the complementary mass chain. Also it may be seen that, if these processes lead to an increased yield of a given mass, they must always do so at the expense of the yield of some other mass. Neutron absorption increases the yield of the mass chain one unit greater than that of the neutron absorber. On the other hand, prompt and delayed neutron emission increase the yield of the mass chain one unit lower in mass than the neutron emitter. The neutron absorption process, however, is dependent on the neutron flux during the fission product formation, whereas the neutron emission processes are independent of the flux. These considerations have been reviewed by Pappas (20).

In order to assess the experimental fission yields in terms of the above processes, it is convenient to fold the fission yield curves over each other as shown in Fig. 3. Since the sum of the mass numbers of corresponding fission fragments together with the number of emitted neutrons must be 236 ($U^{235}+1$ neutron), it is necessary to decide which masses should be made to correspond. Arbitrarily, it has been assumed that most fission fragments are de-excited by the emission of one prompt neutron, and hence the yields of the light mass chains have been plotted in Fig. 3 to correspond to the heavy mass chain such that their combined masses total 234. Since the fission fragments do not all lose the same number of neutrons in de-excitation, there is some justification for this particular matching in spite of the fact that on the average 2.5 neutrons are emitted per fission.

In Fig. 3 it may be seen that the high yield at mass 90 could result from chain branching in the mass 91 chain, but any such simple mechanism would merely displace the indentation in the mass–yield curve and could not account for the apparent displacement of the masses 80–90 in relation to their complementary fragments. This increased width of the mass–yield curve of the light fragments in relation to that of the heavy fragments could result from a greater tendency

towards multiple neutron emission for fragments with masses either less than about 95 or greater than about 139. In view of Fraser's (6) observation that 30% more neutrons are emitted by fragments in the light mass region, it is probable that fragments with mass less than about 95 have greater probability of emitting two neutrons. Such neutron emission would not only increase the width of the light mass–yield curve in relation to that of the heavy fragments, but would also lead to reduced cumulative yields in the mass region where transition from one toward two neutron emission occurs. Since the yields of masses 91 and 92 appear low in relation to that of mass 90, it is possible that many of the primary fission fragments of mass 92 or less de-excite by emission of two neutrons, whereas a smaller fraction of the primary fission fragments of mass 93 or greater emit more than one neutron. Thus not only would the cumulative yields of masses 91 and 92 be reduced in relation to those expected on the basis of single neutron emission, but so also would the yields of other chains of higher mass in this transition region. Correction for this effect could raise the yields of several masses by as much as 0.5% fission yield.

Since some information is available with regard to delayed neutron emitters and fission products with large neutron capture cross sections, it is of interest to consider what influence these may have on the observed fission yields. If fission products are formed at low neutron fluxes and short irradiation times, the effects of neutron capture are minimized. Of isotopes in relatively high yield, only Xe^{135}, Sm^{149}, and Sm^{151} have neutron absorption cross sections large enough to materially affect the observed fission yields. The corrections required by these absorption processes have been discussed in previous papers (21, 17) and the yields reported have been corrected for these effects accordingly. The effects of delayed neutron emission, however, are more difficult to assess. Several delayed neutron emitters have been identified by the half-life of their emission, but only I^{137} and Br^{87} have been given mass assignment with any certainty. The relatively high yield of Kr^{86} in relation to Rb^{87} and the lack of fine structure in the corresponding heavy fragments as shown in Fig. 3 suggests that the delayed neutron activity of Br^{87} could be responsible for the observed fine structure at these masses. In a similar manner, other delayed neutron emitters must introduce a difference between the yields of the light and heavy mass regions. It is suggested that delayed neutron emission by As^{85} may be responsible for the apparently high yield of Kr^{84} and low yield of Kr^{85}. Pappas (20) has summarized the extent to which delayed neutron emitters would affect the mass–yield curve. I^{137} and at least two other delayed neutron emitters with unidentified mass are sufficiently abundant to alter a given mass chain by 0.5% fission yield. Comparison of the light and heavy mass regions of the mass–yield curve as shown in Fig. 3 indicates that only between masses 132 and 138 could such large alterations occur unless they are masked by some form of compensation. From the fission yield data alone, it is difficult to predict which of the isotopes in this mass region (in addition to I^{137}) are the delayed neutron emitters since it appears that other phenomena also influence the observed yields.

It has previously been pointed out (27, 11) that part of the high yields

observed at masses 133 and 134 as well as at the complementary masses 100 and 101 probably result from the preferential formation of nuclides with 82 neutrons in the primary fission act. Since the yields of masses 133 and 134 are considerably greater than those of masses 100 and 101, it is also indicated that the yields of masses 133 and 134 are supplemented by chain branching processes.

Glendenin (7, 8) has postulated that primary fission isotopes reaching the 83 neutron configuration tend to "boil off" a neutron to reach the more stable 82 neutron shell structure. Pappas (20) has extended this postulate to include nuclides with 85, 87, and 89 neutrons. Such chain branching may supplement the yields of masses 133 and 134 but can only do so at the expense of heavier mass chains. Since in Fig. 3 the observed yields in this mass region are higher than the observed yields of the corresponding light mass fragments, it appears that this cannot be the case. It has already been pointed out, however, that the observed cumulative yields in the complementary light mass fragments may have also been reduced by transition from single to multiple neutron emission in this region. The Glendenin–Pappas mechanism, therefore, together with delayed neutron emission may well account for part of the enhanced fine structure at masses 133 and 134.

Pappas (20) has attempted to estimate the influence of neutron "boil-off" on the observed cumulative fission yields. He has predicted the presence of considerable fine structure in addition to that in the region of mass 134 which could extend from mass 136 to mass 144. Although the present data cannot definitely exclude this possibility since yields have not been obtained for masses 138, 139, and 141, the yields above 140 apparently fall on a reasonably smooth curve. Also the accurately determined radiochemical yield at 139 obtained by Reed and Turkevich (22) and the average of values obtained for the yield of mass 141 fit this same smooth curve. In spite of these discrepancies, it appears that at least part of the enhanced yields at masses 133 and 134 must result from the neutron "boil-off" mechanism as described by Pappas. The quantitative treatment of this, however, must await more nuclear data and accurate methods of evaluating the charge distribution of primary fission fragments.

ACKNOWLEDGMENTS

We wish to thank Atomic Energy of Canada Limited for supplying the uranium metal and arranging the neutron irradiation. The financial support of the National Research Council of Canada and Atomic Energy of Canada Limited is gratefully acknowledged.

REFERENCES

1. BERGSTROM, I. M. Siegbahn Commemorative Volume XX. Uppsala. 1951. p. 355.
2. BLADES, A. and THODE, H. G. Unpublished data.
3. BURGUS, W. H. and BALLOU, N. E. Natl. Nuclear Energy Ser. Vol. 9. Paper 180. 1951.
4. CORYELL, C. D. and SUGARMAN, N. Natl. Nuclear Energy Ser. Vol. 9. 1951.
5. FLEMING, W. H. and THODE, H. G. Unpublished result.
6. FRASER, J. S. Phys. Rev. 88: 536. 1952.
7. GLENDENIN, L. E. Ph.D. Thesis, Massachusetts Institute of Technology, Cambridge, Mass. 1949.

8. GLENDENIN, L. E. Mass. Inst. Technol. Tech. Rept. No. 35. 1949.
9. GLENDENIN, L. E. Natl. Nuclear Energy Ser. Vol. 9. Paper 61. 1951.
10. GLENDENIN, L. E. and STEINBERG, E. P. Natl. Nuclear Energy Ser. Vol. 9. Paper 103. 1951.
11. GLENDENIN, L. E., STEINBERG, E. P., INGHRAM, M. G., and HESS, D. C. Phys. Rev. 84: 860. 1951.
12. GRUMMITT, W. E. and WILKINSON, G. Natl. Research Council Can. Rept. CRC-470. 1951.
13. INGHRAM, M. C., HESS, D. C., and HAYDEN, R. J. Phys. Rev. 73: 180. 1948.
14. INGHRAM, M. C., HESS, D. C., and HAYDEN, R. J. Phys. Rev. 74: 98. 1948.
15. KATCOFF, S. and RUBINSON, W. Phys. Rev. 91: 1458. 1953.
16. MACNAMARA, J., COLLINS, C. B., and THODE, H. G. Phys. Rev. 78: 129. 1950.
17. MELAIKA, E. A., PARKER, M. J., PETRUSKA, J. A., and TOMLINSON, R. H. Can. J. Chem. 33: 830. 1955.
18. NIER, A. O. Phys. Rev. 54: 275. 1938.
19. NIER, A. O. Phys. Rev. 79: 450. 1950.
20. PAPPAS, A. C. Mass. Inst. Technol. Tech. Rept. No. 63. 1953.
21. PETRUSKA, J. A., MELAIKA, E. A., and TOMLINSON, R. H. Can. J. Phys. 33: 640. 1955.
22. REED, G. W. and TURKEVICH, A. Phys. Rev. 92: 1473. 1953.
23. THODE, H. G. and GRAHAM, R. L. Can. J. Research, A, 27: 1. 1947.
24. WANLESS, R. K. and THODE, H. G. Can. J. Phys. 33: 541. 1955.
25. WILES, D. R. M.Sc. Thesis, McMaster University, Hamilton, Ont. 1950.
26. WILES, D. R. Ph.D. Thesis, Massachusetts Institute of Technology, Cambridge, Mass. 1953.
27. WILES, D. R., SMITH, B. W., HORSLEY, R., and THODE, H. G. Can. J. Phys. 31: 419. 1953.
28. WILES, D. M. and TOMLINSON, R. H. Can. J. Phys. 33: 133. 1955.
29. YAFFE, L., THODE, H. G., MERRITT, W. F., HAWKINGS, R. C., BROWN, F., and BARTHOLOMEW, R. M. Can. J. Chem. 32: 1017. 1954.

LETTERS TO THE EDITOR

Under this heading brief reports of important discoveries in physics may be published. These reports should not exceed 600 words and, for any issue, should be submitted not later than six weeks previous to the first day of the month of issue. No proof will be sent to the authors.

α^3 Corrections to the Ground State of Helium

In a recent paper (2) Schrodinger-type wave equations were derived for systems of three or more interacting particles. The three-particle case of greatest interest was that of the helium atom. Chandrasekhar and Herzberg (1) have found such close agreement between the best available experimental value of the energy of the ground state and a new theoretical value based on the conventional formulation that it is to be expected that the quantum-theoretical corrections of relative order α^3 contribute nothing to the order required. This has been found to be the case. Calculations have been carried out for 15 likely terms, which together yielded a final correction of the size of 10^{-2} cm.$^{-1}$. Since the corrections involved are all proportional to Z^2 they remain small for all atoms of moderate atomic number. Accordingly, it is considered unnecessary to report the work in any detail. (The contribution of the Lamb Shift has been considered by previous writers.) It is interesting to note that the same result is obtained whether one uses equation [20] or equation [31] of Reference (2) below. The methods employed in carrying out the calculations were essentially those due to Salpeter (3).

1. Chandrasekhar, S. and Herzberg, G. Phys. Rev. 98: 1050. 1955.
2. Robinson, R. O. A. Can. J. Phys. 33: 369. 1955.
3. Salpeter, E. E. Phys. Rev. 87: 328. 1952.

Received September 22, 1955.
Department of Mathematics,
University of Toronto,
Toronto, Ontario.

R. O. A. Robinson

THE PHYSICAL SOCIETY

MEMBERSHIP of the Society is open to all who are interested in Physics.

FELLOWS pay an Entrance fee of £1 1*s*. ($3.00) and an Annual Subscription of £2 2*s*. ($6.00).

STUDENTS: A candidate for Studentship must be between the ages of 18 and 26, and pays an Annual Subscription of 7*s*. 6*d*. ($1.10).

MEETINGS: Fellows and Students may attend all Meetings of the Society including the annual Exhibition of Scientific Instruments and Apparatus.

PUBLICATIONS include the *Proceedings of the Physical Society*, published monthly in two sections, and *Reports on Progress in Physics*, published annually. Volume XVII, 1954, is now available (price 50*s*. ($7.15)). Members are entitled to receive many of the Publications at a reduced rate.

Further information can be obtained from:

THE PHYSICAL SOCIETY

1, LOWTHER GARDENS, PRINCE CONSORT ROAD

LONDON, S.W.7, ENGLAND

CANADIAN JOURNAL OF PHYSICS

Notes to Contributors

Manuscripts

(i) ***General.*** Manuscripts, in English or French, should be typewritten, double spaced, on paper 8½×11 in. **The original and one copy are to be submitted.** Tables and captions for the figures should be placed at the end of the manuscript. Every sheet of the manuscript should be numbered.

Style, arrangement, spelling, and abbreviations should conform to the usage of this journal. Names of all simple compounds, rather than their formulas, should be used in the text. Greek letters or unusual signs should be written plainly or explained by marginal notes. Superscripts and subscripts must be legible and carefully placed.

Manuscripts and illustrations should be carefully checked before they are submitted. Authors will be charged for unnecessary deviations from the usual format and for changes made in the proof that are considered excessive or unnecessary.

(ii) ***Abstract.*** An abstract of not more than about 200 words, indicating the scope of the work and the principal findings, is required, except in Notes.

(iii) ***References.*** References should be listed **alphabetically by authors' names,** numbered, and typed after the text. The form of the citations should be that used in this journal; in references to papers in periodicals, titles should not be given and only initial page numbers are required. All citations should be checked with the original articles and each one referred to in the text by the key number.

(iv) ***Tables.*** Tables should be numbered in roman numerals and each table referred to in the text. Titles should always be given but should be brief; column headings should be brief and descriptive matter in the tables confined to a minimum. Vertical rules should be used only when they are essential. Numerous small tables should be avoided.

Illustrations

(i) ***General.*** All figures (including each figure of the plates) should be numbered consecutively from 1 up, in arabic numerals, and each figure referred to in the text. The author's name, title of the paper, and figure number should be written in the lower left corner of the sheets on which the illustrations appear. Captions should not be written on the illustrations (see Manuscripts (i)).

(ii) ***Line Drawings.*** Drawings should be carefully made with India ink on white drawing paper, blue tracing linen, or co-ordinate paper ruled in blue only; any co-ordinate lines that are to appear in the reproduction should be ruled in black ink. Paper ruled in green, yellow, or red should not be used unless it is desired to have all the co-ordinate lines show. All lines should be of sufficient thickness to reproduce well. Decimal points, periods, and stippled dots should be solid black circles large enough to be reduced if necessary. Letters and numerals should be neatly made, preferably with a stencil (**do NOT use typewriting**) and be of such size that the smallest lettering will be not less than 1 mm. high when reproduced in a cut 3 in. wide.

Many drawings are made too large; originals should not be more than 2 or 3 times the size of the desired reproduction. In large drawings or groups of drawings the ratio of height to width should conform to that of a journal page but the height should be adjusted to make allowance for the caption.

The original drawings and one set of clear copies (e.g. small photographs) are to be submitted.

(iii) ***Photographs.*** Prints should be made on glossy paper, with strong contrasts. They should be trimmed so that essential features only are shown and mounted carefully, with rubber cement, on white cardboard with no space or only a **very** small space (less than 1 mm.) between them. In mounting, full use of the space available should be made (to reduce the number of cuts required) and the ratio of height to width should correspond to that of a journal page (4½×7½ in.); however, allowance must be made for the captions. Photographs or groups of photographs should not be more than 2 or 3 times the size of the desired reproduction.

Photographs are to be submitted in duplicate; if they are to be reproduced in groups one set should be mounted, the duplicate set unmounted.

Reprints

A total of 50 reprints of each paper, without covers, are supplied free. Additional reprints, with or without covers, may be purchased.

Charges for reprints are based on the number of printed pages, which may be calculated approximately by multiplying by 0.6 the number of manuscript pages (double-spaced typewritten sheets, 8½×11 in.) and including the space occupied by illustrations. An additional charge is made for illustrations that appear as coated inserts. The cost per page is given on the reprint requisition which accompanies the galley.

Any reprints required in addition to those requested on the author's reprint requisition form must be ordered officially as soon as the paper has been accepted for publication.

Contents

Page

Vertical Extent of Auroral Arcs and Bands—*B. W. Currie and J. T. Weaver* - 611

On the Efficiency of an Acoustic Line Source with Progressive Phase Shift—*G. J. Thiessen* - - - - - - - - - - - - - 618

Low Energy Neutron Cross Section of Manganese—*R. Krotkov* - - 622

The ν_1 Infrared Band of Ammonia—*C. Cumming* - - - - - - - 635

The Fission Yields of the Cesium Isotopes Formed in the Thermal Neutron Fission of U^{235} and the Neutron Absorption Cross Section of Xe^{135}—*J. A. Petruska, E. A. Melaika, and R. H. Tomlinson* - 640

Gauge-invariant Formulation of Quantum Electrodynamics—*P. A. M. Dirac* - - - - - - - - - - - - - - - - - - - 650

The Fluctuating Field Model of Ferromagnetism with Particular Reference to Nickel—*F. D. Stacey* - - - - - - - - - - - 661

Long Range Forces between Hydrogen Molecules—*F. R. Britton and D. T. W. Bean* - - - - - - - - - - - - - - - - - 668

Field Theoretical Description of the Superconducting State—*Robert E. Pugh* - - - - - - - - - - - - - - - - - - - 679

The Absolute Fission Yields of Twenty-eight Mass Chains in the Thermal Neutron Fission of U^{235}—*J. A. Petruska, H. G. Thode, and R. H. Tomlinson* - - - - - - - - - - - - - - - - - 693

Letter to the Editor:

α^3 Corrections to the Ground State of Helium—*R. O. A. Robinson* - 707

Printed in Canada *by* University of Toronto Press